

Studies of ultracompact H II regions – II. High-resolution radio continuum and methanol maser survey

A. J. Walsh,¹ M. G. Burton,¹ A. R. Hyland² and G. Robinson³

¹Department of Astrophysics and Optics, School of Physics, University of New South Wales, NSW 2052, Australia

²Southern Cross University, Lismore, NSW 2480, Australia

³School of Physics, University College, University of New South Wales, Canberra, ACT 2600, Australia

Accepted 1998 July 23. Received 1998 July 17; in original form 1998 April 15

ABSTRACT

High spatial resolution radio continuum and 6.67-GHz methanol spectral line data are presented for methanol masers previously detected by Walsh et al. (1997). Methanol maser and/or radio continuum emission is found in 364 cases towards *IRAS*-selected regions. For those sources with methanol maser emission, relative positions have been obtained to an accuracy of typically 0.05 arcsec, with absolute positions accurate to around 1 arcsec. Maps of selected sources are provided. The intensity of the maser emission does not seem to depend on the presence of a continuum source. The coincidence of water and methanol maser positions in some regions suggests there is overlap in the requirements for methanol and water maser emission to be observable. However, there is a striking difference between the general proximity of methanol and water masers to both cometary and irregularly shaped ultracompact (UC) H II regions, indicating that, in other cases, there must be differing environments conducive to stimulating their emission. We show that the methanol maser is most likely present before an observable UC H II region is formed around a massive star and is quickly destroyed as the UC H II region evolves. There are 36 out of 97 maser sites that are linearly extended. The hypothesis that the maser emission is found in a circumstellar disc is not inconsistent with these 36 maser sites, but is unlikely. It cannot, however, account for all other maser sites. An alternative model which uses shocks to create the masering spots can more readily reproduce the maser spot distributions.

Key words: masers – stars: formation – ISM: general – H II regions – radio continuum: ISM – radio lines: ISM

1 INTRODUCTION

Ultracompact (UC) H II regions are the small bubbles of ionized gas surrounding a newly formed massive star, embedded in its natal molecular cloud. They have received a considerable amount of attention in recent years because of their effect on the dynamics and energetics of molecular clouds, as well as by being fascinating objects in their own right. They provide a major influence in shaping molecular clouds by virtue of the energy they dump into the medium, whilst still embedded.

Two efficient methods for identifying such regions have been proposed. The first (Wood & Churchwell 1989a, hereafter WCa) involves the selection of candidates based on their far-infrared colours, as detected by *IRAS*. The strong emission of dust, radiating with a blackbody spectrum, peaking around 100 μm , gives the reddest colours of objects listed in the *IRAS* PSC, in the bands of 12, 25 and 60 μm . The second method used to identify UC H II regions is to search for

masing activity and, in particular, 6.67-GHz methanol maser emission, discovered by Menten (1991), as it is a very strong and widespread transition, and is considered to be a signpost of a UC H II region.

Previously (Walsh et al. 1997, hereafter Paper 1) we chose 534 southern UC H II region candidates from the *IRAS* PSC, using the selection criteria of WCa. Of those 534 candidates, we have reported 215 UC H II regions, identified either by association with methanol maser emission at 6.67 GHz or by identification of a compact radio source. Unfortunately, the original survey suffered from poor spatial resolution because of a large primary beam of 3.3 arcmin, so that we could not be sure of the association between methanol masers and UC H II regions. UC H II regions are also gregarious and so a large beam may also pick up emission from more than one UC H II region. It is the purpose of this paper to present high (arcsec) resolution data for both the methanol maser emission and any associated compact continuum sources in order to determine the nature of the association between UC H II regions and methanol masers.

2 OBSERVATIONS AND DATA REDUCTION

The observations were made using the Australia Telescope Compact Array (ATCA) during 1994 July/August and 1995 January/February. The ATCA is an array of six 22-m antennas on an east–west baseline with the widest separation being 6 km. Since the ATCA is a synthesis telescope, observations of each object were made by making a series of short integration cuts, of 2 min each, a number of times, spaced over a period of 12 h. Typically five cuts were taken on each object, but some have fewer because of bad weather. The effect of this is to decrease the sensitivity of the final image and to increase the relative inaccuracies of derived positions of unresolved maser sources. Observations of program sources were interspersed with calibrator sources every 30 min. The ATCA can simultaneously observe two frequencies. The first selected frequency was chosen to be the 8.64-GHz continuum over a bandwidth of 128 MHz (with 32 channels). The second frequency was chosen so as to observe the 6.67-GHz methanol maser emission. The bandwidth at this frequency is 4 MHz, with 1024 channels, giving a velocity resolution of 0.18 km s^{-1} and a velocity coverage of 180 km s^{-1} . The observing frequency was varied between 6.667, 6.668, 6.669 and 6.670 GHz, as appropriate, to take into account the radial velocities of the maser sources observed in Paper 1.

The data were processed using the `aips` data reduction package.¹ Each frequency was processed separately. The radio continuum data at 8.64 GHz were averaged into a single frequency channel, using `avspc`. Bad data were interactively edited with `tvflg`, antenna gain solutions were found with `atcalib` and then calibrated with `atclcal`. Single source files were created, and calibrations were applied with `split`. The resulting source files were then imaged and cleaned using `mx`, with typically 500 cleaning iterations. The image maps were then visually inspected for evidence of radio continuum emission.

The spectral line data at 6.67 GHz were reduced in a similar fashion, except that the data were not compressed into a single frequency channel, to preserve the spectral information, and the instrumental bandpass was removed with `bandpass` before single source files were created, with `split`. After individual source files were created, each UV source file was continuum fitted using `uvlsf` so that separate images of the continuum emission at 6.67 GHz and methanol emission could be made. The spectral line data were corrected for the motion of the array with respect to the local standard of rest, using `cvel`, and then both continuum and spectral line images were made using `mx`. The final images were inspected for continuum and maser emission in a fashion similar to the 8.64-GHz data.

The positions of each methanol maser spot were determined to an accuracy of 1.8 arcsec for each field, and then more accurate positions were determined using the method of ‘super resolution’ used by Norris et al. (1993). For each maser spot, an image was made using only the channels in which that maser spot was dominant. The emission was then Gaussian fitted using `jmf` to accurately determine the position of the maser emission, assuming it is unresolved. We estimate that the relative uncertainties of individual maser spots in a single field is 50 mas for the majority of cases. This increases for masers weaker than about 1 Jy, up to 0.5 arcsec for the weakest sources imaged, at 0.3 Jy. There is also considerable uncertainty in the positional accuracy in declination for any source closer than 10° to the celestial equator. We estimate that a strong maser at a declination of -5° would have an associated

maser spot declination error of ± 0.1 arcsec and may increase to larger than 2 arcsec for sources at a declination of -1° . It is estimated that the absolute positional uncertainty of any features will be 1 arcsec. These estimates are made by correlating the positions of the same maser spots that were obtained in both observing runs. A total of 29 maser spots could be used to experimentally determine the errors. We believe that the effect of any proper motions of the maser spots over the short interval of 6 months between the two runs will be minimal.

As a result of the nature of the short cut integrations used, only the simplest morphologies of resolved continuum sources are easily discernible from artefacts. Any interpretation of morphologies is thus limited to the overall shapes of resolved regions. Furthermore, radio continuum sources close to a declination of 0° are greatly elongated in the declination axis. No interpretation is placed on the morphologies of such continuum sources. The 1σ sensitivity limits are typically 1 mJy at 8.64 GHz and 10 mJy at 6.67 GHz, for the continuum images. The flux limit on the methanol maser emission is limited to detecting a single peak within the spectrum and is typically 0.5 Jy, although it is possible to image some weaker sources by using the known velocity coverage of a maser source from Paper 1 and Caswell et al. (1995a), and imaging over that velocity range.

In Paper 1, it was noted that some of the listed maser flux densities were underestimated, since the Parkes beam may not have been centred on the maser emission. With the accurate positions of the methanol maser and continuum emission obtained in this paper, it is possible to correct for the profile of the ATCA primary beam for most sources using `pbcor`. The HPBW of the ATCA primary beam is approximately 8.6 arcmin, so that rescaling of flux densities is only accurate out to about 5 arcmin from the pointing centre. Beyond this the uncertainties in rescaling become too large because of the low efficiency of the beam.

3 RESULTS

There are 276 observed fields, including 193 of the maser and UC H II regions identified in Paper 1 and a selection of other *IRAS* sources with no previously detected maser or radio continuum emission. The remaining 22 *IRAS* sources with methanol and/or radio continuum emission listed in Paper 1 were not observed because of poor conditions. Each field chosen was centred on the relevant *IRAS* position. Out of the 276 fields, a total of 364 sites were found which had either methanol maser emission, a compact radio continuum source, or both. There are 233 sites that exhibit methanol emission; only 46 of these have associated radio continuum emission. There are a further 131 sites that exhibit radio continuum but no methanol emission, making a total of 177 sites with continuum emission. There are 68 fields observed in which there is no detectable methanol or continuum emission; these are listed in Table 1. There are also three sources listed in Table 1 that exhibit methanol maser emission, but could not be located in the cleaned image. This may be a result of strong emission far from the pointing centre, being picked up in the sidelobes.

Details for those sources showing methanol and/or continuum emission are given in Table 2. The first column lists the associated *IRAS* name. Columns 2 and 3 give the Galactic coordinates for the *IRAS* point source, which was used as the pointing centre. Columns 4–7 contain information on the methanol maser emission: columns 4 and 5 list the methanol maser offset position from the *IRAS* position. Column 6 lists the peak flux density for the methanol emission. Column 6 also has an identifying letter that corresponds

¹ Provided by the ATNF.

Table 1. The observed sources in our data set with no positive methanol or radio continuum identification.

00445-1207 ^a	07278-1826	16475-4609	18060-1816
05173-0555	07333-1838	16557-4002	18067-1921
05283-0412	07358-3243	17149-3916 ^b	18072-1954 ^d
05304-0435	07395-1437	17178-3742	18092-1742
05327-0529	07399-1435	17234-3405 ^c	18159-1648 ^b
05331-0515	07502-2618	17242-3513 ^c	18234-1444A
05338-0624	08438-4340	17260-3445 ^b	18246-1032
05363-0702	08563-4711	17352-3153 ^c	18263-1036
05375-0731	09006-4830	17430-2822 ^b	18308-0911
05394-0151	09017-4814	17430-2900	18310-0806
05400-0154	09018-4816 ^b	17431-2846	18342-0655
05396-0153	09230-5148	17432-2855	18360-0537
06046-0603	09238-5153	17440-2823	18411-0338 ^b
06343-1036	10049-5657	17441-2910	18420-0512
06361-0142	10309-5745	17443-2821	18451-0332
06529-0755	11101-5829 ^b	17474-2637	18491-0207
06547-1012	16112-4943 ^b	17488-1741	18595-3712
07207-1435	16186-5044	17527-2439	19590-1249

^a Planetary nebula.

^b Methanol detected in Paper 1, but is not evident in these data, because of increased noise levels and/or variability of the maser source.

^c Methanol emission is present, but cannot be located in the CLEANED image.

^d Observed velocity range did not cover methanol emission.

to the positions of selected methanol spots in the images of Figs 1 and 2. Column 7 lists the radial velocity for the methanol spot. Columns 8–12 contain information on the radio continuum emission: columns 8 and 9 list the RA and Dec. offset positions for the radio continuum from the *IRAS* pointing centre, respectively. Column 10 lists the 8.64-GHz continuum peak flux density, column 11 lists the 6.67-GHz continuum peak flux density. Integrated fluxes have not been derived here, as the poorly sampled data makes it difficult to obtain accurate flux measurements. The peak flux densities are listed as a guide to the brightness of each region, although this number does not take into account the extended morphologies of some of the continuum sources. Column 12 lists the proposed morphological type for the continuum emission, where U means unresolved, I means irregularly shaped, C means cometary shaped, D means double peaked and P means partially extended (see Section 4.3 for definitions of the morphological types).

Sources listed in Table 2 and indicated with an asterisk (*) have not been corrected for the profile of the primary beam. This is because their offset positions are too great for an accurate rescaling to be performed. Instead, the uncorrected flux densities are listed, which will be considerably lower than the true values.

Cleaned images of selected radio continuum sources are shown as contour maps in Fig. 1. The criterion for inclusion of a continuum source in this figure is that either the emission is extended in some way, or that there is methanol maser emission close to the continuum emission. Unresolved continuum sources with no associated methanol emission are not shown as all the relevant information on them is contained in Table 2. The positions of the methanol spots are shown either by their associated letter from Column 6 of Table 2, or by a ‘plus’ (+) symbol. The letters were only used when there was more than one maser spot, but not so many that the letters would become unreadable. Fig. 2 shows offset positions for the methanol maser spots from the *IRAS* pointing centre, as listed in Table 2. Only

those sites of methanol emission with four or more maser spots are shown. In some cases the positions of the maser spots are in both Figs 1 and 2. These cases are shown in Fig. 2 to indicate the letter for the associated maser spot, since the continuum contour plot would be too crowded to show the individual letters.

3.1 Comments on individual sources of interest

This section contains details of fields that are relevant to the results presented in this paper. Fields which are illustrative of the major characteristics of the data set are also described. Some other fields of major importance have been detailed in Paper 1.

IRAS 13471-6120. The methanol emission has also been observed with the ATCA by Norris *et al.* (1993) and our relative positions of the maser spots correlate well, although there is an absolute offset of around 1 arcsec. We have detected a new methanol spot, with a radial velocity of -54.5 km s^{-1} (A). The maser emission is slightly offset from the centre of the unresolved continuum emission, but is still within the continuum contours. Caswell, Vaile & Forster (1995b) reported methanol and OH maser emission from this source. The position of the OH emission appears to be 0.5 arcsec offset from the methanol emission, but within the continuum emission. This is not apparent from our image in Fig. 1, as there is an offset of 1 arcsec in the absolute position with that of Caswell *et al.*, assuming the methanol emission reported here is coincident with that of Caswell *et al.*

IRAS 16484-4603. The relative positions of the methanol spots agree with those of Norris *et al.* (1993). New features are seen in our data, namely A and B. The position of the methanol emission with respect to the continuum is similar to that of *IRAS* 13471-6120. The continuum emission seems to be slightly extended to the west, with the methanol also on the west side of the centre of the continuum emission. The radio continuum image of Ellingsen, Norris & McCulloch (1996) indicates that the emission is extended to the north-east and that the angular position of the methanol maser spots is perpendicular to this continuum emission. OH maser emission is also reported by Caswell *et al.* (1995b) in three locations, two of which are within the continuum emission contours, the third lying about 4 arcsec to the north of the continuum emission. Water maser emission is reported close to the continuum emission by Forster & Caswell (1989). It is not clear whether the OH and water maser emission sites are offset from the continuum or not, because of the absolute positional uncertainty.

IRAS 16533-4009. There are two distinct sites of methanol emission, separated by 0.23 pc (assuming a near kinematic distance of 2.5 kpc), in which the individual spots of both sites correspond well with the relative positions published by Norris *et al.* (1993). An unresolved continuum source is found close to the southerly site of methanol emission, along with two OH maser emission sites. Both sites of methanol emission seem to have a linear structure. The southerly linear structure is extended radially with respect to the continuum emission.

IRAS 17016-4124. There are two separate sites of methanol emission. The first is within the contours of continuum emission. The second is offset by 40 mpc (assuming a distance of 2.7 kpc) to the west of the centre of the continuum emission. The shape of the continuum emission is cometary (about 80 mpc long), with the methanol emission found towards the ‘head’ of the continuum. OH and water maser emission is reported by Forster & Caswell (1989), both are found towards the ‘tail’ of the continuum cometary region. The methanol site overlying the continuum has weak evidence for a linear structure, which is pointing perpendicular to the cometary

Table 2. List of the 364 UC HII regions detected either by methanol maser emission or a compact radio continuum source. Each source denoted with an asterisk (*) indicates that the provided flux or flux density has not been corrected for the beam profile, and the numbers stated are most certainly underestimates.

IRAS name	IRAS		Methanol Maser					Radio Continuum					
	Galactic coordinates ^a		Offset (arcsec)	Peak flux density		Radial velocity (km s ⁻¹)	RA	Dec.	Peak flux density ^b		Morph Type ^c		
	<i>l</i>	<i>b</i>		RA	Dec.				(Jy beam ⁻¹)	(mJy beam ⁻¹)			
05393–0156	206.5620	−16.3396							−55.2	47.6	6	<14	U
05391–0152	206.4792	−16.3487							40.4	−137.4	25	<9	U
06053–0622	213.7034	−12.6017	17.83	2.76	10.6	A	12.7	7.0	−7.7	180	180	I	
			17.83	2.75	109	B	11.6						
			17.80	2.22	40	C	11.0						
06084–0611	213.8821	−11.8359							−6.2	2.8	28	26	U
07299–1651	232.6214	0.9962	3.05	1.94	1.4	A	23.2	−3.3	3.5	1	<7	U	
			3.05	2.04	94	B	22.5						
			3.02	1.97	16.7	C	22.0						
			3.05	1.99	5.0	D	21.3						
07427–2400	240.3153	0.0712							1.9	−1.8	12	<18	U
08189–3602	254.6604	0.2052							−5.0	−45.8	23	<30	U
08337–4028	259.9414	−0.0406	−6.80	4.16	2.5		−1.3				<1	<11	
08470–4243	263.2486	0.5145	1.25	−5.67	4.9	A	14.3				<1	<15	
			1.50	−5.81	5.9	B	12.9						
			1.48	−5.82	22.3	C	12.0						
08546–4254	264.2918	1.4705							27.2	212.5	9	<18	U
									80.8	104.4	5	<18	U
08576–4334	265.1476	1.4426							13.4	19.8	7	9	I
09002–4732	268.4200	−0.8472							1.24	−11.6	510	490	C
09015–4843	269.4557	−1.4717	13.43	8.93	4.5		56.0		6.3	−10.1	1	<7	U
09149–4743	270.2614	0.8358							87.9	112.7	14	<13	U
09227–5146	274.0063	−1.1471							5.7	13.4	<40	67	I
10303–5746	285.3477	0.0022	−41.59	6.88	1	A	2.3	−5.2	1.3	2.7	<10	C	
			−41.30	6.73	9	B	0.4						
			−41.28	6.90	1	C	−6.4						
			−41.40	6.91	1	D	−7.6						
10460–5811	287.3711	0.6447	−0.28	−1.83	4	A	−1.3			<1	<15		
			−0.27	−1.85	140	B	−2.0						
			−0.25	−1.82	24	C	−2.6						
10555–6242	290.4085	−2.9128	5.08	−8.79	2.4		−16.2			<1	<12		
11097–6102	291.2740	−0.7124	−22.45	−15.52	2.5	A	−26.9	−9.5	10.5	380	430	I	
			5.67	12.94	2.0	B	−28.4						
			5.63	12.83	90	C	−29.4						
			5.67	12.84	180	D	−29.9						
			5.67	12.92	55	E	−30.6						
11298–6155	293.8280	−0.7453	2.86	−1.94	3.6		36.7	2.8	3.2	12	14	I	
11304–6206	293.9497	−0.8929						3.2	−8.0	52	50	P	
11332–6258	294.5116	−1.6235	2.12	8.64	1.2	A	−9.1			<1	<10		
			1.85	8.58	8.9	B	−10.4						
			2.03	8.40	3.3	C	−11.2						
			1.95	8.38	5.6	D	−12.0						
			2.10	8.31	1.6	E	−13.4						
11368–6312	294.9728	−1.7296	68.57	20.84	30		−12.5	−0.3	7.5	1	<11	C	
12015–6305	297.6584	−0.9755						6.0	11.9	20	19	U	
12091–6129	298.2623	0.7400	−1.06	−2.64	11		−30.2			<1	<14		
12146–6212	299.0125	0.1308	0.84	−9.7	6		18.2			<1	<9		
12272–6240	300.5048	−0.1781	−2.76	7.76	2.3	A	8.2			<1	<10		
			−2.67	7.74	4.0	B	7.4						
12320–6122	300.9687	1.1520	−0.92	−16.60	3.1		−37.4	−1.1	−16.3	130	150	C	
12326–6245	301.1345	−0.2249						6.9	−3.5	210	190	U	
								7.3	4.3	170	230	U	
12405–6238	302.0324	−0.0620	−0.05	2.00	9	A	−34.9	−0.9	4.9	100	100	C	
			−0.26	1.87	3.9	B	−35.8						
			−0.05	4.32	0.8	C	−39.9						

Table 2 – continued

IRAS name	Galactic coordinates ^a <i>l</i>	<i>b</i>	Methanol Maser					Radio Continuum					
			IRAS			Offset (arcsec)	Peak flux density (Jy beam ⁻¹)	Radial velocity (km s ⁻¹)	RA	Dec.	Offset (arcsec)	Peak flux density ^b (mJy beam ⁻¹)	
			RA	Dec.								Morph Type ^c	
13080–6229	305.1937	0.0355	27.20	−57.77	24	A	−32.6	7.2	−9.3	90	160	C	
			27.24	−57.75	37	B	−33.4						
			27.59	−58.43	5	C	−37.2						
			29.01	−108.71	1	D	−42.9						
13092–6218	305.3526	0.1975	53.26	−44.55	0.4	A	−34.0	18.1	47.3	<100	77	U	
			47.29	−167.60	2.9	B	−36.6						
13111–6228	305.5532	0.0146						33.7	−5.2	7	<10	C	
								−100.1	−84.8	4	<10	U	
13134–6242	305.7982	−0.2482						−1.8	24.0	2	<10	U	
13291–6249	307.5596	−0.5864						4.3	−1.6	50	60	C	
13471–6120	309.9196	0.4791	3.64	−1.52	0.7	A	−54.5	4.2	−1.1	350	310	U	
			3.79	−0.65	110	B	−58.1						
			3.89	−0.72	270	C	−58.6						
			3.90	−0.79	640	D	−59.9						
			3.66	−1.07	80	E	−61.0						
			3.55	−0.97	80	F	−61.9						
			3.62	−1.18	180	G	−62.5						
			3.87	−1.38	75	H	−63.0						
			−0.08	−1.59	0.5	A	34.0		−0.1	1.3	150	160	P
			0.22	−1.53	4.0	B	32.4						
14050–6056	312.1086	0.3092	48.98	−164.28	15	A	−50.1	−0.4	−0.6	70	100	I	
			48.96	−164.43	6.5	B	−51.1						
			48.88	−164.00	1.7	C	−51.8						
			48.92	−164.24	1.7	D	−53.3						
14095–6102	312.5965	0.0474	3.86	−10.92	0.4	A	−60.0	1.5	−0.6	7	7	C	
			8.58	−6.21	2.9	B	−64.5						
			7.88	−6.45	11.6	C	−68.1						
14159–6038	313.4585	0.1926	39.86	4.37	0.4	A	−5.6	−2.8	−1.2	40	50	I	
			38.64	4.81	2.0	B	−7.5					U	
			38.58	4.85	3.4	C	−9.0						
			38.61	4.81	16	D	−9.5						
			38.60	4.78	8.2	E	−11.7						
			38.62	4.83	2.7	F	−12.3						
			33.85	11.40	7	A	−41.4				<1	<8	
			33.86	11.41	6	B	−42.9						
			33.85	11.38	4	C	−45.5						
			11.94	4.16	8	D	−53.3						
14212–6131	313.7634	−0.8624	11.91	4.20	18	E	−54.1	<1	<1	<8	<11		
			11.92	4.22	40	F	−54.8						
			11.86	4.26	6	G	−56.6						
			−32.20	3.16	1	A	7.4						
			−32.22	3.23	3	B	6.7						
			−32.18	3.21	10	C	5.7						
			−32.19	3.27	3	D	4.5						
			−32.21	3.24	6	E	4.2						
			−32.22	3.24	111	F	3.4						
			−32.21	3.24	20	G	3.0						
			−32.16	3.26	3	H	1.6						
			64.14	−20.78	3	J	0.5						
			64.46	−20.77	11	K	−0.2						
14394–6004	316.3675	−0.3664	64.28	−20.81	40	L	−0.9	<1	<1	<8	<11		
			64.28	−20.71	1	M	−2.5						
			64.54	−20.77	6	N	−3.2						
			64.49	−20.76	6	O	−4.5						
			64.31	−20.82	7	P	−5.1						
			67.83	−29.93	4	Q	−5.8						

Table 2 – continued

IRAS name	IRAS		Methanol Maser					Radio Continuum				
	Galactic coordinates ^a		Offset (arcsec)	Peak flux density (Jy beam ⁻¹)	Radial velocity (km s ⁻¹)	RA	Dec.	Offset (arcsec)	Peak flux density ^b (mJy beam ⁻¹)	8.64 GHz	6.67 GHz	Morph Type ^c
	<i>l</i>	<i>b</i>										
14404–5942	316.6396	−0.0838	6.72	−8.72	3	A	−16.3			<1		<9
			6.79	−8.74	5	B	−17.3					
			6.82	−8.76	14	C	−18.1					
			6.83	−8.75	109	D	−20.0					
			6.73	−8.74	22	E	−22.5					
			6.66	−8.44	2	F	−23.7					
			6.76	−8.66	1	G	−24.2					
14416–5937	316.8095	−0.0698	−14.18	42.57	3.1	A	−42.2	−43.7	21.2	<24	40	I
			−14.19	42.41	0.9	B	−44.9					
			−14.18	42.57	3.1	D	−46.9					
			−14.18	42.63	0.7	E	−48.1					
14567–5846	318.9174	−0.1681	144.86	−37.67	6	A	−32.0	−17.4	−7.6	120	130	C
			144.85	−37.64	41	B	−33.1					
			144.84	−37.41	27	C	−33.8					
			144.86	−37.47	685	D	−34.8					
			144.87	−37.49	55	E	−36.4					
			144.85	−37.27	66	F	−37.0					
			144.84	−37.10	47	G	−37.5					
14594–5824	319.3959	−0.0093	144.76	−37.21	10	H	−38.2					
								18.0	−4.8	57	48	D/C
15061–5814	320.2522	−0.2964	−87.21	1.27	1.1	A	−58.6	−81.4	6.2	130	130	C
			−87.21	1.28	5.6	B	−59.5					
			−87.42	1.28	5.6	C	−60.9					
			−87.32	1.27	14	D	−61.5					
			−87.21	1.27	17	E	−62.0					
			−87.10	1.27	26	F	−62.5					
			−86.99	1.37	3.9	G	−63.5					
			−87.22	1.46	1.7	H	−69.7					
			−87.16	1.35	1.0	J	−70.5					
15061–5828	320.1242	−0.5009	1.94	−8.59	3.0	A	−10.4			<1		<11
			1.98	−8.74	1.7	B	−11.0					
15122–5801	321.0571	−0.5204	−145.31	68.34	3	A	−55.0			<1		<10
			−145.25	68.36	3	B	−55.7					
			−145.32	68.35	3	C	−56.0					
			−145.30	68.35	8	D	−58.0					
			−145.33	68.34	5	E	−58.6					
			−152.24	57.70	3	F	−59.1					
			−152.23	57.72	3	G	−60.0					
			−145.31	68.33	94	H	−61.1					
			−145.48	68.34	39	J	−61.6					
			−145.46	68.34	49	K	−62.3					
			−152.23	58.03	3	L	−64.2					
			−152.23	58.16	17	M	−65.8					
			−152.23	58.11	17	N	−66.6					
			−152.23	58.10	6	O	−67.1					
			−145.38	68.34	3	P	−68.8					
15254–5621	323.4592	−0.0793	−2.17	0.94	12.9		−67.1	−1.8	1.6	270	240	U
			16.77	−23.80	200	A	−47.7			<1		<20
15278–5620	323.7400	−0.2544	16.77	−23.80	400	B	−48.2					
			16.77	−23.80	650	C	−48.8					
			16.77	−23.80	550	D	−49.7					
			16.77	−23.80	1750	E	−50.6					
			16.77	−23.80	2550	F	−51.2					
			16.69	−23.80	100	G	−52.1					
			16.69	−23.80	60	H	−52.5					
			16.90	−23.78	60	J	−52.8					
			16.84	−23.67	60	K	−53.3					
			17.10	−23.26	6	L	−56.3					
			20.18	−24.76	3	M	−57.4					

Table 2 – *continued*

IRAS name	IRAS		Methanol Maser					Radio Continuum				
	Galactic coordinates ^a		Offset (arcsec)	Peak flux density (Jy beam ⁻¹)	Radial velocity (km s ⁻¹)	RA	Dec.	Offset (arcsec)	Peak flux density ^b (mJy beam ⁻¹)	8.64 GHz	6.67 GHz	Morph Type ^c
	<i>l</i>	<i>b</i>										
15360–5554	324.9222	−0.5645	10.33	−6.37	0.7	−78.6	11.4	−6.7	80	80	C	
15408–5356	326.6551	0.5919	−84.24	25.21	0.4	A	−36.2	−40.6	−33.9	43	<58	I (a)
			−84.24	25.26	7.6	B	−40.9	33.5	56.0	33	<58	I (b)
			−84.26	25.23	11.5	C	−43.3					
15437–5343	327.1197	0.5117	1.39	−1.88	4	A	−83.8	−0.6	64.8	12	<13	U
			1.54	−2.36	1	B	−85.1					
			1.68	−2.39	70	C	−87.3					
			1.75	−2.48	8.5	D	−89.2					
			1.64	−2.52	13	E	−89.7					
15520–5234	328.8078	0.6322	−0.71	4.09	170	A	−44.0	−1.4	3.3	220	200	D/C
			−1.25	4.10	188	B	−44.6					
			−0.49	4.11	59	C	−45.5					
			−1.25	3.96	120	D	−46.4					
15539–5353	328.1911	−0.5710	68.85	170.57	4	A	−33.3			<2	<11	
			68.93	170.92	14	B	−35.2					
			68.98	170.99	54	C	−36.6					
			82.45	253.37	568	D	−37.7					
			82.45	253.43	238	E	−38.1					
			82.45	253.41	96	F	−38.8					
			69.67	170.97	132	G	−43.4					
			69.46	171.01	280	H	−44.5					
			69.48	171.03	470	J	−45.0					
			69.50	171.13	78	K	−45.6					
			83.26	253.74	25	L	−49.0					
			83.21	253.52	82	M	−49.7					
15557–5215	329.4566	0.5057	3.75	52.09	0.3	A	−61.2			<1	<10	
			41.43	20.24	0.3	B	−65.6					
			41.59	20.80	3.1	C	−70.7					
			41.41	20.69	8.3	D	−72.1					
			41.75	20.71	2.2	E	−72.7					
			41.65	20.64	2.0	F	−73.1					
15567–5236	329.3375	0.1473	1.74	6.06	9.3		−106.7	3.8	−0.4	<20	270	C
15596–5301	329.4036	−0.4576	−9.70	−34.90	1	A	−63.8			<2	<10	
			−5.27	−31.34	139	B	−66.9					
			−9.76	−34.84	52	C	−67.5					
			−9.76	−34.84	18	D	−68.4					
			−9.24	−34.76	1	E	−69.3					
			−9.49	−35.03	41	F	−70.7					
			−9.69	−35.00	1	G	−71.8					
			−5.26	−31.04	1	H	−73.1					
16060–5146	330.9489	−0.1739	30.42	−12.48	5.5		−87.8	32.4	−9.4	280	290	I
16065–5158	330.8826	−0.3694						37.1	660.0	28*	<100	I (a)
								−57.0	588.2	<100	68*	C (b)
16071–5142	331.1260	−0.2393	26.87	2.24	16	A	−84.5	22.9	1.8	21	17	C
			26.80	2.27	9	B	−85.2					
			26.76	2.31	5	C	−85.8					
16076–5134	331.2754	−0.1882	7.21	7.14	179	A	−78.3			<5	<9	
			7.22	7.14	59	B	−79.0					
			7.12	7.16	22	C	−80.5					
			7.15	7.16	23	D	−81.0					
			7.17	7.13	55	E	−81.8					
			7.15	7.04	13	F	−82.7					
			7.24	7.10	32	G	−83.4					
			7.18	7.17	5	H	−84.4					
			7.13	7.16	6	J	−84.7					
			7.13	7.17	38	K	−85.2					
16085–5138	331.3331	−0.3389	41.22	2.33	1	A	−65.0			<4	<14	
			41.07	2.29	51	B	−65.5					
			41.25	2.41	45	C	−66.6					
			−91.80	125.58	93	D	−67.0					

Table 2 – continued

IRAS name	IRAS		Methanol Maser					Radio Continuum					
	Galactic coordinates ^a		Offset (arcsec)	Peak flux density (Jy beam ⁻¹)	Radial velocity (km s ⁻¹)	RA	Dec.	Offset (arcsec)	Peak flux density ^b (mJy beam ⁻¹)	8.64 GHz	6.67 GHz	Morph Type ^c	
	<i>l</i>	<i>b</i>											
16128–5109	332.1533	−0.4447	−214.30	−86.60	6.3	A	−58.7	10.6	−8.9	<100	120	U	
			−214.26	−86.45	1.5	B	−60.0						
			−214.24	−86.46	7.6	C	−61.5						
16132–5039	332.5413	−0.1284	124.47	−74.16	0.7	A	−51.0	<2	<10	<10	<10	U	
			96.74	−3.33	3.3	B	−55.9						
16158–5055	332.6529	−0.6115	208.91	160.47	1.7	A	−47.2	<6	<27	<27	<27	U	
			25.15	−23.87	3.5	B	−50.7						
16159–5012	333.1681	−0.1036	20.72	−33.88	1.0	A	−43.9	−23.2	−4.4	4	12	U	
16172–5028	333.1286	−0.4292		26.66	−28.26	1.9	B						
				−7.30	−30.85	1.9	C						
				−7.52	−30.84	9.0	D						
				−7.58	−30.84	8.4	E						
				−109.64	−199.15	8.8	F						
				−0.60	−12.81	9	A						
				−0.48	−12.98	1	B						
				−0.62	−12.91	7	C						
16175–5002	333.4686	−0.1619		−0.63	−12.89	45	D						
				−0.79	−12.87	1.4	E						
				−0.73	−12.87	1.0	F						
16177–5018	333.3061	−0.3645						−5.4	−147.8	<100	290	U	
16272–4837	335.5824	−0.2841	7.89	6.20	8	A	−44.5	180.3	−109.2	<100	190	U	
				22.82	−7.80	1.5	B						
				22.85	−7.66	102	C						
				7.79	5.96	5	D						
				7.77	6.12	29	E						
				7.82	6.06	2	F						
				21.56	−5.05	17	G						
				21.53	−5.02	40	H						
				21.45	−4.87	1	J						
				21.37	−5.04	8	K						
				21.22	−4.94	11	L						
				21.33	−4.83	1	M						
				−5.22	−124.39	9	N						
				−5.23	−124.33	14	O						
				−5.20	−124.45	5	P						
				−5.16	−124.62	19	Q						
				−5.20	−8.83	15	A						
				−5.03	−8.62	3	B						
				−4.91	−8.29	3	C						
16297–4757	336.3610	−0.1367		−5.02	−8.22	3	D						
				−5.04	−8.44	6	E						
				−70.17	26.27	3	A	−74.3	114.4	32.3	25	26	
				−70.36	26.39	5	B	−74.9					
				−70.04	26.50	29	C	−76.4					
				−233.43	−28.62	13	D	−77.1					
				−233.37	−28.57	8	E	−77.5					
				−69.99	26.76	4	F	−78.0					
				−69.92	26.92	6	G	−79.6					
16313–4729	336.8721	−0.0144		−70.16	26.51	3	H	−81.7					
				13.70	−30.54	45	A	−39.8	7.5	18.2	6	<13	
				13.89	−30.75	10	B	−40.5					
				13.70	−30.74	50	C	−41.5					
				13.70	−30.82	35	D	−42.1					
				13.71	−30.86	40	E	−45.4					
				13.71	−30.46	10	F	−47.9					
				13.70	−30.56	15	G	−48.6					

Table 2 – continued

IRAS name	IRAS Galactic coordinates ^a <i>l</i> <i>b</i>		Methanol Maser					Radio Continuum				
			Offset (arcsec)	Peak flux density (Jy beam ⁻¹)	Radial velocity (km s ⁻¹)	RA	Dec.	RA	Dec.	Peak flux density ^b (mJy beam ⁻¹) 8.64 GHz 6.67 GHz	Morph Type ^c	
	<i>l</i>	<i>b</i>	RA	Dec.	(km s ⁻¹)							
16318–4724	336.9927	-0.0227	13.70	-30.52	20	H	-52.1					
			13.71	-30.37	307	J	-53.4					
			13.61	-30.62	151	K	-54.0					
16330–4725	337.1210	-0.1736	14.79	-8.06	20		-126.0	-1.7	-10.1	9	16	I
16344–4658	337.6156	-0.0606	35.30	-176.22	2.3		-77.5	2.9	5.8	41	52	U
			-9.80	-6.00	15	A	-42.0			<4	<13	
			-9.86	-6.01	15	B	-42.4					
			-9.84	-5.97	17	C	-43.2					
			-9.87	-5.90	8	D	-43.8					
			-10.55	-5.63	2	E	-48.0					
			-10.59	-5.54	3	F	-48.7					
			88.13	0.48	11	G	-57.1					
			88.03	0.51	2.7	H	-61.3					
			88.00	0.48	7	J	-62.1					
16348–4654	337.7034	-0.0519	8.49	1.86	8	A	-44.2	8.1	2.7	84	57	C
			7.83	2.60	16	B	-49.3					
			7.68	2.64	75	C	-50.5					
			7.65	2.49	25	D	-51.2					
			7.63	2.79	58	E	-52.9					
			7.65	2.73	36	F	-53.4					
			7.69	2.86	117	G	-54.8					
			7.73	2.16	4	H	-55.4					
			7.69	2.14	3.5	J	-55.7					
16351–4722	337.4027	-0.4004	8.43	1.02	77	A	-39.9	7.8	-1.3	28	57	I (a)
			8.05	0.13	3	B	-41.7	53.6	11.3	20	<15	P (b)
16359–4635	338.0696	0.0176	35.70	3.42	1	A	-38.2	28.1	2.1	160	170	C
			35.66	3.44	0.5	B	-39.2					
			16.72	-8.51	0.8	C	-40.1					
			35.70	3.40	0.5	D	-41.9					
			27.70	8.87	7.9	E	-44.1					
			27.77	8.56	12	F	-53.2					
16371–4617	338.4383	0.0571	-16.31	-15.91	1.5	A	-29.1	-11.8	-0.7	45	44	I
			-16.31	-15.86	30	B	-30.4					
			-16.32	-15.87	1.6	C	-32.0					
			-16.29	-15.83	1.5	D	-33.0					
16374–4701	337.9171	-0.4656	-18.12	30.85	2	A	-36.5	2.9	47.0	100	96	C
			-18.16	30.71	24	B	-38.0					
			-18.00	30.55	24	C	-38.9					
16376–4542	338.9256	0.3856						-16.7	-30.8	44	74	P
16381–4629	338.4049	-0.2034	243.74	42.42	47	A	-50.1	-3.0	1.1	31	40	U
			243.71	42.42	90	B	-50.7					
			243.74	42.43	44	C	-51.8					
			243.74	42.44	61	D	-52.1					
			243.75	42.45	18	E	-53.2					
			243.75	42.38	3	F	-54.9					
16387–4612	338.6828	-0.0862						-9.3	0.5	15	15	D
16421–4532	339.5634	-0.0909	143.41	-32.14	1.4	A	-30.3			<1	<9	
			143.33	-32.34	1.6	B	-30.6					
			143.28	-32.30	6.5	C	-31.5					
16424–4531	339.6225	-0.1227	-7.15	3.77	38	A	-32.5			<1	<10	
			-7.13	3.78	98	B	-33.1					
			-7.14	3.86	55	C	-33.7					
			-6.83	3.14	27	D	-34.9					
			-6.98	3.18	69	E	-36.2					
			-6.99	3.22	42	F	-37.1					
			-6.86	3.54	47	G	-37.8					
16445–4516	340.0526	-0.2375	21.08	-8.76	35		-59.8	24.8	-3.9	71	79	C
16445–4459	340.2529	-0.0512						-23.5	0.9	23	22	C

Table 2 – continued

IRAS name	IRAS Galactic coordinates ^a		Methanol Maser					Radio Continuum				
			Offset (arcsec)	Peak flux density (Jy beam ⁻¹)	Radial velocity (km s ⁻¹)	RA	Dec.	RA	Dec.	Peak flux density ^b (mJy beam ⁻¹)	8.64 GHz	6.67 GHz
	<i>l</i>	<i>b</i>										
16455–4531	339.9724	−0.5314	36.53	4.84	3	A	−89.5	36.6	4.5	71	59	U
			−34.04	−82.04	10	B	−89.9					
			−34.11	−82.05	52	C	−91.2					
			−34.13	−81.99	8	D	−92.2					
			−34.30	−81.95	3	E	−94.2					
			−34.52	−81.88	21	F	−94.9					
			−34.35	−81.88	1	G	−95.8					
			−34.29	−81.88	35	H	−96.7					
			−34.37	−81.80	10	J	−97.4					
			−34.31	−81.87	39	K	−98.1					
			−34.19	−81.86	2	L	−99.1					
			−34.30	−81.88	1	M	−99.6					
			−34.27	−81.93	16	N	−100.7					
			−34.24	−81.91	15	O	−101.8					
			−34.25	−81.95	1	P	−102.5					
			−34.26	−81.94	9	Q	−103.0					
			−34.23	−81.88	10	R	−103.7					
16450–4517	340.1006	−0.3152	−224.26	−131.11	23		−59.8			<1	<10	
16474–4610	339.6833	−1.2070	−3.30	−10.34	60	A	−21.6			<1	<10	
			−3.31	−10.29	12	B	−22.4					
			−3.29	−5.20	6	C	−34.1					
			−3.31	−9.97	8.5	D	−38.5					
16484–4603	339.8865	−1.2611	−12.28	−1.12	12	A	−30.4	−12.2	−1.2	4	<8	C
			−12.30	−1.25	49	B	−31.8					
			−12.45	−1.26	30	C	−32.6					
			−12.56	−1.18	100	D	−33.2					
			−12.61	−1.22	370	E	−34.1					
			−12.47	−1.26	430	F	−34.8					
			−12.43	−1.28	890	G	−35.4					
			−12.10	−1.63	250	H	−35.9					
			−12.31	−1.58	620	J	−36.8					
			−12.20	−1.61	410	K	−37.6					
			−11.96	−1.76	490	L	−38.5					
			−12.07	−1.72	1320	M	−38.8					
16506–4512	340.7869	−1.0200					11.0	8.4	29	41	P	
16513–4316A	342.3634	0.1031	−93.87	96.20	0.7	A	−3.6	−8.4	102.7	4	<7	I
			−93.94	96.17	0.4	B	−5.1					
			−93.81	96.17	0.7	C	−6.2					
16533–4009	345.0098	1.7901	−15.88	21.75	8	A	−11.0	−6.7	4.3	140	150	U
			−15.84	21.64	10	B	−12.1					
			−15.75	21.43	24	C	−13.0					
			−16.43	22.16	0.7	D	−14.2					
			−15.72	21.66	8	E	−15.8					
			−7.38	4.58	3	F	−16.2					
			−7.30	4.58	48	G	−17.0					
			−7.41	4.50	75	H	−17.6					
			−7.36	4.54	375	J	−18.1					
			−7.30	4.60	16	K	−19.5					
			−7.30	4.49	28	L	−19.8					
			−7.23	4.58	71	M	−20.5					
			−7.22	4.62	175	N	−22.0					
			−7.23	4.55	147	O	−22.7					
			−7.11	4.57	5	P	−23.5					
			−7.20	4.61	13	Q	−23.9					
16547–4247	343.1262	−0.0620					3.8	0.1	5	<7	U	
16561–4006	345.3930	1.3991					−17.7	−60.2	5	<14	U	
16566–4204	343.9107	0.1134	8.85	78.88	9	A	14.3	8.8	78.8	24	<7	U
			8.88	78.89	3	B	13.5					
			8.86	78.94	8	C	12.1					
			8.89	78.90	5	D	11.2					

Table 2 – continued

IRAS name	IRAS		Methanol Maser					Radio Continuum						
	Galactic coordinates ^a	<i>l</i>	<i>b</i>	Offset	Peak flux	Radial	Offset	Peak flux density ^b	Morph	Type ^c				
				(arcsec)	density (Jy beam ⁻¹)	velocity (km s ⁻¹)	RA	Dec.	8.64 GHz	6.67 GHz				
16586–4142	344.4245	0.0451		−7.23 −7.14	−8.24 3	10 B	−71.6 −72.3	−2.1	5.8	82	120	I		
16594–4137	344.5832	−0.0252		−8.63	−1.68	1.7	1.5	−7.5	−1.3	6	<11	U		
17006–4215	344.2204	−0.5931		−55.13	74.07	113	A −54.97 −55.17 −54.11 −54.83 −54.75 −54.03 −54.47 −54.74 −54.72	−19.9 74.26 74.08 73.55 74.00 73.82 73.28 73.84 73.95 73.95	−20.7 9 C D 1.7 F G H J K	2.0	0.6	140	140	I
17008–4040	345.4990	0.3536		28.40 28.54 27.19 27.38 27.43 27.51 27.21 27.30 27.19 27.20	4.47 3.89 3.99 3.91 3.71 3.96 3.94 3.38 3.61 3.69	170 150 215 120 250 150 65 70 5 3	A B C D E F G H J K	−14.4 −14.7 −15.8 −16.8 −18.0 −18.7 −19.3 −19.8 −21.3 −22.3	85.7	−116.6	200	220	C	
17016–4124	345.0014	−0.2204		12.26 12.25 12.21 12.23 12.17 15.48 15.96 15.90 16.21 15.97 15.72 16.08 16.08 12.71 15.74 12.65	−2.41 −2.38 −2.33 −2.36 −2.48 −3.15 −3.10 −3.08 −2.95 −3.07 −3.31 −3.19 −3.24 −2.46 −3.39 −2.37	9 120 250 75 22 74 36 13 10 11 14 7 6 8 1.2 1.1	A B C D E F G H J K L M N O P Q	−21.6 −22.3 −22.6 −23.1 −23.9 −26.7 −26.8 −27.4 −27.7 −28.1 −28.4 −29.2 −30.0 −30.5 −31.3 −32.0	15.7	−2.4	200	160	C	
17028–4050	345.5888	−0.0496						−155.7	108.1	20	<30	P		
17031–4037	345.8037	0.0467		69.14	95.14	1.9	−10.5	−3.4	4.3	12	13	P		
17052–4001	346.5244	0.0808						−15.0	1.6	45	71	C		
17059–4132	345.3995	−0.9413		81.46	51.47	0.6	−14.0	46.1	0.8	300	280	U		
17079–3905	347.5903	0.2178		109.64 109.75 107.51 114.74 1.18 1.18 1.18	104.85 104.93 105.67 107.89 −31.29 −31.15 −31.53	10.4 1.5 4.5 0.7 0.6 1.2 1.2	A B C D E F G	−92.0 −93.3 −96.7 −97.8 −101.7 −102.2 −102.8	−78.2	92.8	10	<16	I	
17096–3856	347.9043	0.0437		−27.05 −27.04 −14.02 −26.94 −13.99 −14.01	11.89 11.90 −173.33 11.94 −173.32 −173.34	2.5 3.2 6.1 0.5 1.2 1.9	A B C D E F	−27.3 −27.7 −29.4 −30.3 −34.0 −35.3	15.7	−161.5	110	140	C	
17130–3756	349.0921	0.0918		−39.18 −39.55 −41.01 −41.01	26.42 26.65 27.80 27.73	31 2 3 3	A B C D	−76.7 −77.7 −80.5 −81.7	−38.8	84.0	8	<16	I	

Table 2 – continued

IRAS name	IRAS		Methanol Maser					Radio Continuum				
	Galactic coordinates ^a		Offset (arcsec)	Peak flux density (Jy beam ⁻¹)	Radial velocity (km s ⁻¹)	RA	Dec.	Offset (arcsec)	Peak flux density ^b (mJy beam ⁻¹)	8.64 GHz	6.67 GHz	Morph Type ^c
	<i>l</i>	<i>b</i>										
17136–3617	350.5037	0.9562						2.7	−1.0	290	290	C
17136–3816	348.8962	−0.1870	−29.63	0.56	1.0		1.3	−30.9	2.0	52	37	I
17143–3700	350.0146	0.4332	2.37	2.27	1.3	A	−31.0	2.3	1.9	81	98	P
			2.46	2.25	1.4	B	−31.8					
			2.63	1.06	0.9	C	−36.3					
17160–3707	350.1027	0.0853	10.69	1.44	4	A	−62.4	113.7	−1.3	76	<47	U
			10.55	1.40	5	B	−64.5					
			10.52	1.80	2.9	C	−65.5					
			10.46	1.50	7	D	−66.6					
			6.66	1.05	1	E	−68.0					
			10.27	1.32	18	F	−74.1					
17165–3554	351.1594	0.6999	21.19	3.06	1.6	A	−2.9	41.5	9.2	6	<65	I
			28.18	9.06	9.4	B	−5.4					
			11.69	−4.45	4.1	C	−6.3					
			0.39	−2.17	1.0	D	−10.6					
17166–3656	350.3334	0.0945	−153.09	−45.13	22	A	−62.2	−19.3	2.4	38	12	C
			−153.08	−45.14	9.4	B	−64.0					
			−43.30	74.47	11.1	C	−65.7					
			−152.97	−45.07	1.4	D	−66.9					
17167–3854	348.7267	−1.0479	−60.20	−58.22	68	A	−3.5	−119.5	−42.1	500	400	C
			−60.19	−58.24	20	B	−4.2					
			−60.14	−58.25	11	C	−5.1					
			−60.20	−58.24	14	D	−5.6					
			−60.17	−58.28	23	E	−6.6					
			−30.94	24.48	53	F	−7.5					
			−30.94	24.47	47	G	−8.1					
			−60.15	−58.28	53	H	−9.1					
			−60.08	−58.31	43	J	−10.5					
			−60.08	−58.31	14	K	−11.2					
			−30.93	24.28	4	L	−11.8					
			−60.16	−58.24	2	M	−12.3					
			−60.30	−57.86	7	N	−15.6					
			−60.22	−58.01	1	O	−16.2					
			−60.20	−58.19	2	P	−17.0					
17175–3544	351.4193	0.6412	−1.47	113.63	1	A	0.3	−15.2	0.4	530	620	C
			−1.51	113.61	2	B	−1.0					
			−1.51	113.57	26	C	−2.7					
			−1.51	113.87	3	D	−5.4					
			−1.62	113.78	4	E	−6.2					
			−15.93	−1.32	120	F	−6.7					
			−16.11	−1.24	120	G	−7.5					
			−19.48	3.46	45	H	−8.0					
			−16.18	0.22	40	J	−8.4					
			−16.02	0.49	80	K	−8.7					
			−1.56	113.76	80	L1	−9.4					
			−19.37	3.12	84	L2	−9.4					
			−16.73	0.61	3000	M	−10.7					
			−19.09	3.04	2000	N	−11.4					
17220–3609	351.5833	−0.3499	6.01	−10.89	4	A	−91.2	5.5	−11.7	340	280	U
			5.21	−12.36	28	B	−94.4					
			5.18	−11.95	12	C	−95.6					
			5.79	−11.09	0.4	D	−98.2					
			6.45	−11.47	0.5	E	−99.5					
17233–3606	351.7757	−0.5428	−21.17	9.56	200	A	1.6	−8.5	11.5	50	66	C
			−21.13	9.62	200	B	1.0					
			−21.13	9.50	0.9	C	−0.3					
			−21.13	9.49	1.0	D	−0.6					
			−21.11	9.65	0.6	E	−2.5					

Table 2 – *continued*

IRAS name	IRAS		Methanol Maser					Radio Continuum				
	Galactic coordinates ^a		Offset (arcsec)	Peak flux density (Jy beam ⁻¹)	Radial velocity (km s ⁻¹)	RA	Dec.	Offset (arcsec)	Peak flux density ^b (mJy beam ⁻¹)	8.64 GHz	6.67 GHz	Morph Type ^c
	<i>l</i>	<i>b</i>										
17238–3516	352.5211	−0.1550						−7.9	−11.6	8	<14	U
								44.1	−139.0	10	<14	U
17258–3637	351.6328	−1.2525						0.4	2.2	430	650	I
17271–3439	353.4162	−0.3670	−33.40	−5.01	64	A	−20.3	−34.0	−4.9	200	160	C
			−33.41	−5.01	41	B	−21.0					
			−33.40	−4.97	20	C	−21.5					
			−33.43	−4.92	6	D	−21.8					
			−33.40	−4.85	11	E	−22.4					
17278–3541	352.6298	−1.0670	18.27	−37.20	5	A	6.6			<1	<9	
			17.98	−37.36	30	B	5.4					
			17.87	−37.19	6	C	−1.7					
			0.88	1.66	168	D	−3.0					
			0.91	1.67	40	E	−3.7					
			0.99	1.67	4	F	−4.5					
			0.79	1.80	6	G	−7.0					
17279–3311	354.7218	0.3034	15.04	0.77	16	A	93.7	15.4	1.3	150	180	C
			15.03	0.84	6	B	92.5					
			15.06	0.83	1	C	91.8					
			−718.30	13.27	0.7*	D	−17.0					
			−718.10	13.33	1.1*	E	−23.2					
			−718.02	13.40	2.1*	F	−24.5					
17302–3245	355.3456	0.1449	−10.34	−0.75	8	A	19.8	−11.1	0.3	110	110	C
			−12.26	8.83	10.2	B	9.8					
			−12.32	8.87	1.0	C	8.9					
17402–2938	359.1372	0.0304	−3.09	2.95	1	A	−1.2			<1	<9	
			−2.87	2.85	2	B	−1.7					
			−2.96	3.04	3	C	−2.0					
			−3.09	3.07	4	D	−2.5					
			−3.13	3.01	4	E	−3.0					
			−2.94	3.05	3	F	−3.7					
			−2.89	2.93	13	G	−4.0					
17403–3032	358.3812	−0.4761	−44.54	−17.76	0.4	A	12.8	30.9	4.3	100	100	U
			−44.50	−17.76	0.7	B	10.1					
			−44.55	−17.33	4	C	2.0					
			−44.68	−17.32	9	D	1.4					
			−44.64	−17.29	24	E	0.8					
			31.25	2.27	2.0	F	−6.2					
17429–2823	0.4955	0.1833	−12.58	12.41	10	A	0.8	66.9	93.2	63	69	I
			−12.57	12.41	6	B	−0.6					
			−12.57	12.46	5	C	−1.1					
			−12.65	12.47	5	D	−2.5					
			−12.59	12.49	4	E	−3.7					
			−12.51	12.41	0.4	F	−4.3					
			−12.59	12.40	0.9	G	−5.1					
			−12.58	12.39	1.0	H	−7.0					
			−12.57	12.54	1.5	J	−7.6					
			−12.54	12.30	1.6	K	−8.0					
			−12.67	14.27	1.0	L	−9.0					
			−12.66	14.21	1.6	M	−10.0					
			−12.59	12.29	0.5	N	−11.2					
17430–2844	0.2201	−0.0088	−39.34	−9.68	2.6	A	49.4	−43.8	−21.8	5	<15	P
			−39.34	−9.64	1.6	B	42.1					
17432–2835	0.3811	0.0174						−2.4	47.9	17	<10	I
17436–2807	0.8118	0.1781	24.68	85.06	6.7	A	3.5			<2	<10	
			24.62	85.02	0.6	B	2.4					
17439–2845	0.3138	−0.1995	7.38	2.94	2	A	26.5	14.1	−9.6	14	8	U
			6.98	2.05	20	B	19.2	12.2	2.2	9	<8	U
			6.94	2.07	26	C	18.0					

Table 2 – continued

IRAS name	Galactic coordinates ^a <i>l</i>	<i>b</i>	Methanol Maser				Radio Continuum					
			IRAS			Offset (arcsec)		Peak flux density (Jy beam ⁻¹)	Radial velocity (km s ⁻¹)	Offset (arcsec)		Peak flux density ^b (mJy beam ⁻¹)
			RA	Dec.	(Jy beam ⁻¹)	RA	Dec.	8.64 GHz	6.67 GHz	Morph Type ^c		
17441–2822	0.6652	−0.0338	6.94	2.10	5	D	17.3					
			6.87	2.03	7	E	16.4					
			6.88	2.02	12	F	15.1					
			6.84	2.03	5	G	14.6					
			−4.75	51.92	0.3	A	76.2	11.4	2.0	520	490	C (a)
			−4.37	52.27	3	B	73.2	28.0	−25.7	260	<110	C (b)
			−12.73	12.50	33	C	72.2	40.7	71.9	390	170	C (c)
			−12.73	12.50	8	D	71.5	−11.9	90.6	340	<110	I (d)
			−12.73	12.52	12	E	70.4	−67.3	−44.0	140	<110	U
			67.62	83.52	5	F	69.9					
			−12.42	12.40	14	G	69.0					
			67.72	83.56	31	H	68.5					
			67.69	83.52	5	J	67.8					
			67.68	83.53	3.6	K	66.9					
			67.73	83.58	4.8	L	66.5					
			67.69	83.52	1.2	M	65.1					
			5.66	−5.59	1.4	N	60.4					
			5.70	25.73	3.0	O	58.0					
			−12.52	−77.68	5	P	52.5					
			−12.48	−77.69	3	Q	51.8					
			−12.49	−77.61	3	R	51.5					
			32.05	−95.44	2	S	51.1					
17455–2800	1.1270	−0.1066	−12.54	−77.80	21	T	50.6					
			−12.61	−77.75	28	U	50.2					
			−12.62	−77.79	74	V	49.0					
			19.87	−71.10	30	W	47.9					
			91.11	27.52	4.6		−20.8	1.1	0.6	27	33	I
			−10.39	−28.20	19	A	19.3	−9.9	−31.0	70	93	I
			−10.36	−28.31	7	B	18.2					
			−10.46	−28.30	14	C	17.7					
			−10.70	−28.52	26	D	17.2					
			−10.42	−28.59	14	E	16.0					
17470–2853	0.5547	−0.8500	−10.25	−28.61	9	F	15.3					
			−10.30	−28.63	30	G	14.4					
			−10.32	−28.65	60	H	13.6					
			−10.50	−28.69	32	J	12.1					
			−10.59	−28.71	52	K	11.6					
			−10.68	−28.72	27	L	10.8					
			−12.85	−26.19	0.5	M	8.5					
			−341.37	−122.33	2.0*	A	18.0	4.5	3.7	39	37	C
			−341.44	−122.49	2.5*	B	6.1					
			−341.32	−122.58	9*	C	3.0					
17559–2420	5.4768	−0.2433					41.8	−26.5	14	<20	U	
17574–2403	5.8880	−0.3983	119.77	−17.28	0.8	A	10.1	−23.5	1.8	960	740	I
			119.79	−17.24	0.5	B	9.2					
17577–2320	6.5531	−0.0947	18.76	−67.38	1.1	A	13.2	6.4	11.0	14	27	I
			62.43	200.03	11	B	0.5					
17591–2228	7.4701	0.0605					9.5	−1.6	42	<15	I	
17599–2148	8.1390	0.2278	4.80	−4.96	5.0		20.0	16.3	−3.0	30	30	I
18006–2422	5.9807	−1.1909					93.6	−65.8	69	<27	I (a)	
							−149.0	−87.4	46	<27	C (b)	
18021–1950	10.0925	0.7502	116.79	−38.46	1.2		1.2	44.9	0.9	61	45	C
18032–2137	8.6612	−0.3421	120.07	22.65	11	A	44.0	58.0	1.1	390	380	C
			119.97	22.78	166	B	42.8					
			119.89	22.67	23	C	41.4					
			119.88	22.66	24	D	40.9					
			57.33	1.31	8	E	39.0					
18032–2032	9.6152	0.1976	19.88	3.30	20	A	6.3	20.2	4.6	49	29	P
			19.84	3.38	75	B	5.5					

Table 2 – continued

IRAS name	Galactic coordinates ^a <i>l</i>	<i>b</i>	Methanol Maser				Radio Continuum							
			IRAS				Offset (arcsec)	Peak flux density (Jy beam ⁻¹)	Radial velocity (km s ⁻¹)	RA	Dec.	Offset (arcsec)	Peak flux density ^b (mJy beam ⁻¹)	Morph Type ^c
			RA	Dec.										
18048–2019	9.9937	−0.0299	16.23	15.45	100	C	3.0							
			16.23	15.45	250	D	1.9							
			16.22	15.49	4500	E	1.1							
			16.20	15.44	100	F	−0.2							
			16.15	15.50	30	G	−2.1							
			−20.85	−20.60	1	A	47.9	17.3	6.8	2	<10		U	
			−21.04	−20.65	35	B	47.0							
			−20.97	−20.57	6	C	46.3							
			−21.01	−20.61	28	D	43.0							
			−21.00	−20.63	16	E	41.9							
18056–1952	10.4662	0.0310	−20.99	−20.63	12	F	40.8							
			22.44	13.13	7	A	76.4	22.2	13.0	63	44	P (a)		
			22.46	13.21	9	B	76.0	−16.8	−6.3	42	45	C (b)		
			22.42	13.20	10	C	75.3							
			22.39	13.22	68	D	74.8							
			22.39	13.20	11	E	74.4							
			22.33	13.17	13	F	74.0							
			22.36	13.23	23	G	72.2							
			17.85	47.31	8	H	65.1							
			17.85	47.27	9	J	64.5							
			16.24	51.95	3	K	62.2							
			16.21	51.98	3	L	61.5							
			22.75	13.04	4	M	59.9							
			22.02	13.14	16	N	59.2							
			17.92	47.67	0.7	O	58.0							
18056–1954	10.4443	0.0070	79.68	−44.23	2	A	78.2			<10	<10			
			79.45	−44.47	26	B	73.2							
			79.48	−44.50	18	C	71.6							
			79.58	−44.45	6	D	70.4							
			79.55	−44.44	9	E	68.0							
18060–2005	10.3130	−0.1519	−41.85	−33.72	0.6	A	20.0	−36.3	−29.9	50	60	C		
			20.70	108.57	5	B	16.7							
			20.74	108.68	16	C	15.5							
			20.73	108.70	16	D	14.3							
			41.38	16.24	5	E	13.0							
			41.42	16.27	52	F	12.2							
			41.39	16.29	83	G	11.4							
			41.49	16.28	124	H	9.9							
			−128.88	−34.94	2.0	J	7.8							
			−128.89	−34.78	68	K	4.5							
			−128.93	−34.88	1.8	L	2.6							
			−128.88	−34.68	1.6	M	2.2							
18064–2020	10.1567	−0.3542						−30.3	15.0	46	<100	U		
								16.7	152.7	<40	110	I		
18067–1927	10.9622	0.0157	−27.69	−1.08	13	A	24.7	−27.0	−1.3	150	100	C		
			−27.70	−1.15	20	B	24.4							
18075–1956	10.6259	−0.3869	−6.54	6.30	1.1	A	5.9	−14.4	−2.2	740	610	C		
			−6.49	6.36	2.6	B	4.6							
			−6.56	6.44	1.0	C	3.7							
			−6.40	6.17	1.0	D	2.2							
			−165.19	103.42	1.6	E	−6.2							
			−165.03	103.03	4.1	F	−8.0							
18089–1732	12.8887	0.4898	1.85	−1.67	58	A	39.2			<1	<10			
			1.82	−1.64	15	B	38.7							
			1.90	−1.61	13	C	37.6							
			1.92	−1.71	6	D	36.6							
			2.01	−1.54	5	E	34.6							

Table 2 – continued

IRAS name	IRAS Galactic coordinates ^a <i>l</i> <i>b</i>		Methanol Maser					Radio Continuum				
			Offset (arcsec)	Peak flux density (Jy beam ⁻¹)	Radial velocity (km s ⁻¹)	RA	Dec.	RA	Dec.	Peak flux density ^b (mJy beam ⁻¹) 8.64 GHz 6.67 GHz	Morph Type ^c	
	<i>l</i>	<i>b</i>	RA	Dec.	(Jy beam ⁻¹)							
			2.92	-0.54	47	F	33.6					
			2.38	-0.62	2	G	32.7					
			1.98	-1.61	1.0	H	31.6					
			1.97	-1.67	0.8	J	30.0					
18090–1832	12.0254	-0.0315	-0.23	0.08	64		107.5	-185.7	-107.4	14	<15	I
18094–1840	11.9498	-0.1592	-53.39	-27.41	1.1	A	48.3	-136.4	-113.2	15	<17	D/C
			-53.40	-27.39	0.7	B	47.5					
			-136.29	-113.34	4.3	C	43.6					
			-136.27	-113.39	61	D	43.1					
			-136.26	-113.37	87	E	42.6					
			-136.34	-113.35	2.6	F	41.5					
			-136.41	-113.43	12	G	40.2					
18097–1825A	12.2161	-0.1142	-24.35	8.82	0.7	A	67.9	-52.7	-3.9	79	91	C
			-34.26	-124.70	0.9	B	29.7					
			-6.75	-54.79	1.9	C	26.2					
			-45.14	-30.58	1.5	D	20.5					
			-49.55	-0.90	11	E	19.7					
			-45.12	-30.77	1	F	17.0					
18098–1814	12.3718	-0.0329						147.0	156.3	13	<16	C
18099–1841	11.9922	-0.2752	-10.75	2.44	0.6		59.5			<1	<20	
18110–1854	11.9358	-0.6132	7.94	-3.37	6	A	43.4	10.6	-1.5	230	250	C
			7.97	-3.23	7.1	B	42.1					
			7.88	-3.42	6	C	41.1					
			7.97	-3.23	8	D	40.3					
			8.00	-3.21	23	E	39.6					
			7.98	-3.42	44	F	32.0					
			7.98	-3.50	2	G	30.2					
18117–1753	12.9068	-0.2589	-631.46	-577.56	1*	A	58.5			<1	<24	
			-631.25	-577.93	6.5*	B	57.7					
			-631.25	-577.89	2*	C	56.9					
			-631.13	-577.99	4.8*	D	52.2					
			-631.09	-578.08	1.5*	E	51.3					
			7.54	3.15	305	F	39.9					
			7.37	3.19	350	G	39.1					
			7.59	2.86	60	H	38.5					
			7.22	3.00	8	J	37.2					
			7.20	3.03	13	K	35.9					
			7.17	3.01	4	L	35.2					
18134–1942	11.4994	-1.4848	-1.71	-7.46	20	A	16.2			<1	<10	
			-1.79	-7.53	13	B	15.3					
			-1.83	-7.43	48	C	14.8					
			-1.73	-7.39	81	D	14.3					
			-1.88	-7.29	18	E	13.4					
			-1.90	-7.26	30	F	13.0					
			-1.83	-7.23	6	G	10.0					
			-1.82	-7.67	13	H	8.9					
			-1.78	-7.54	12	J	8.0					
			-1.81	-7.40	35	K	7.2					
			-1.78	-7.61	190	L	6.7					
			-1.81	-7.58	180	M	6.3					
18141–1615	14.6060	0.0128	-15.64	0.11	0.8	A	25.5	-34.7	-10.8	2	<7	U
			-15.54	-0.02	0.5	B	24.7					
			-15.55	-0.04	1.2	C	23.3					
18162–2048	10.8403	-2.5913						2.9	2.9	4	<21	U
18174–1612	15.0324	-0.6675	34.25	-10.18	13	A	23.2	-15.5	28.9	67	54	I
			34.02	-10.16	33	B	21.1					
18182–1433	16.5817	-0.0468	18.37	4.37	1.2	A	68.6			<1	<12	
			18.47	4.46	10	B	63.9					
			18.45	4.47	20	C	61.9					
			18.56	4.23	22	D	59.3					

Table 2 – continued

IRAS name	IRAS Galactic coordinates ^a		Methanol Maser					Radio Continuum				
			Offset (arcsec)	Peak flux density (Jy beam ⁻¹)	Radial velocity (km s ⁻¹)	RA	Dec.	Offset (arcsec)	Peak flux density ^b (mJy beam ⁻¹)	8.64 GHz	6.67 GHz	Morph Type ^c
	<i>l</i>	<i>b</i>	RA	Dec.				RA	Dec.			
18217–1252	18.4599	−0.0051	18.60	4.29	5	E	58.4	−2.0	6.0	150	140	C
			18.50	4.20	1.1	F	57.0					
18232–1154	19.4883	0.1400	−1.69	3.79	23	A	49.2	−0.6	−3.5	19	<25	U
			−1.71	4.23	1	B	47.2					
18236–1205	19.3636	−0.0240	−37.79	12.03	5.1	A	24.2	20.5	1.0	17	9	C
			−37.73	12.39	1.0	B	23.0					
18239–1228	19.0710	−0.2824	−37.76	12.07	6.6	C	22.4	<1	<10	<1	<10	I
			−121.22	0.29	8.8	D	21.5					
18244–1155	19.6096	−0.1326	−37.85	12.08	16	E	20.9	28.0	8.9	64	54	I
			−121.30	0.46	2.8	F	18.0					
18248–1158	19.6087	−0.2356	21.94	−6.05	2	A	28.7	325.1	−173.3	<4	60*	I
			21.82	−6.00	5	B	27.8					
18253–1130	20.0783	−0.1384	21.83	−5.95	18	C	27.0	−1.55	3.8	210	280	C
			21.83	−5.99	6	D	25.3					
18265–1517	16.8683	−2.1582	21.81	−5.96	10	E	24.7	0.7	−26.3	60	32	D
			−5.18	−15.47	8	A	18.6					
18282–0951	21.8722	0.0085	−5.61	−15.16	16	B	17.2	−3.9	12.8	180	130	U
			−5.66	−15.14	2	C	15.3					
18290–0924	22.3588	0.0642	−5.67	−15.21	24	D	14.8	−46.3	133.5	3	<8	P (b)
			−4.91	33.51	5.5		20.6					
18310–0825	23.4571	0.0682	−10.24	−4.23	1.1	A	85.0	6.6	8.0	18	22	I
			−10.44	−3.87	10	B	80.0					
18311–0809	23.7082	0.1685	−10.13	−4.99	2.0	C	77.0	−1.55	3.8	210	280	C
			−46.31	134.03	10.6	A	88.0					
18314–0720	24.4673	0.4910	−46.28	133.98	8.5	B	87.0	−46.3	133.5	3	<8	D
			−46.18	134.28	1.4	C	84.8					
18316–0602	25.6469	1.0534	−46.09	133.57	1.1	D	82.0	−2.1	13.0	40	57	U
			17.29	4.34	2	A	42.4					
18317–0757	23.9547	0.1508	17.32	3.76	90	B	41.7	17.3	4.9	1	<7	U
			17.49	3.28	2	C	41.1					
18317–0845	23.2453	−0.2400	17.65	3.20	2	D	40.8	7.2	0.2	79	120	I
			20.84	35.73	3.5	A	64.8					
18319–0834	23.4337	−0.2062	20.86	35.75	6.1	B	64.0	19.1	77.2	10	17	U
			−64.99	45.63	2	A1	107.3					
18324–0820	23.6995	−0.1942	−65.78	58.83	2	A2	107.3	24.11	15.98	4	<2	<9
			−65.01	45.38	7	B	105.9					
18324–0820	23.6995	−0.1942	−65.01	45.49	45	C	104.2	24.11	15.98	4	77.6	U
			−64.90	45.46	26	D	103.6					
18324–0820	23.6995	−0.1942	−64.80	45.40	60	E	102.9	24.11	15.98	4	77.6	U
			−64.77	45.40	27	F	102.3					
18324–0820	23.6995	−0.1942	−64.78	45.67	9	G	101.7	24.11	15.98	4	77.6	U
			−65.87	59.22	1.6	H	99.8					
18324–0820	23.6995	−0.1942	−65.91	59.35	25	J	98.2	24.11	15.98	4	77.6	U
			−65.91	59.37	21	K	97.5					
18324–0820	23.6995	−0.1942	−65.94	59.39	21	L	96.6	24.11	15.98	4	77.6	U
			−65.94	59.39	20	M	95.7					
18324–0820	23.6995	−0.1942	24.14	16.04	27	A	81.4	<2	<9	<9	<9	U
			24.12	16.07	16	B	78.5					
18324–0820	23.6995	−0.1942	24.15	15.98	9	C	78.0					
			24.11	15.98	4	D	77.6					

Table 2 – continued

IRAS name	IRAS Galactic coordinates ^a <i>l</i> <i>b</i>	Methanol Maser					Radio Continuum							
					Offset (arcsec)		Peak flux density (Jy beam ⁻¹)	Radial velocity (km s ⁻¹)				Peak flux density ^b (mJy beam ⁻¹)	Morph Type ^c	
		RA	Dec.		RA	Dec.			8.64 GHz	6.67 GHz				
18335–0711	24.8455 0.0906	24.21	16.03	3	E	76.6								
		24.15	15.95	11	F	76.2								
		24.15	16.10	2	G	74.9								
		-68.90	-190.38	16	A	114.6						<3		<16
		-68.80	-190.43	45	B	113.9								
		-68.78	-190.53	143	C	113.3								
		-70.12	-189.35	23	D	112.2								
		-70.12	-189.42	59	E	111.7								
		17.98	8.58	2	F	110.8								
		-69.98	-189.99	14	G	110.3								
		17.93	8.69	24	H	109.7								
		-69.17	-191.02	104	J	107.9								
		-69.20	-190.84	80	K	107.6								
18353–0628	25.6954 0.0277	-69.08	-191.12	4	L	106.7								
		-28.22	72.48	14	A	100.0						-33.3		D
		-28.15	72.20	38	B	96.2								
		-28.15	72.19	386	C	95.5								
		-28.21	72.30	130	D	94.8								
		-28.21	72.26	33	E	93.6								
		-28.28	72.22	16	F	92.3								
		-28.30	72.24	27	G	92.0								
		-28.25	72.32	24	H	91.2								
		-28.24	72.26	67	J	89.8								
		177.27	50.71	5	A	99.0						69.4		C
		177.46	51.05	5	B	96.6								
		177.46	51.05	7	C	93.8								
18361–0627	25.7905 -0.1407	177.49	50.99	65	D	91.5								
		177.51	50.99	40	E	90.7								
		18385–0512	27.1815	-0.0782								18.0		U
		18403–0417	28.1999	-0.0499	-233.13	92.06	49	A	101.0			-1.0	5.1	P
					-1.09	3.86	2.0	B	98.7				140	
18416–0420	28.2949 -0.3766				-0.97	3.35	1.0	C	97.2					
					51.66	14.69	3.1	A	93.1			-51.1		I
					51.68	14.59	6.2	B	92.3					
					51.47	14.53	6.2	C	82.9					
					51.44	14.69	12	D	82.5					
					51.45	14.74	13	E	82.0					
					51.47	14.66	68	F	81.0					
					51.57	14.55	2.1	G	80.2					
					51.56	15.16	3.1	H	79.7					
					-78.93	-9.91	1.2	J	40.4					
18421–0348	28.8342 -0.2440				-29.42	70.96	0.5	A	99.8				<1	
					25.01	-20.54	70	B	91.7					<10
					25.07	-20.32	40	C	90.9					
					24.69	-19.93	35	D	85.7					
					24.81	-20.16	16	E	84.9					
					24.86	-20.26	19	F	84.2					
					24.95	-20.31	92	G	83.2					
					24.96	-20.68	3	H	81.7					
					24.95	-20.25	11	J	81.0					
18434–0242	29.9564 -0.0170				133.75	22.34	3	A	104.5			-0.5	-0.5	I
					133.74	22.72	11	B	103.9					
					133.77	22.46	9	C	103.4					
					133.87	22.67	4	D	102.5					
					-66.94	-336.90	7*	E	101.8					
					-66.92	-337.14	12*	F	101.2					
					-3.74	1.51	16	G	100.1					
					-4.19	-0.45	13	H	98.9					
					133.65	22.41	19	J	98.2					
					-4.31	-0.40	5	K	97.7					

Table 2 – continued

IRAS name	IRAS		Methanol Maser					Radio Continuum					
	Galactic coordinates ^a		Offset (arcsec)	Peak flux density (Jy beam ⁻¹)	Radial velocity (km s ⁻¹)	RA	Dec.	<1	<18	Peak flux density ^b (mJy beam ⁻¹)	8.64 GHz	6.67 GHz	Morph Type ^c
	<i>l</i>	<i>b</i>											
18440–0148	30.8179	0.2739	-4.19	0.13	65	L	96.5						
			-4.37	0.77	158	M	95.7						
			4.31	4.89	0.6	A	110.1						
			4.26	0.55	5.0	B	104.6						
			176.44	-203.30	24	C	87.5						
			176.44	-202.88	29	D	85.7						
			176.42	-204.85	18	E	85.2						
			176.21	-199.08	1.8	F	76.1						
			77.86	-189.09	27	G	48.8						
			-280.94	78.43	3.0		43.2	-9.9	5.9	89	110	I	
18443–0210	30.5363	0.0180	-72.51	183.95	5.0	A	110.0	26.6	3.3	180	150	I	
18446–0150	30.8621	0.1204	-72.57	183.24	10.9	B	107.5						
			-72.31	181.79	12	C	107.1						
			-72.31	184.38	4.0	D	104.3						
			-72.34	182.41	9.9	E	103.8						
			-72.36	183.44	26	F	103.2						
			-72.34	183.33	36	G	102.9						
			-72.34	183.14	79	H	101.8						
			-72.37	183.17	30	J	100.5						
			-72.40	182.05	6	K	99.7						
			-72.40	182.62	16	L	98.9						
18449–0115	31.4148	0.3062	-7.34	-9.61	2.0	A	105.0	-4.0	5.2	31	40	I	
			-7.27	-9.22	9.0	B	103.4						
			-7.15	-10.42	2.0	C	99.0						
			-7.73	-10.32	7.0	D	95.8						
			-7.58	-10.01	2.0	E	94.2						
			-7.54	-8.49	1.0	F	92.4						
			103.72	181.31	5.8	A	108.2	-58.5	-172.9	45	<38	I	
18450–0200	30.7616	-0.0532	103.95	180.97	21	B	101.2						
			96.77	183.75	13	C	92.8						
			-4.82	-1.34	75	D	91.8						
			-4.85	-1.52	36	E	90.9						
			-4.83	-1.36	4	F	89.9						
			-4.91	-2.52	6	G	88.6						
			-48.71	-208.41	141	H	88.0						
			-49.43	-207.94	9	J	87.3						
			-49.42	-206.89	13	K	85.9						
			-147.59	51.46	24	A	16.2	5.9	12.7	19	<12	U	
18452–0141	31.0665	0.0510	-147.76	49.10	11	B	15.5						
			-40.42	3.01	46	A	112.0	-45.9	6.2	22	<14	I	
			-41.45	3.01	35	B	111.5						
			-40.21	2.61	39	C	110.8						
			-40.12	2.45	83	D	110.0						
			-40.31	2.96	10	E	108.5						
			-40.03	1.45	3	F	107.6						
			-40.03	3.13	26	G	107.0						
			-40.06	2.04	30	H	105.9						
			-40.09	2.22	18	J	105.2						
18461–0136	31.2413	-0.1094	-40.10	1.62	4	K	104.3	6.4	16.7	53	74	I	
								-24.76	11.7	8	<19	I	
18469–0132	31.3978	-0.2638											

^a The Galactic coordinates are the same as the coordinates of the IRAS point source and the pointing centre for each observed field.^b Non-detected radio continuum emission is shown with the value for the upper limit preceded by a < sign, to indicate the non-detection.^c Lower-case letters listed in parentheses (e.g. IRAS 15408–5356) refer to the radio continuum emission shown as a contour plot in Fig. 1, which is labelled similarly. Those unresolved sources with no associated maser emission are not shown in Fig. 1.

flow. The other offset methanol site has a similar linear structure, pointing in a similar direction.

IRAS 17175-3544. This source is better known as NGC 6334F. The continuum emission is of cometary shape, about 44 mpc across (assuming a distance of 1.7 kpc). Methanol emission is found scattered within the head of the cometary shape, along with OH emission, detected by Gaume & Mutel (1987). OH and water maser emission is also reported by Forster & Caswell (1989) within the tail of the cometary continuum emission. We also find a separate site of methanol emission 40 mpc to the side of the continuum emission. Our data agree well with those of Ellingsen et al. (1996), although the continuum emission they find extended to the south-east is below our lowest contour and is not evident in Fig. 1. A third, presumably unrelated, maser site is located approximately 2 arcmin north of NGC 6334F.

IRAS 17470-2853. The radio continuum emission consists of an unresolved strong source, with weaker emission extending away from the unresolved source, to the north-west. The extent of this emission, including both sources, is 0.7 pc, assuming a distance of 9.1 kpc. It is not clear whether the extended emission is associated with the unresolved source. Methanol maser emission is found at the edge of the unresolved continuum source, at the point where the two continuum features would meet. OH maser emission is also located close to this point (Forster & Caswell 1989). A single spot of methanol emission is found within the weak, extended continuum. Water maser emission, detected by Forster & Caswell (1989), is found between the two continuum features. The positions of the maser sources do indicate that the two continuum features are linked.

IRAS 18032-2032. Our continuum image shows a single unresolved source, but the deeper image of Hofner & Churchwell (1996) indicates a second continuum source 12 arcsec to the north-west. At the position of this second continuum source, we find a site of maser emission, comprising five maser spots. There are also two maser spots associated with the first continuum source, overlying the continuum emission contours, but offset to the south of the centre of emission by 1 arcsec. Hofner & Churchwell also report a line of water maser emission leading from one continuum emission source to the other, and interpret this as a ridge of star forming activity.

IRAS 18110-1854. The continuum emission is cometary in shape, and methanol emission is found beyond the head of the continuum contours. The position of the methanol emission also agrees with that of water maser emission reported by Hofner & Churchwell (1996).

4 DISCUSSION

4.1 IRAS selection criteria

It is found that the regions with maser and/or continuum emission tend to have bright *IRAS* sources. In fact, 96 per cent of the *IRAS* sources which have methanol or continuum emission within 1 arcmin of the *IRAS* position have 100 μm flux densities greater than 500 Jy, whereas 69 per cent of all of the 534 candidates have 100 μm fluxes greater than 500 Jy. We cannot say whether the weaker *IRAS* sources represent some contamination of the original *IRAS* selection criteria (explained in Paper 1), since it may be that the weaker sources are further away and therefore we are less likely to detect methanol or continuum emission from them. As there is no radial velocity information for those *IRAS* sources with no maser emission, we cannot derive distance estimates and test this hypothesis. However, van der Walt (1997) has shown that those fainter *IRAS* sources are most likely contamination of embedded

non-ionizing stars, as a result of the broader distribution of them about the Galactic plane. Similarly, Ramesh & Sridharan (1997) have shown that the *IRAS* PSC selection criteria of WCa may include up to 75 per cent of sources other than UC H II regions. They suggest that these *IRAS* sources may be the result of embedded non-ionizing stars, or of high mass equivalents of class 0 objects.

4.2 The association of methanol and continuum emission

Fig. 3 shows the distribution of the projected sizes of radio continuum regions when maser emission is present (allowing us to determine the distance). The top histogram includes all extended continuum emission regions that do not have any methanol emission projected on to the radio continuum contours. The lower histogram shows the size of the extended continuum regions that exhibit methanol maser emission projected on to the continuum contours. It is clear that the continuum sources with maser emission are generally considerably smaller than those without, and quantified by a Kolmogorov-Smirnov (K-S) test, which shows the two distributions have only a 0.7 per cent chance of coming from the same population. Also, no continuum source is found with associated methanol emission greater than 180 mpc in projected size. This suggests that the maser emission is detectable before the continuum emission and is associated with young, and therefore small, UC H II regions, probably being destroyed as the UC H II region expands. This agrees well with the hypothesis stated in Paper 1 that the masers are present before the UC H II region develops.

The mechanism for pumping the methanol maser, although not clearly understood, is generally considered to be linked to the radio continuum emission (Menten 1991). We can now test this hypothesis, by comparing the incidences of methanol and radio continuum emission. As stated in Section 3, most sites of maser emission are not associated with any detectable continuum emission. Furthermore, we can place stringent limits on the association of methanol and continuum emission by examining the relationship between them. In Table 2, we have provided peak flux densities only as a guide to the brightness of the continuum emission, so we cannot directly compare maser and continuum fluxes. We can, however, compare the distribution of the brightness of maser emission that is and is not associated with detected radio continuum emission. If the maser emission were closely associated with radio continuum emission, we would expect the strength of the maser emission to be dependent on the proximity of the continuum source. We have tested this in the three histograms shown in Fig. 4. Here we plot the distribution of the number of maser sources as a function of a measure of the integrated maser luminosity. The integrated luminosity measure is just the summation of the flux contributions of each maser spot within a given site multiplied by the square of the distance to the site. Three histograms are shown: the top one for all maser sites that have no associated continuum emission within a 0.2-pc projected distance; the middle histogram for those maser sites within a 0.2-pc projected distance of the peak position of a radio continuum source, and are therefore likely to be associated; the bottom histogram shows those maser sites that are actually projected on top of the radio continuum contours, so that they lie directly in front of the continuum source, along our line of sight. If the maser emission is affected by the proximity of a radio continuum source, then we would expect the distribution of the top and middle histograms to be different. A K-S test indicates that they are drawn from the same distribution, with 61 per cent probability. Hence, we find little evidence to suggest that the intensity of the maser emission is affected by radio continuum emission.

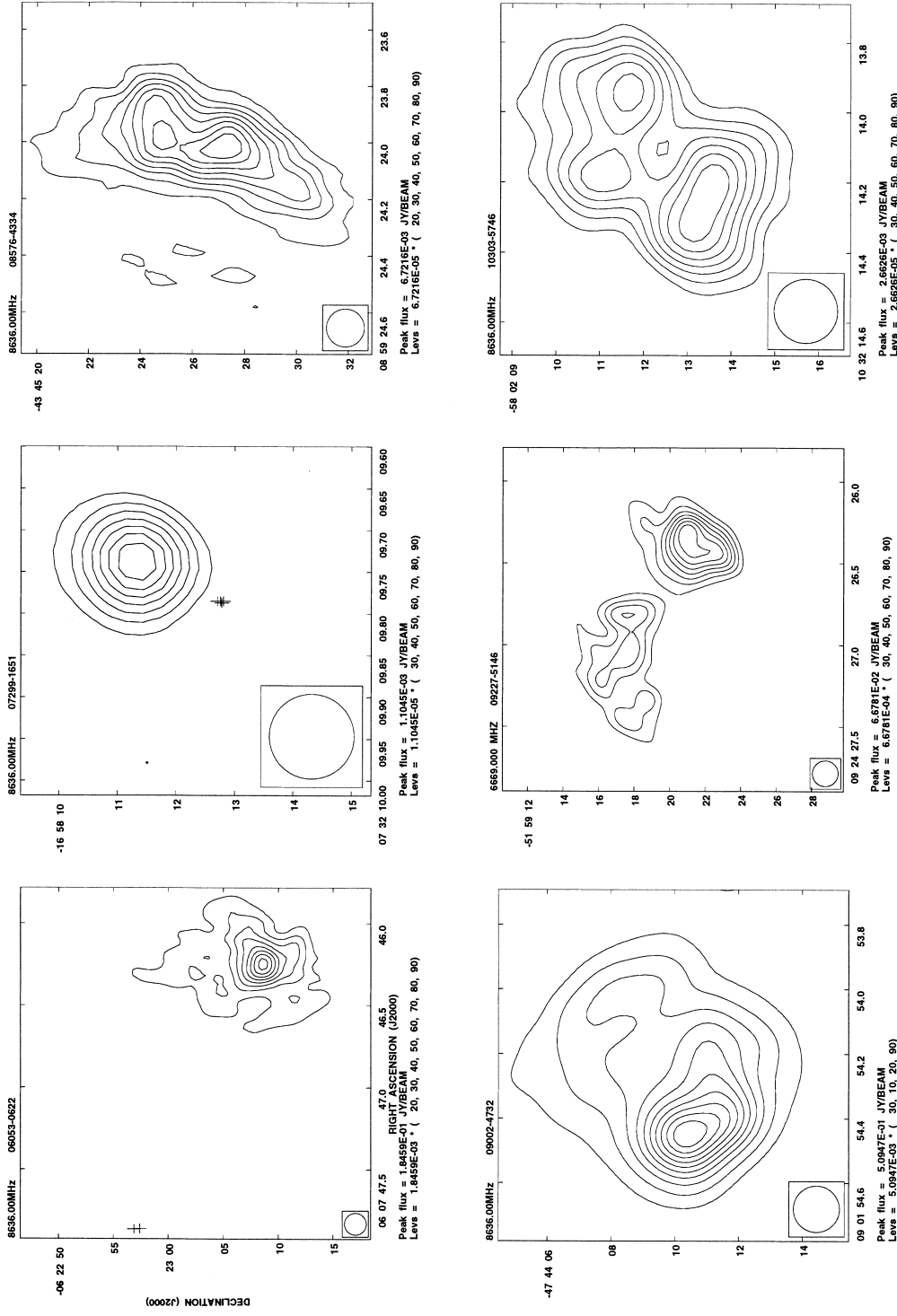
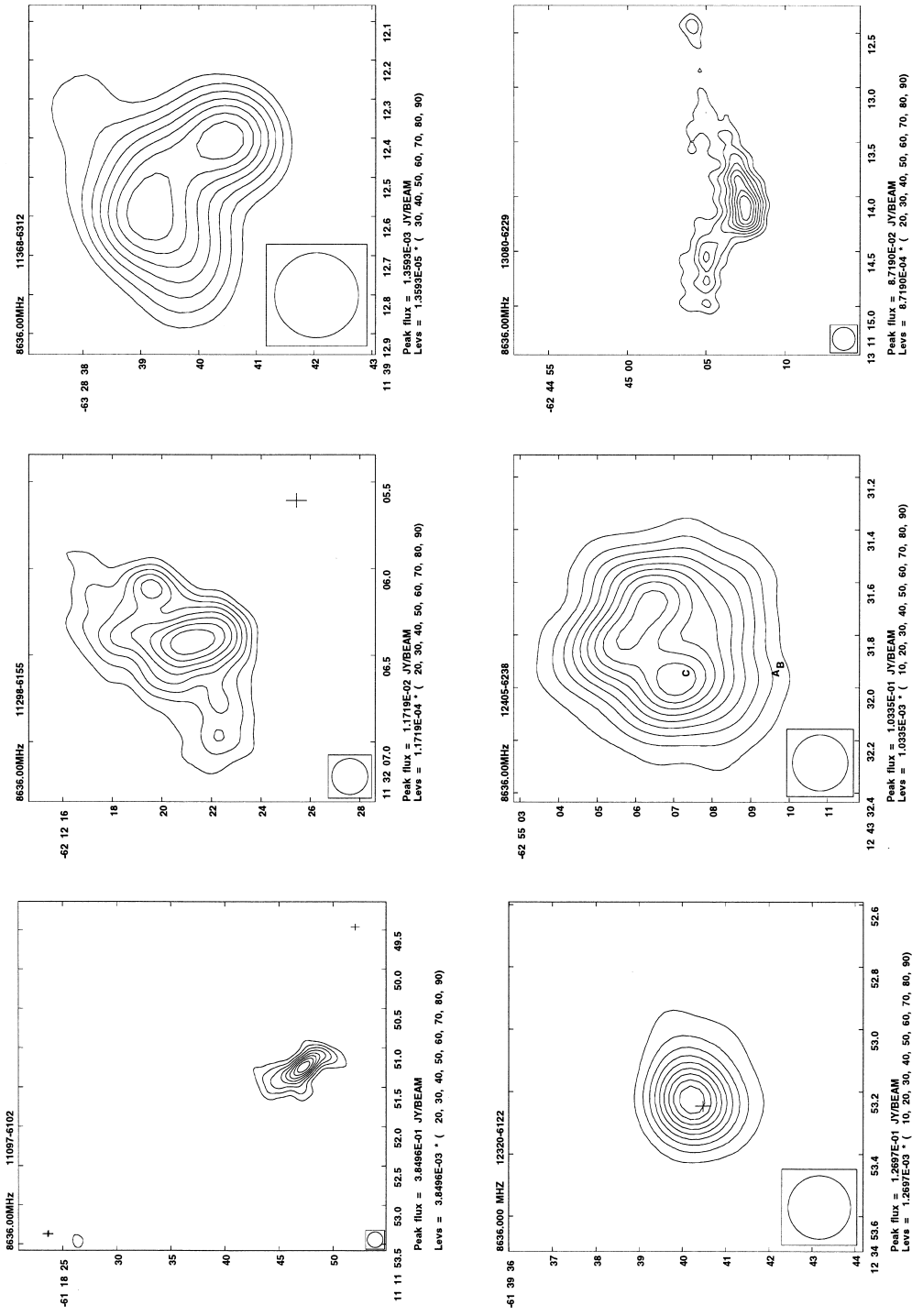
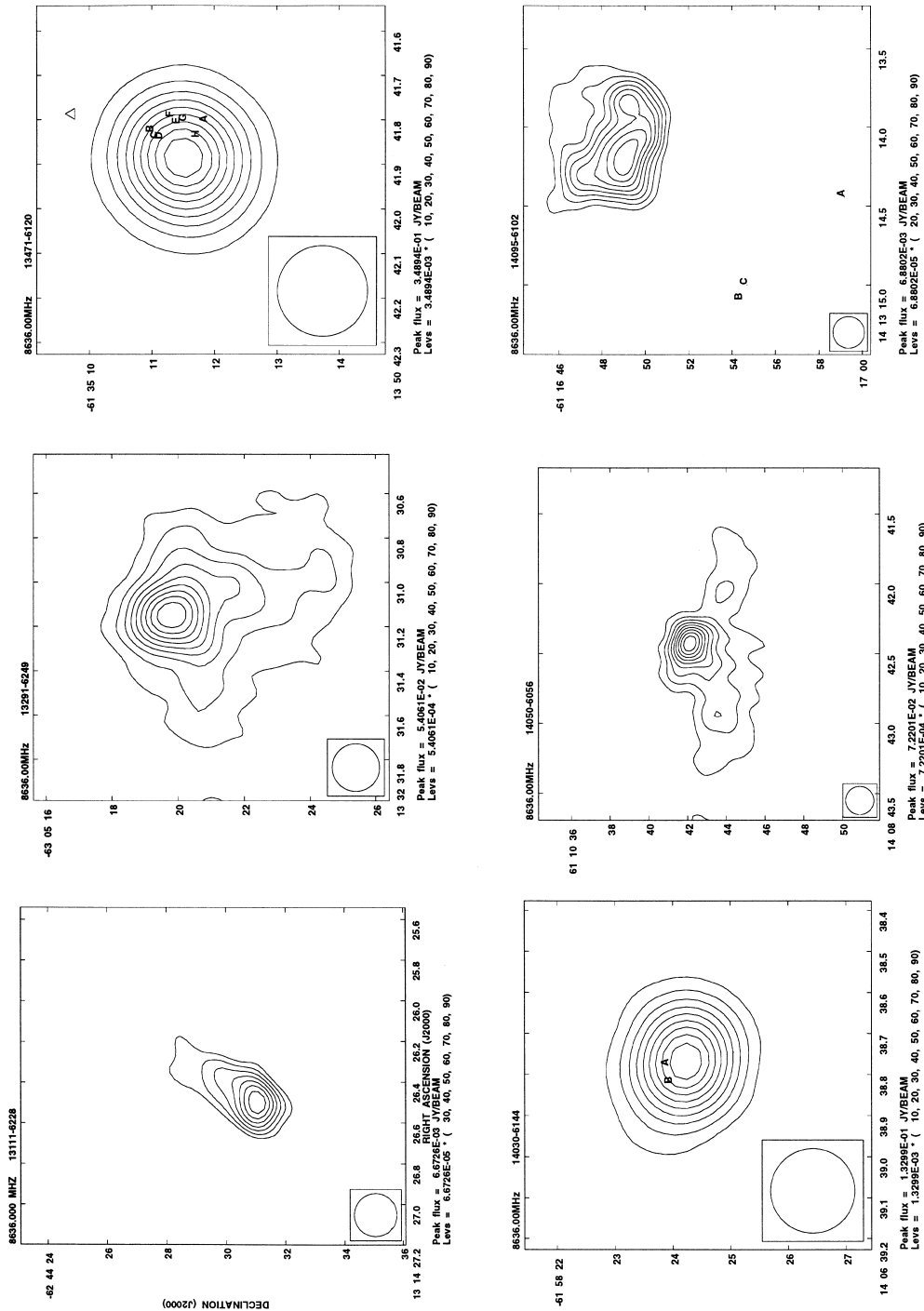
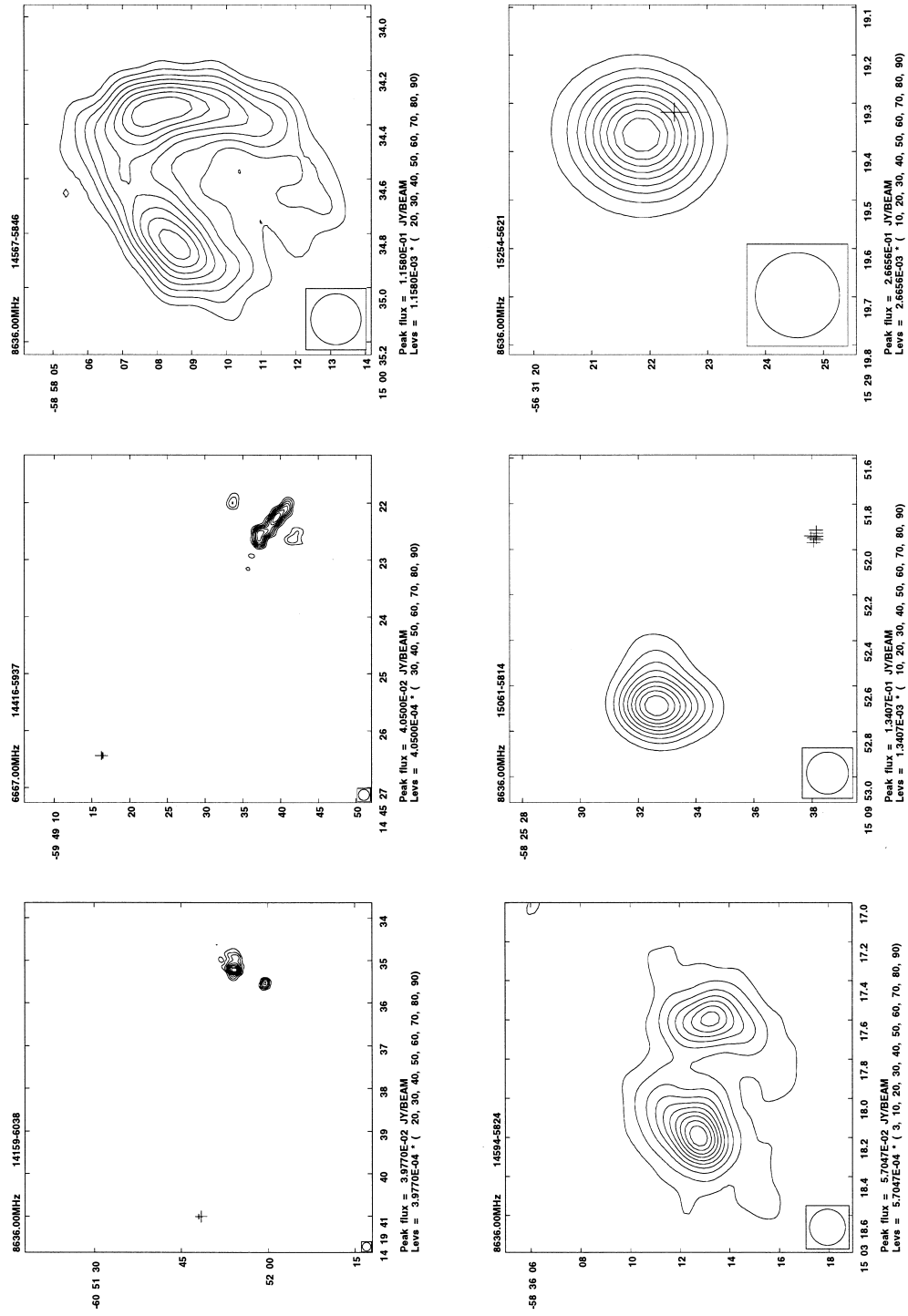
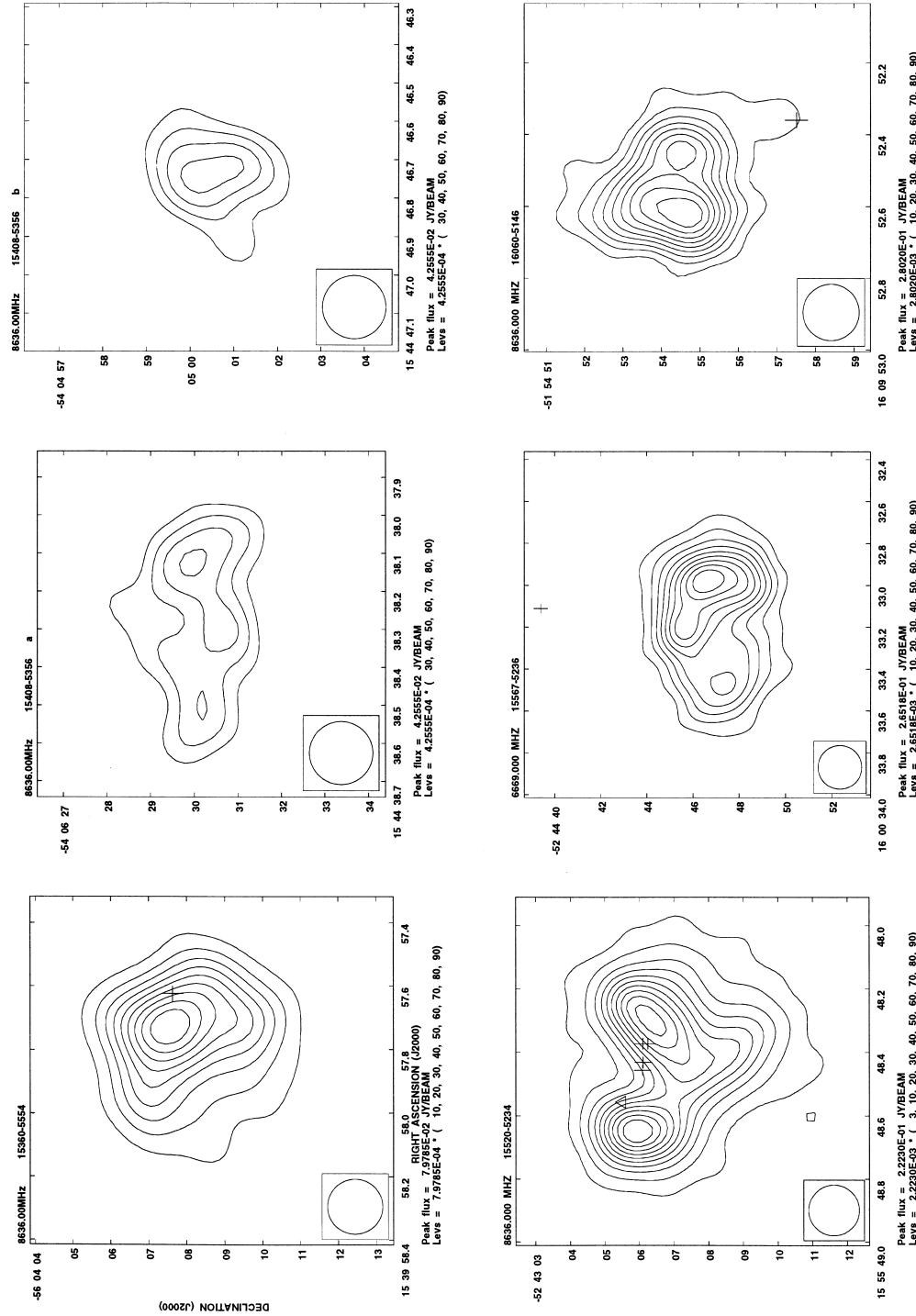


Figure 1. Radio continuum and methanol maser maps of selected sources. The map axes are labelled in J2000 coordinates. Radio continuum sources are shown as contour plots, with frequency and source name at the top of each plot. The contour levels vary depending on the strength of the radio continuum emission and are listed at the bottom of each plot. Not all radio continuum sources are shown here. Those sources that are unresolved, with no nearby maser emission, are excluded as all relevant information is provided in Table 2. Radio continuum sources within a few degrees of the Galactic plane have virtually no declination information, thus the contour maps shown provide little information in this direction. They are provided to show relationships between the radio continuum and maser positions, even though no interpretation is made on their morphologies. Multiple sources within the same field are labelled with the name of the *IRAS* source and a lower case letter, such as '16351-4722' and '16351-4722 b'. Methanol maser emission is shown by either a 'plus' (+) or by a letter, corresponding to the letter of column 6 in Table 2. Polygons indicate previous OH maser detections: triangle – Caswell et al. (1995b); square – Sevenster et al. (1997); diamond – Forster & Caswell (1989); pentagon – Ho et al. (1983); circle – Gaume & Muiel (1987). The stars indicate the positions of previous water maser detections: 5-pointed star – Forster & Caswell (1989); 6-pointed star – Hofner & Churchwell (1996).

**Figure 1 – continued**

**Figure 1 – continued**

**Figure 1 – continued**

**Figure 1 – continued**

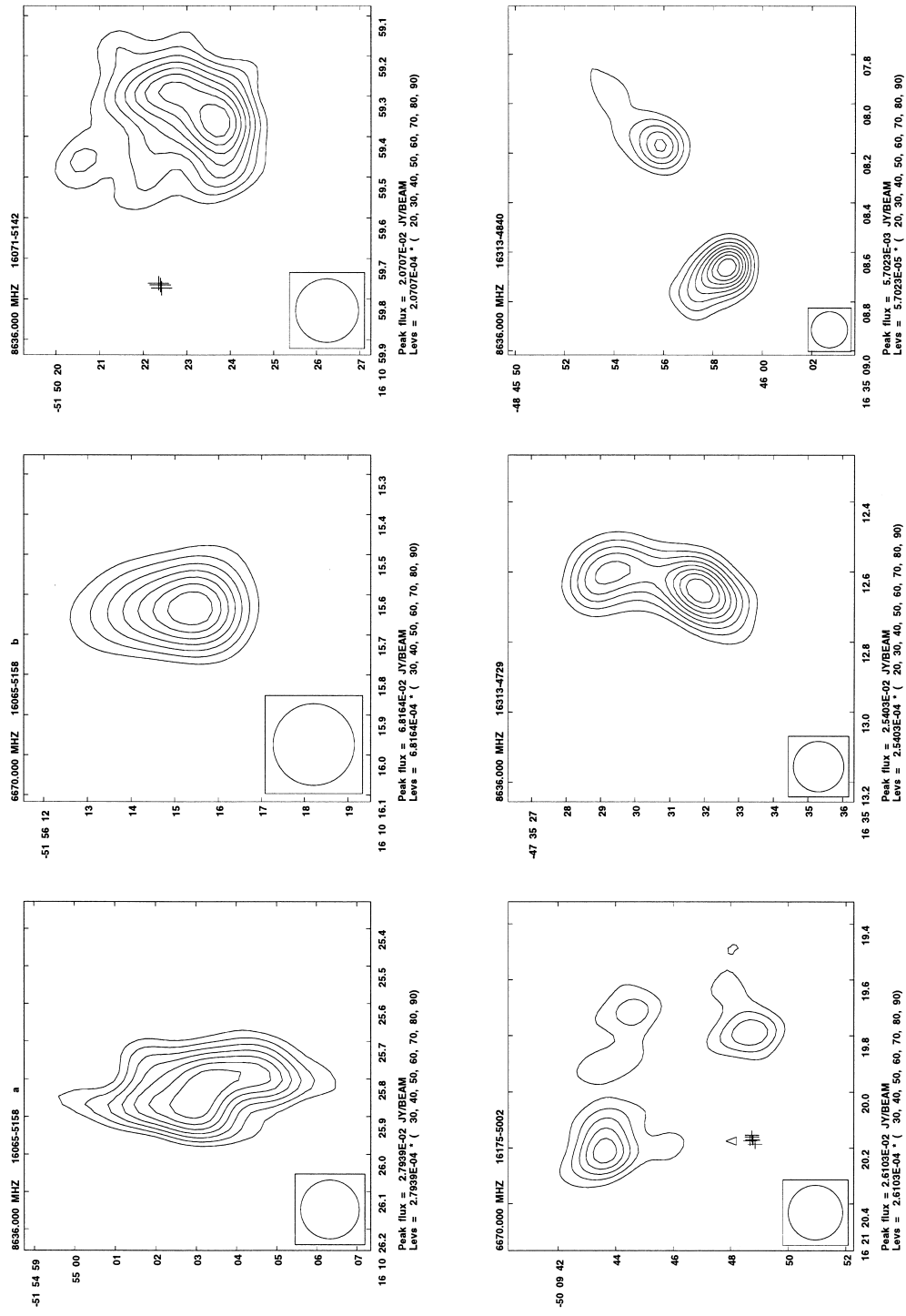
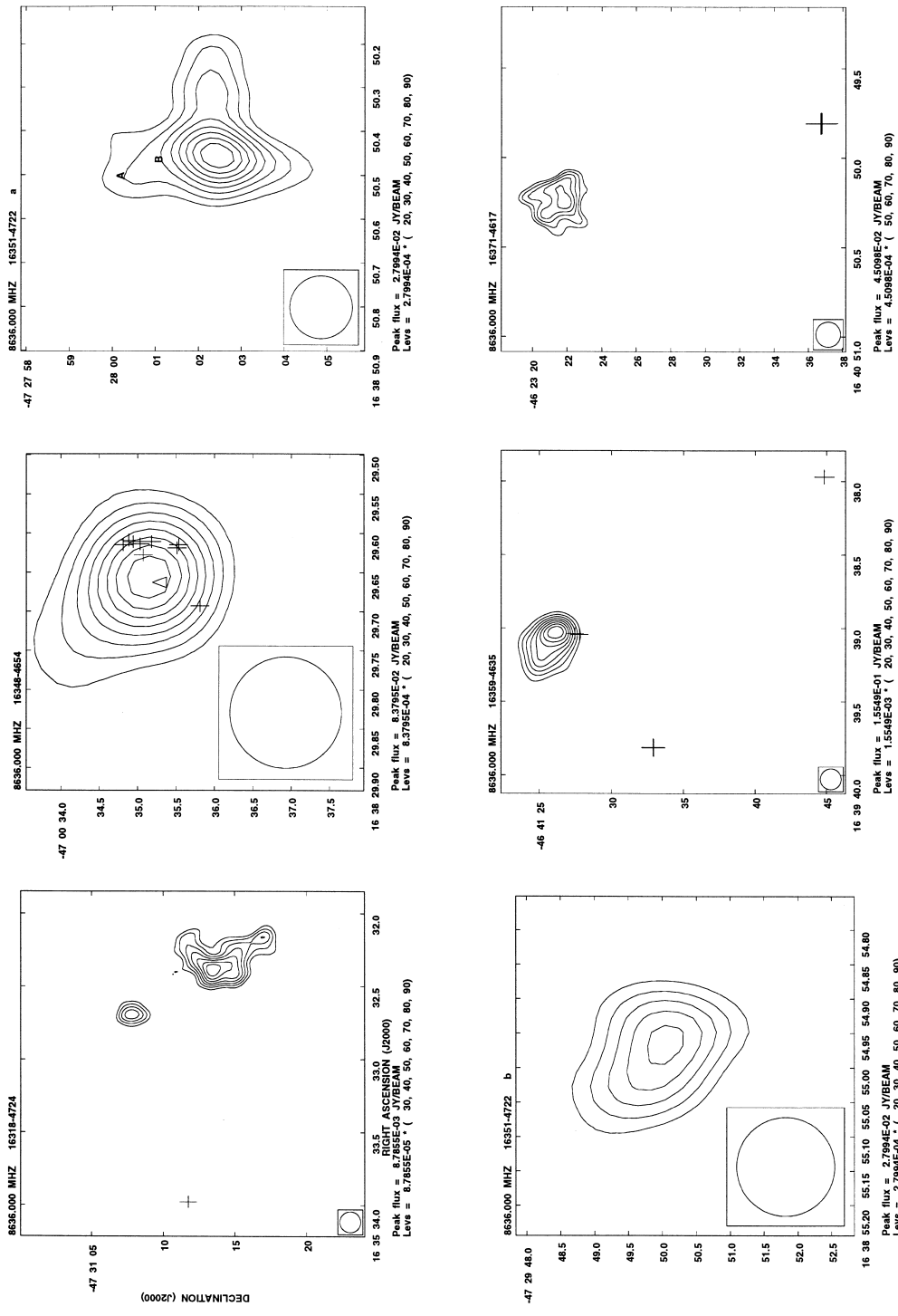


Figure 1 – continued

**Figure 1 – continued**

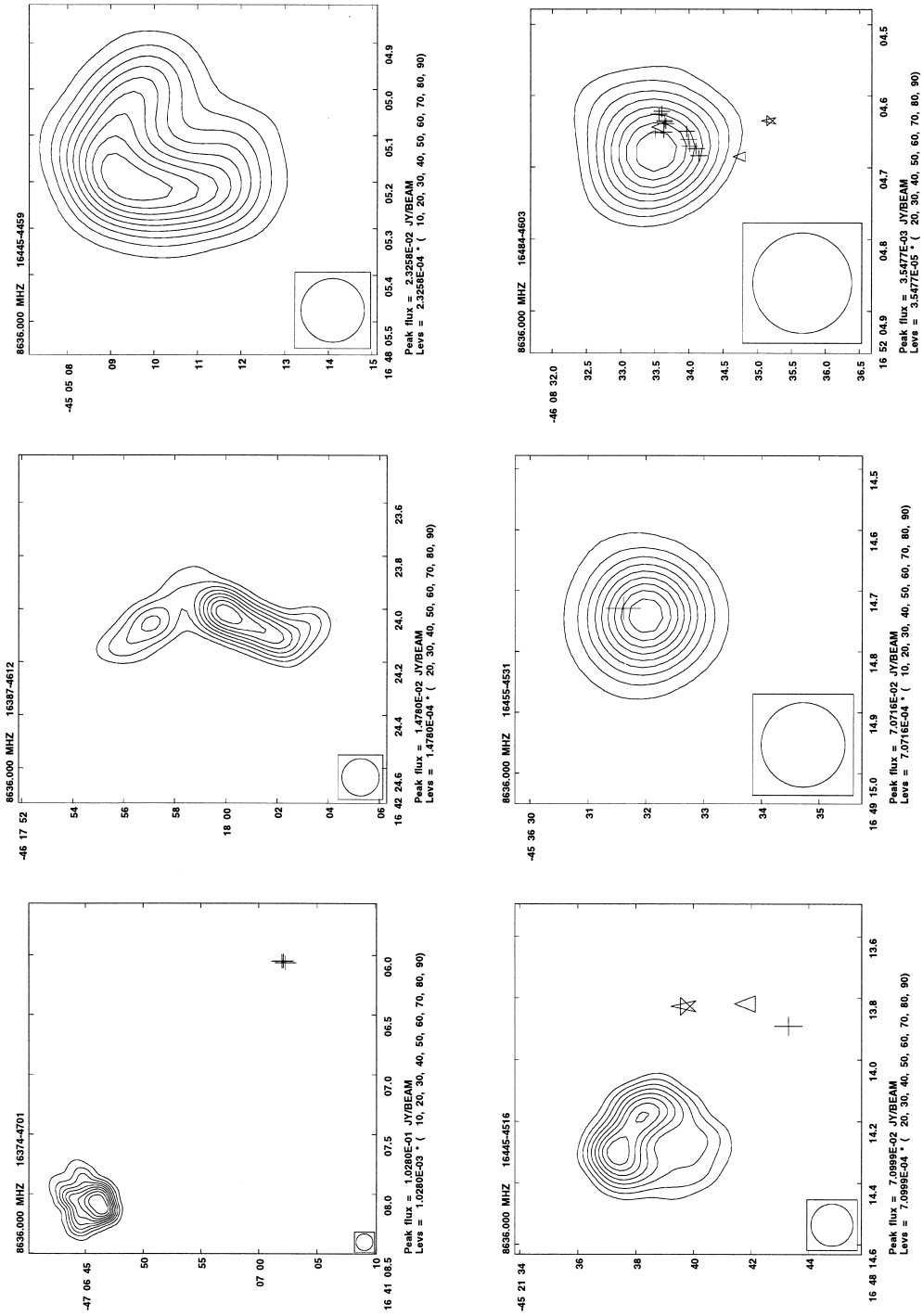
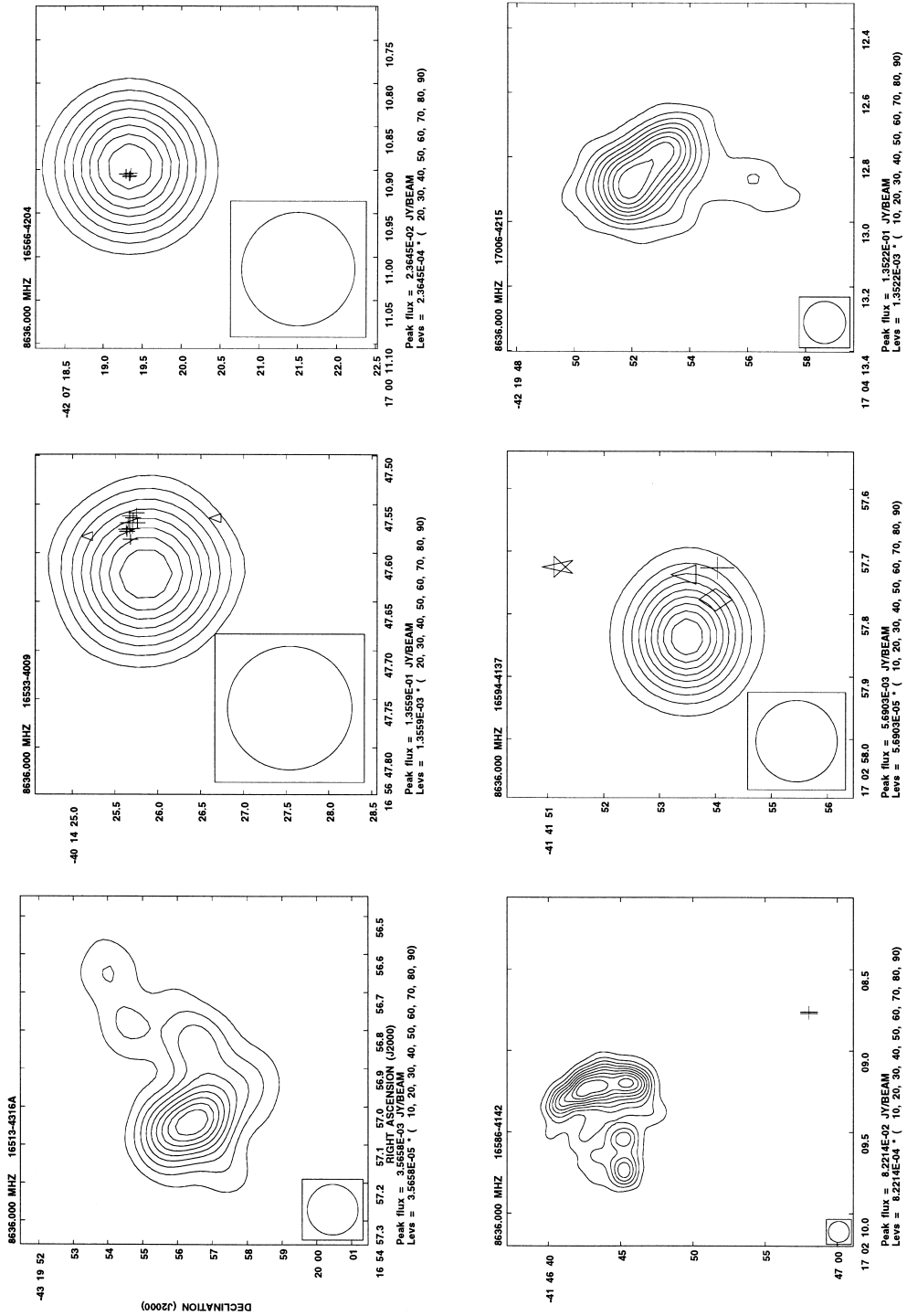
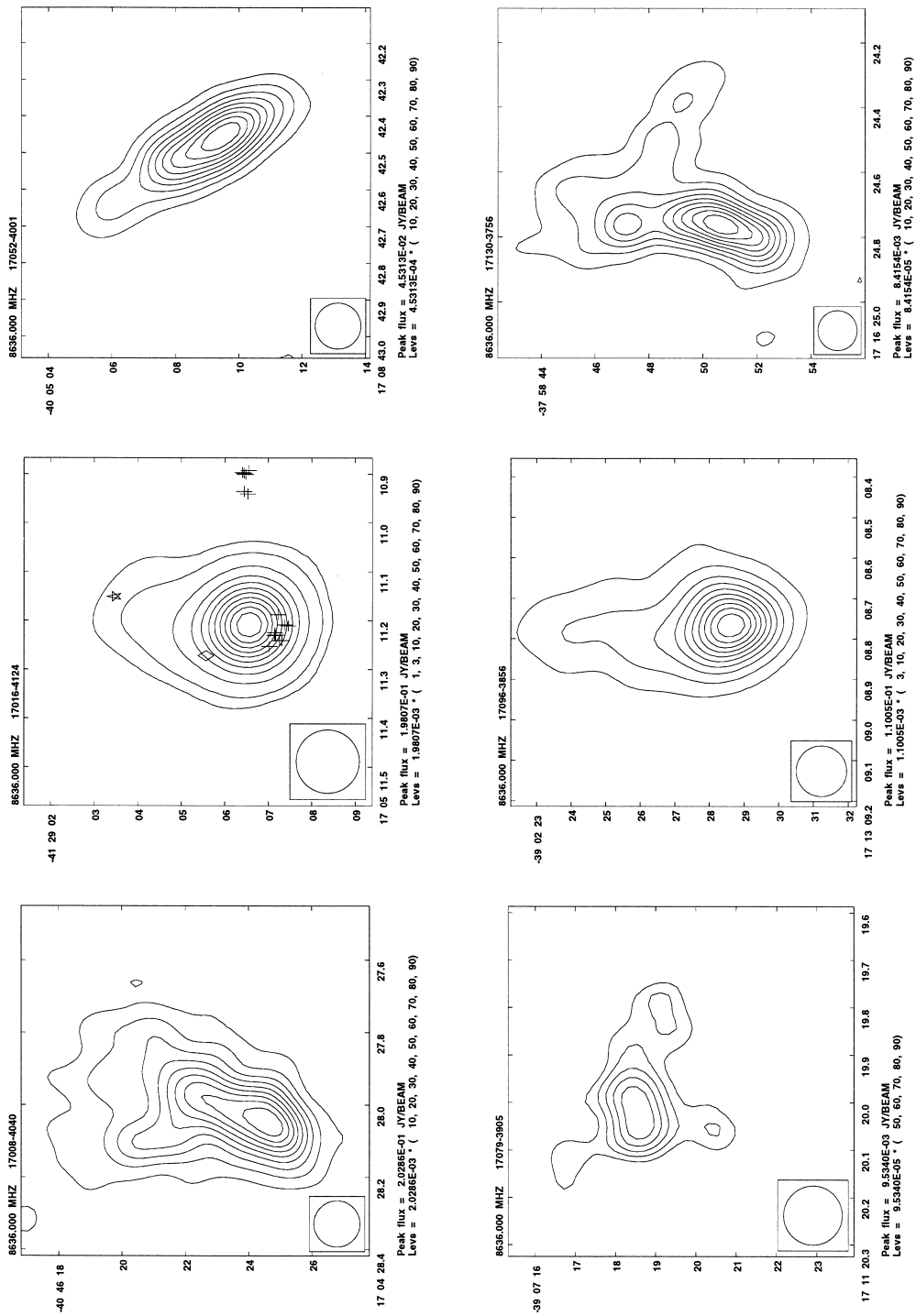
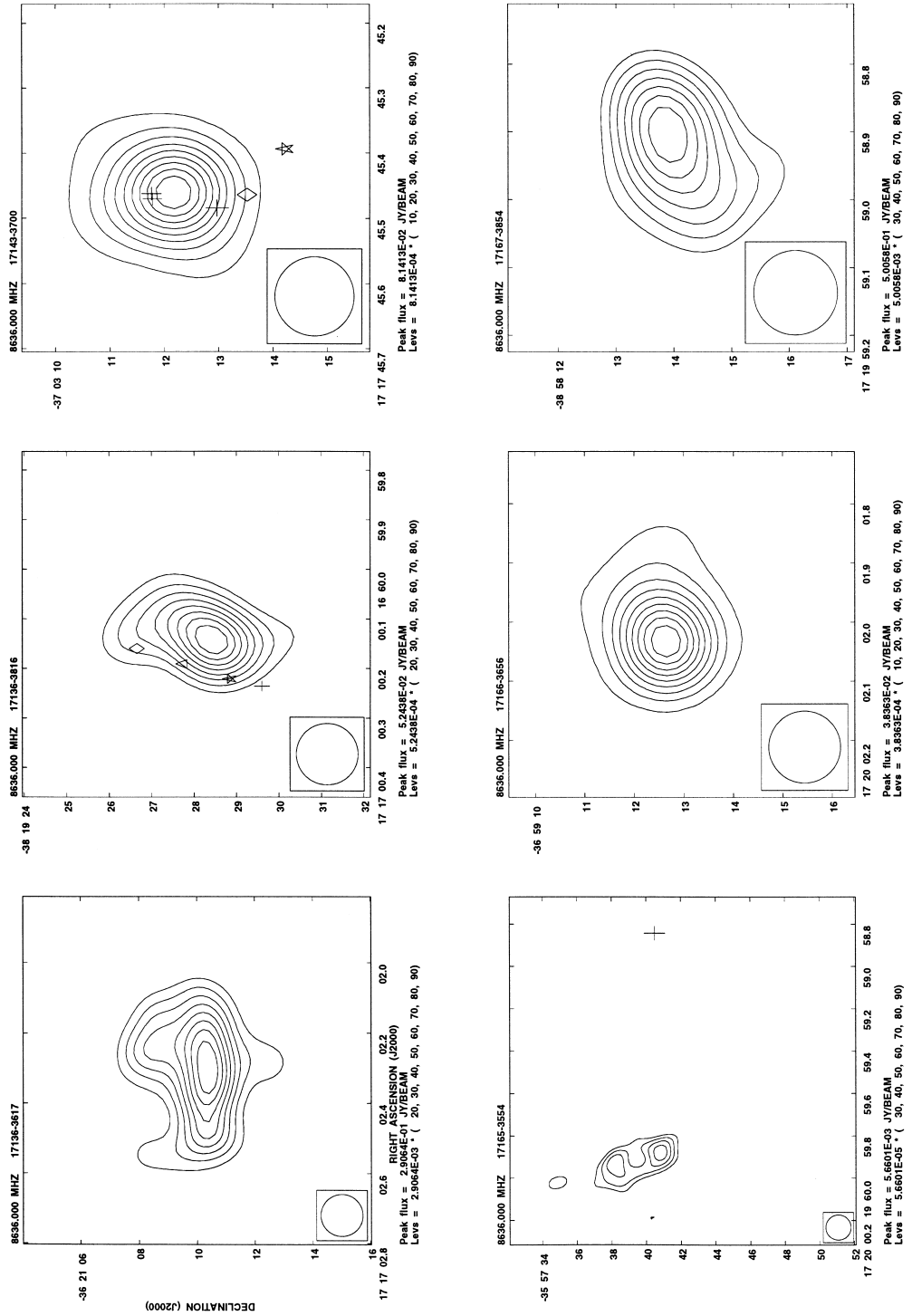
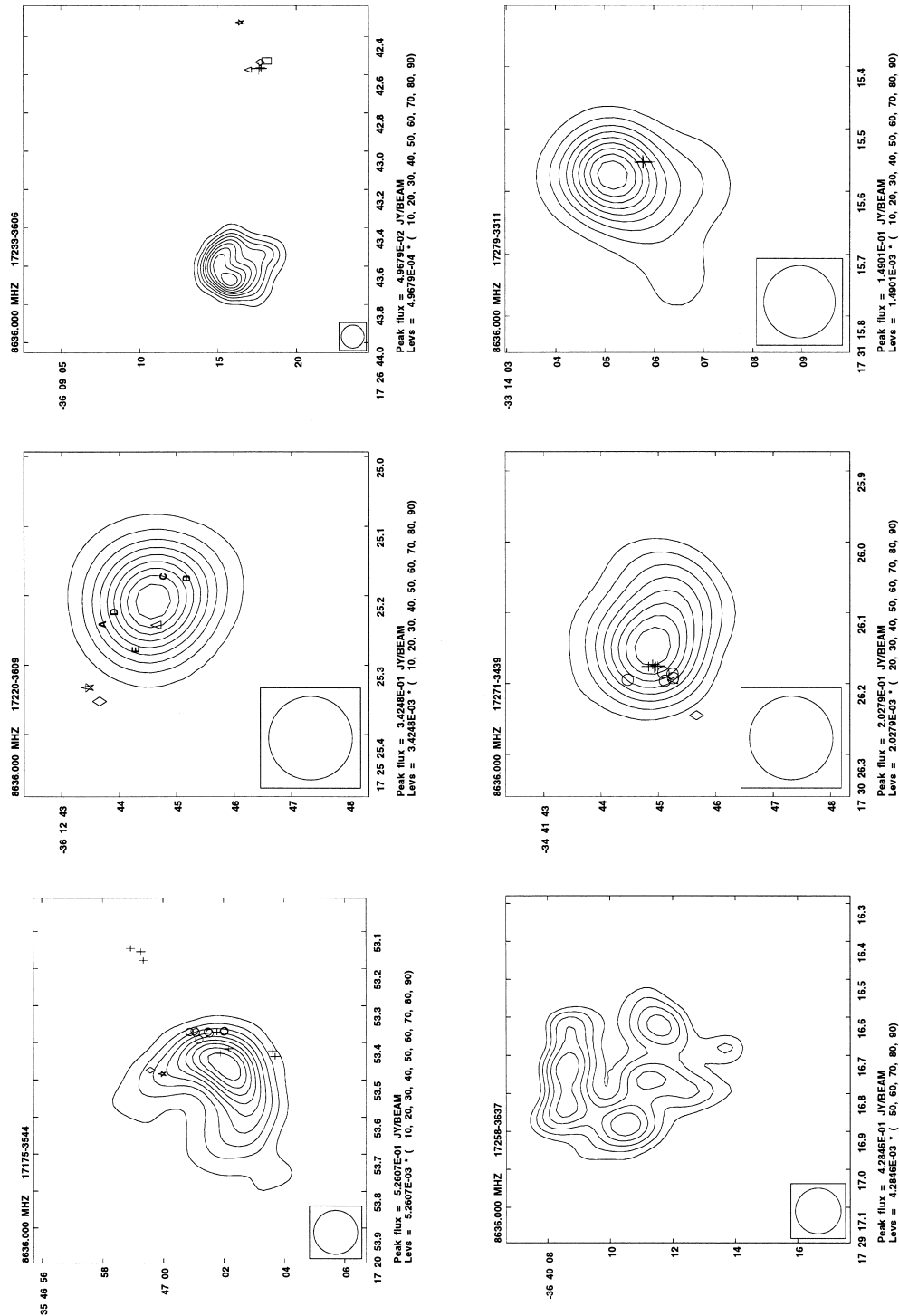


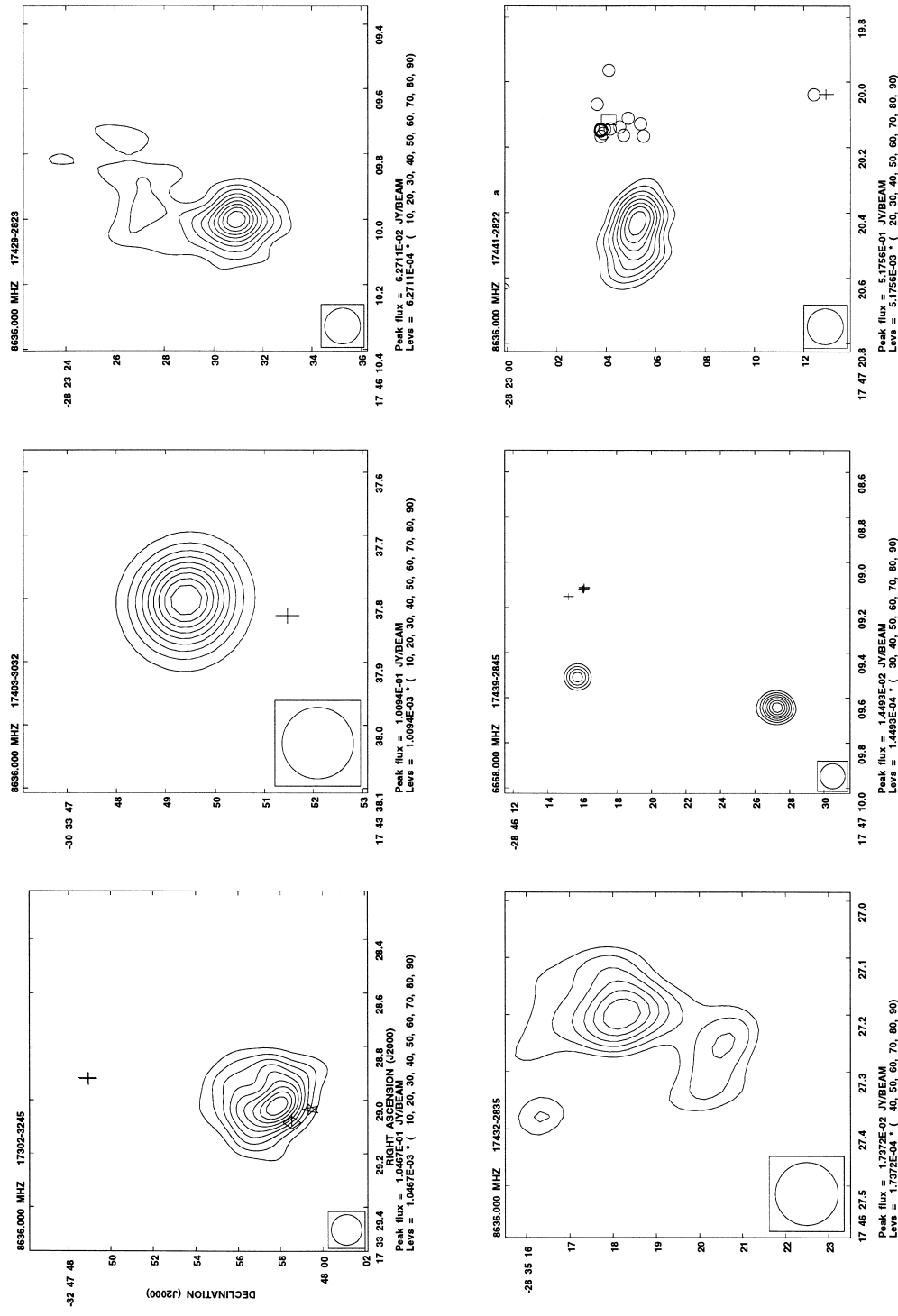
Figure 1 – continued

**Figure 1 – continued**

**Figure 1 – continued**

**Figure 1 – continued**

**Figure 1 – continued**

**Figure 1 – continued**

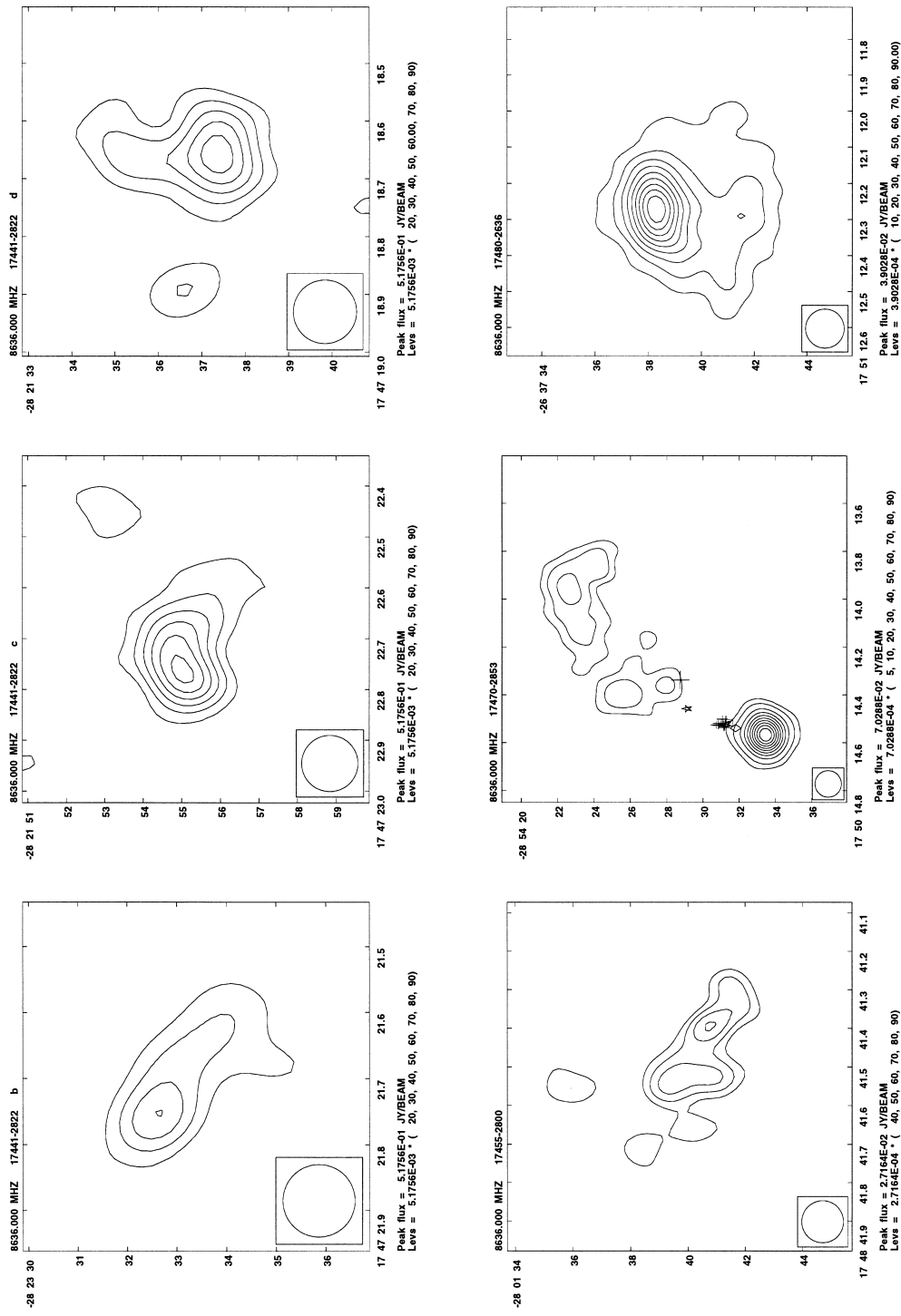
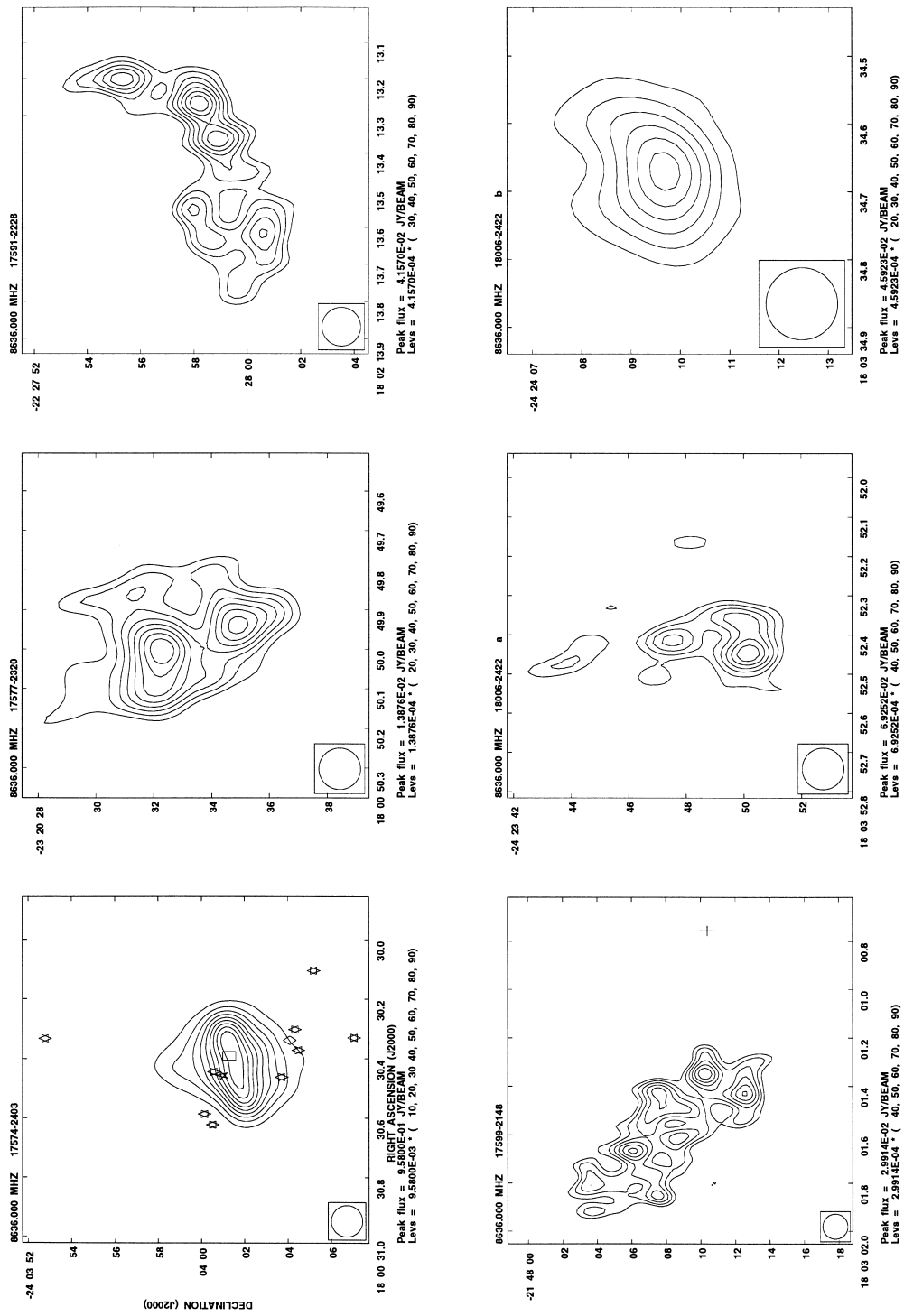


Figure 1 – continued

**Figure 1 – continued**

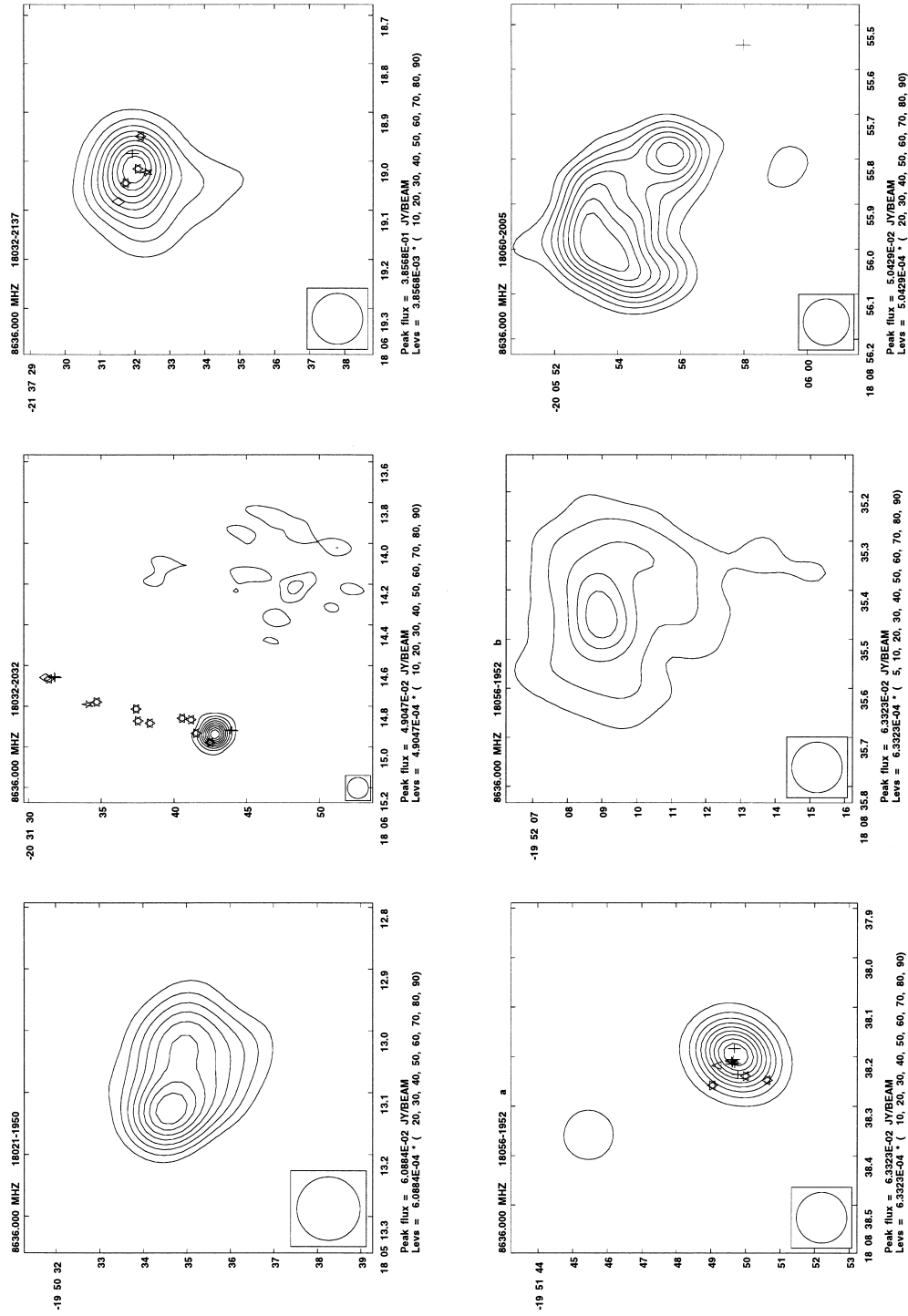
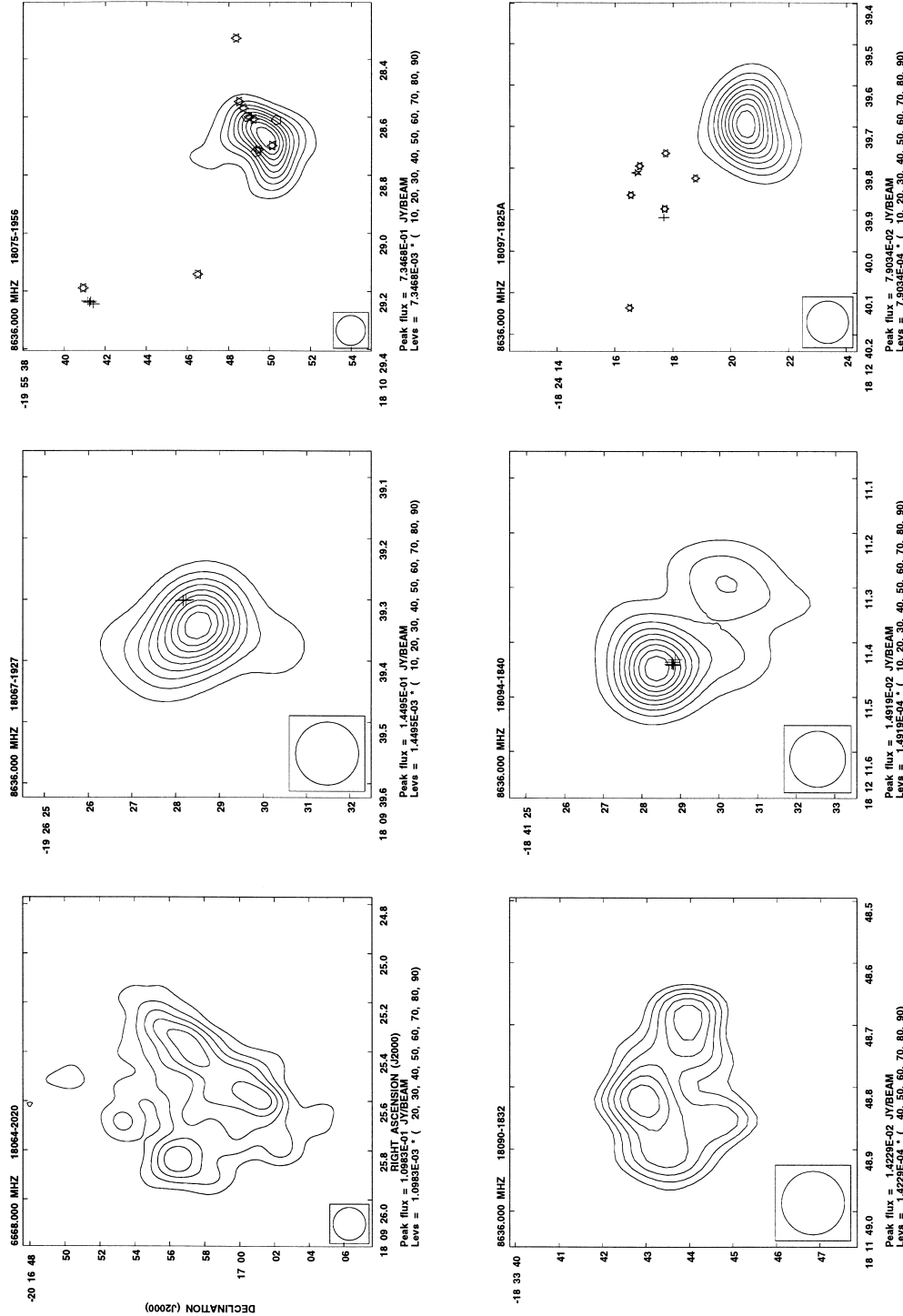
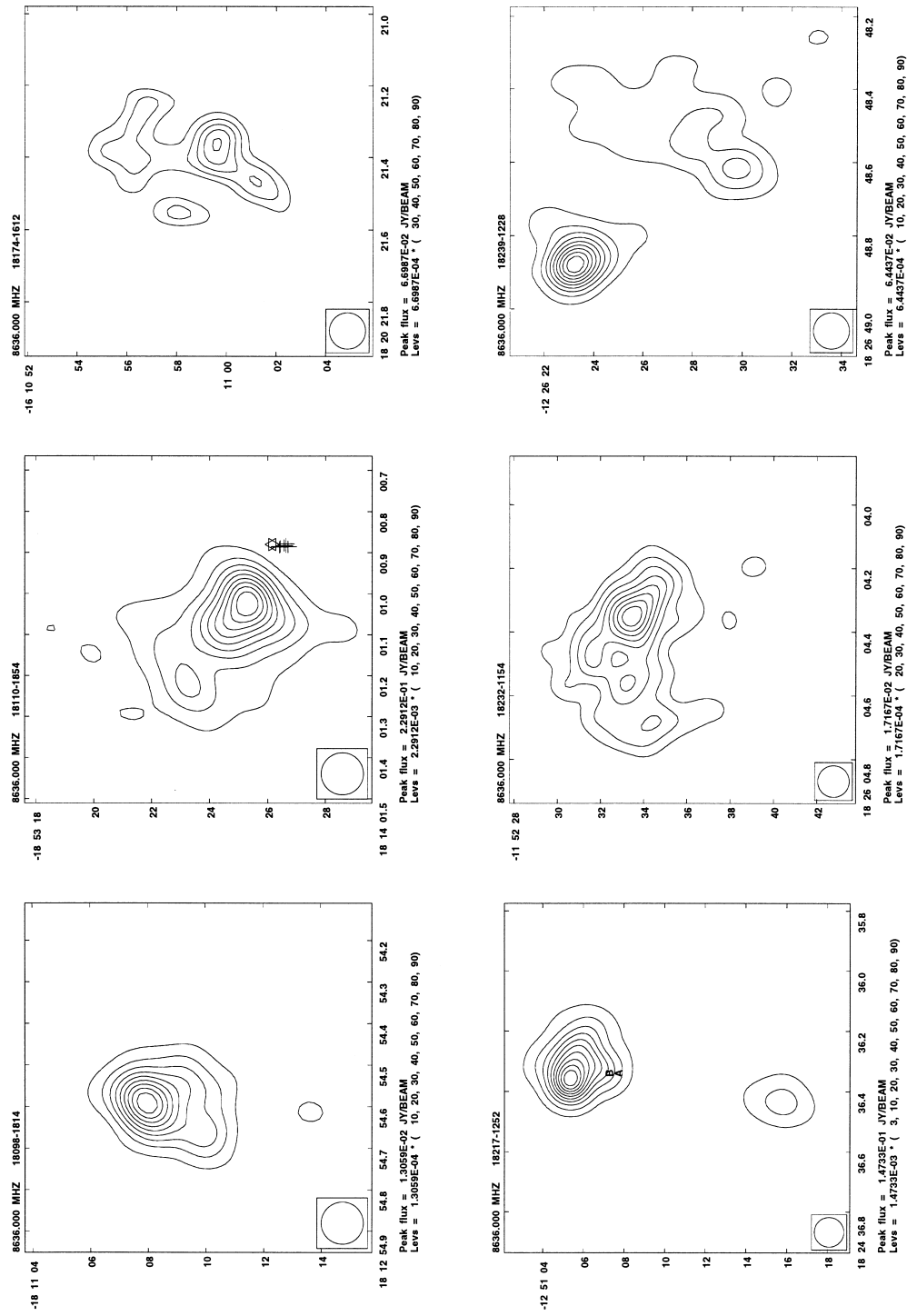
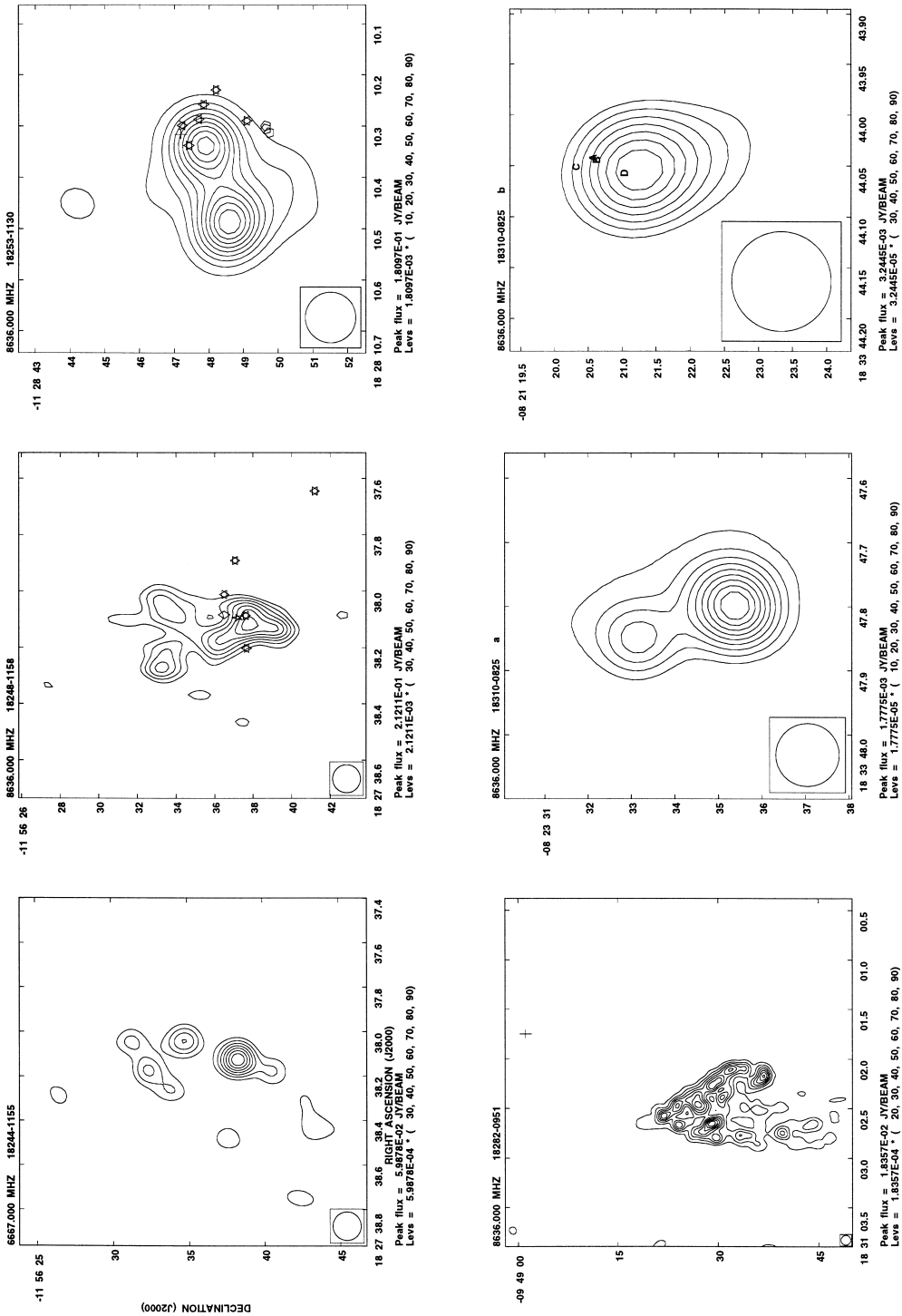


Figure 1 – continued

Figure 1 – *continued*

**Figure 1 – continued**

**Figure 1 – continued**

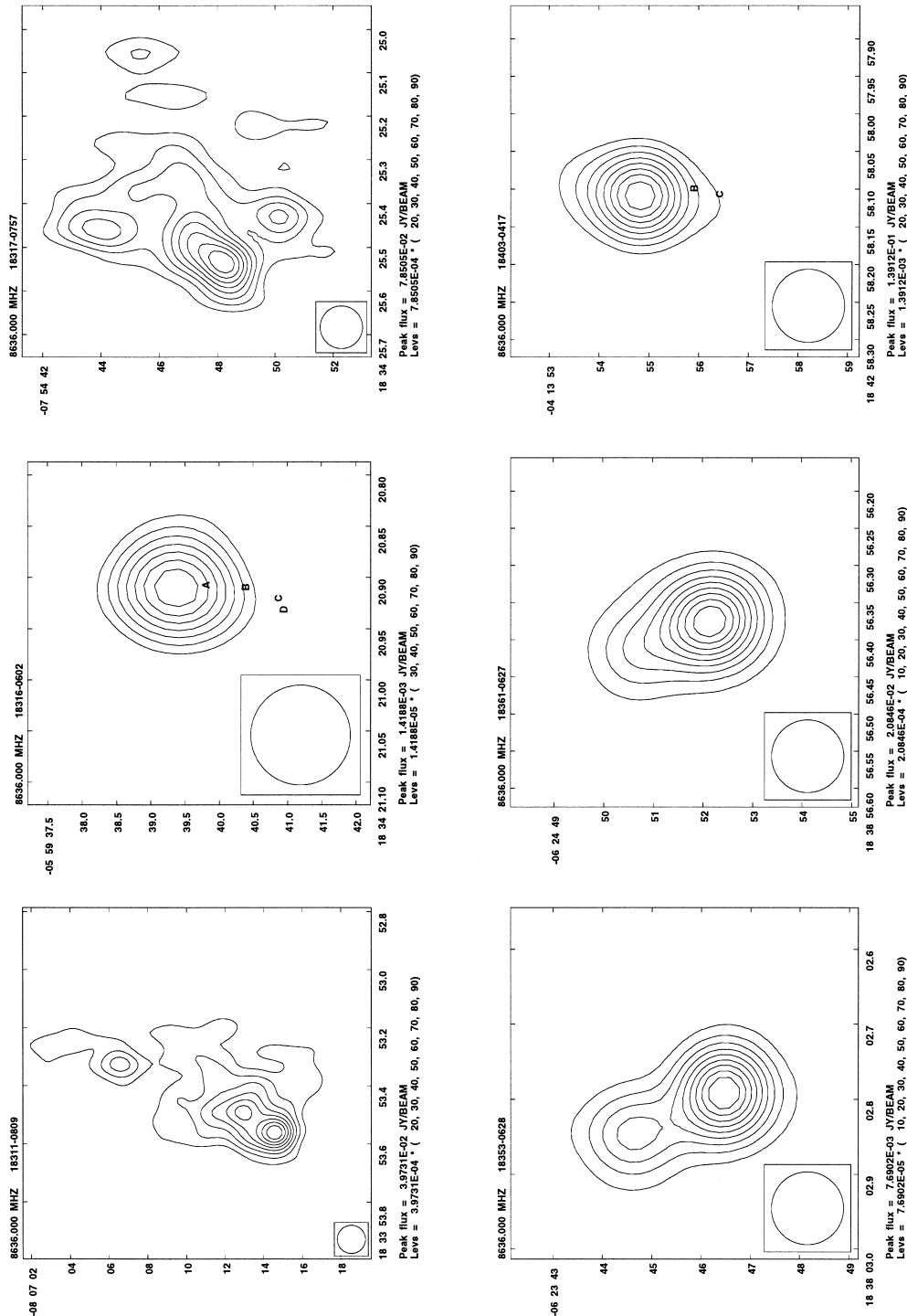
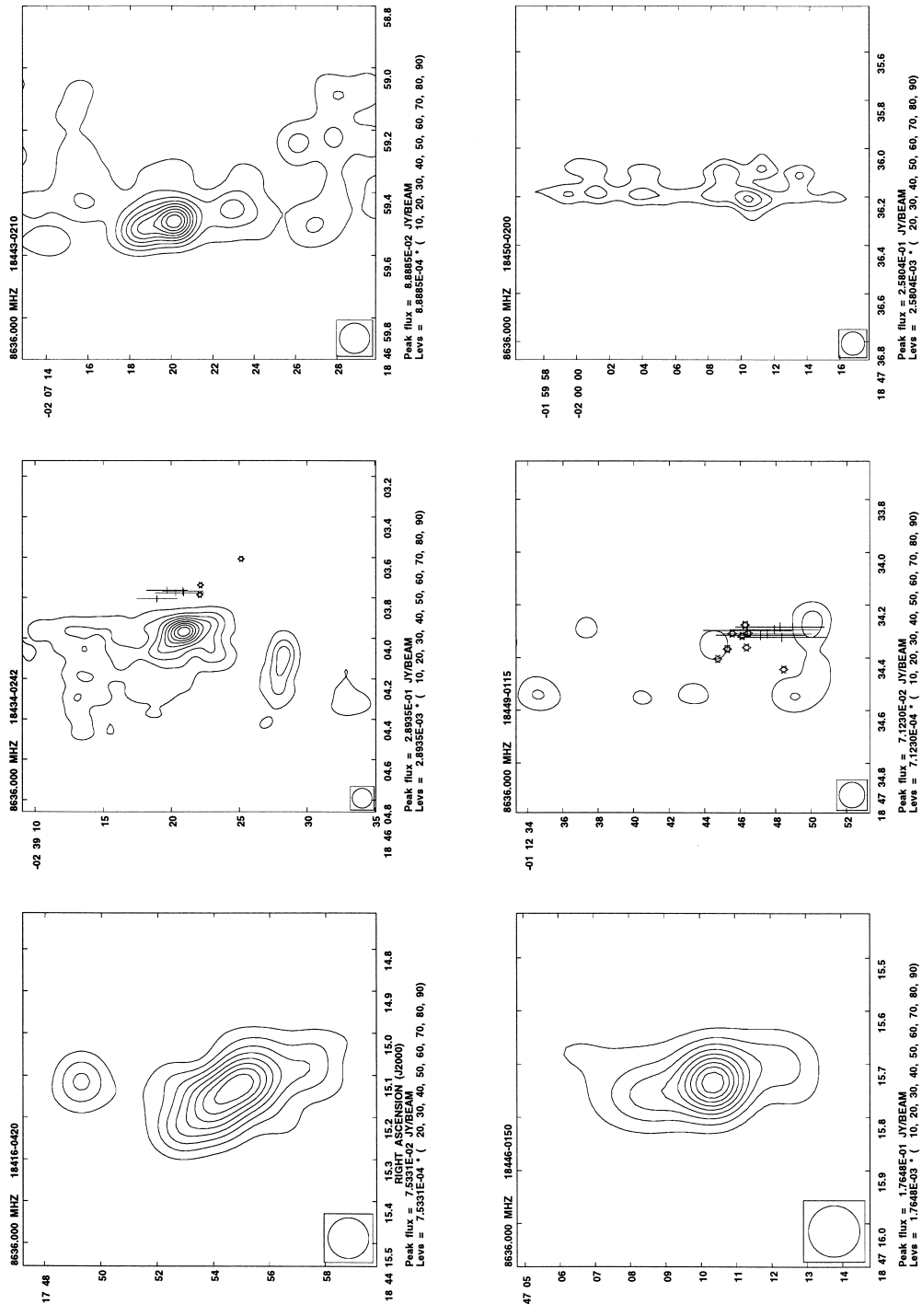


Figure 1 – continued

**Figure 1 – continued**

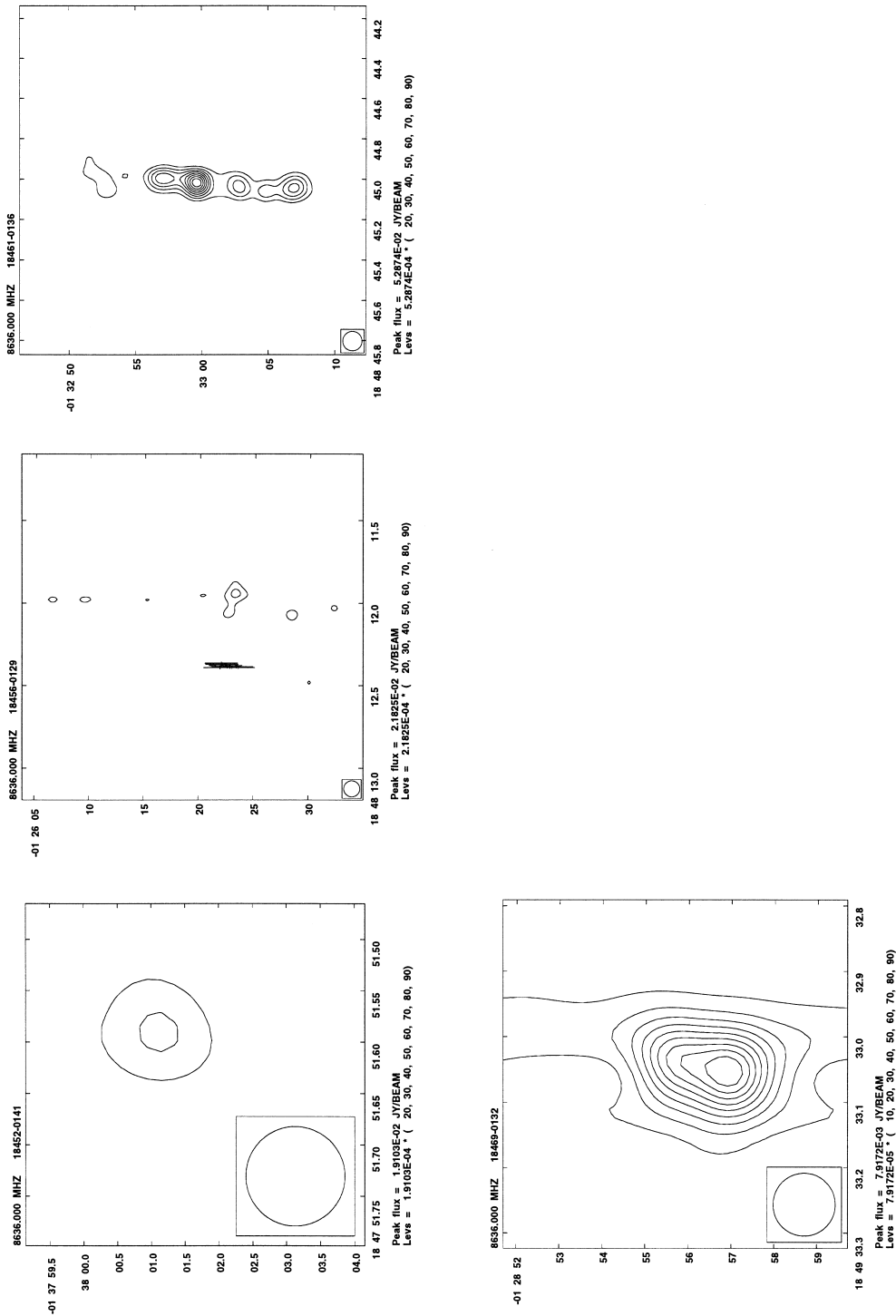


Figure 1 – continued

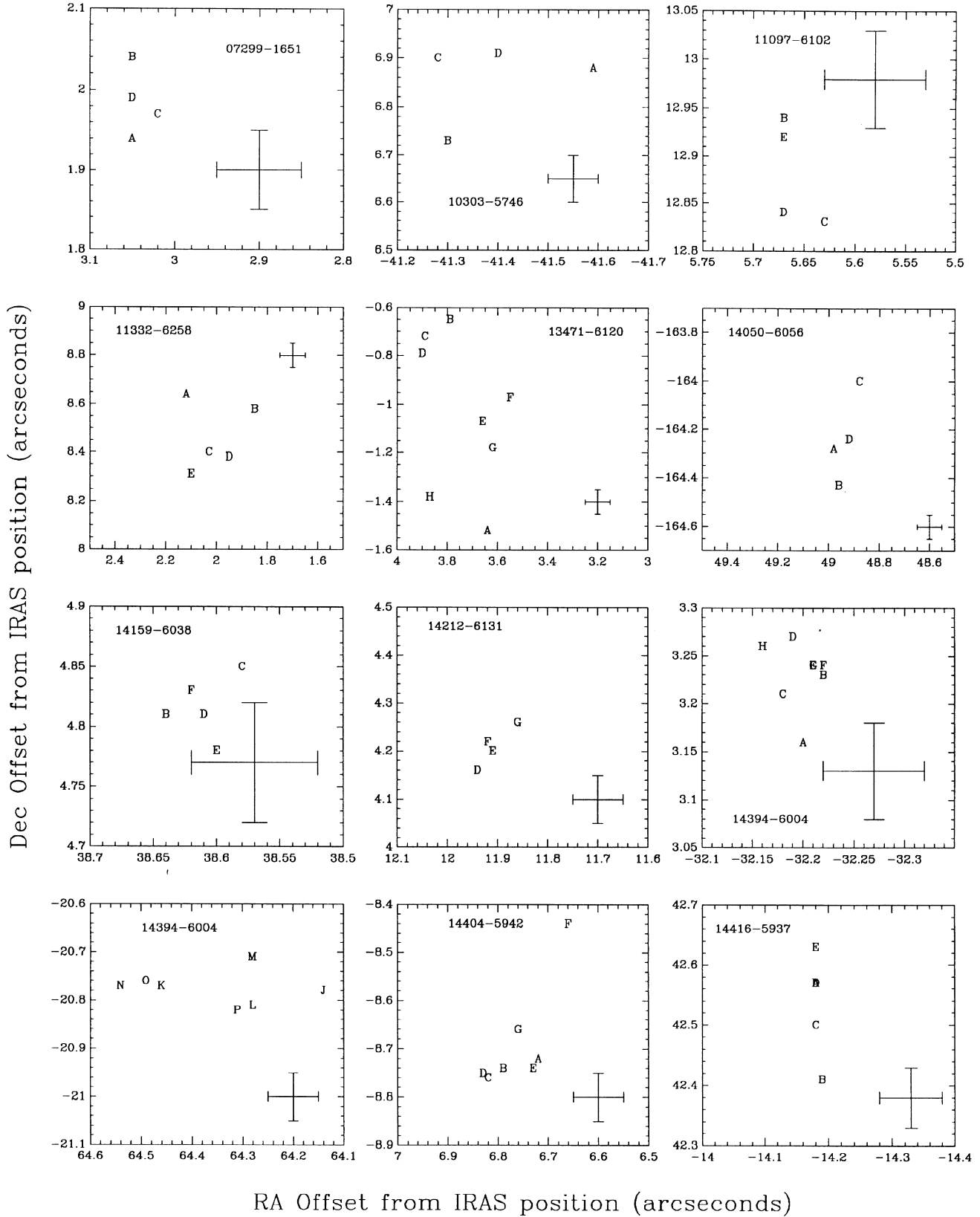


Figure 2. Relative positions of maser spots within an individual maser site. The offsets are in arcsec from the *IRAS* source. Only those maser sites with four or more spots are shown. The typical size of the error bars on each maser spot are shown by a representative error bar, usually in the bottom right corner of each plot.

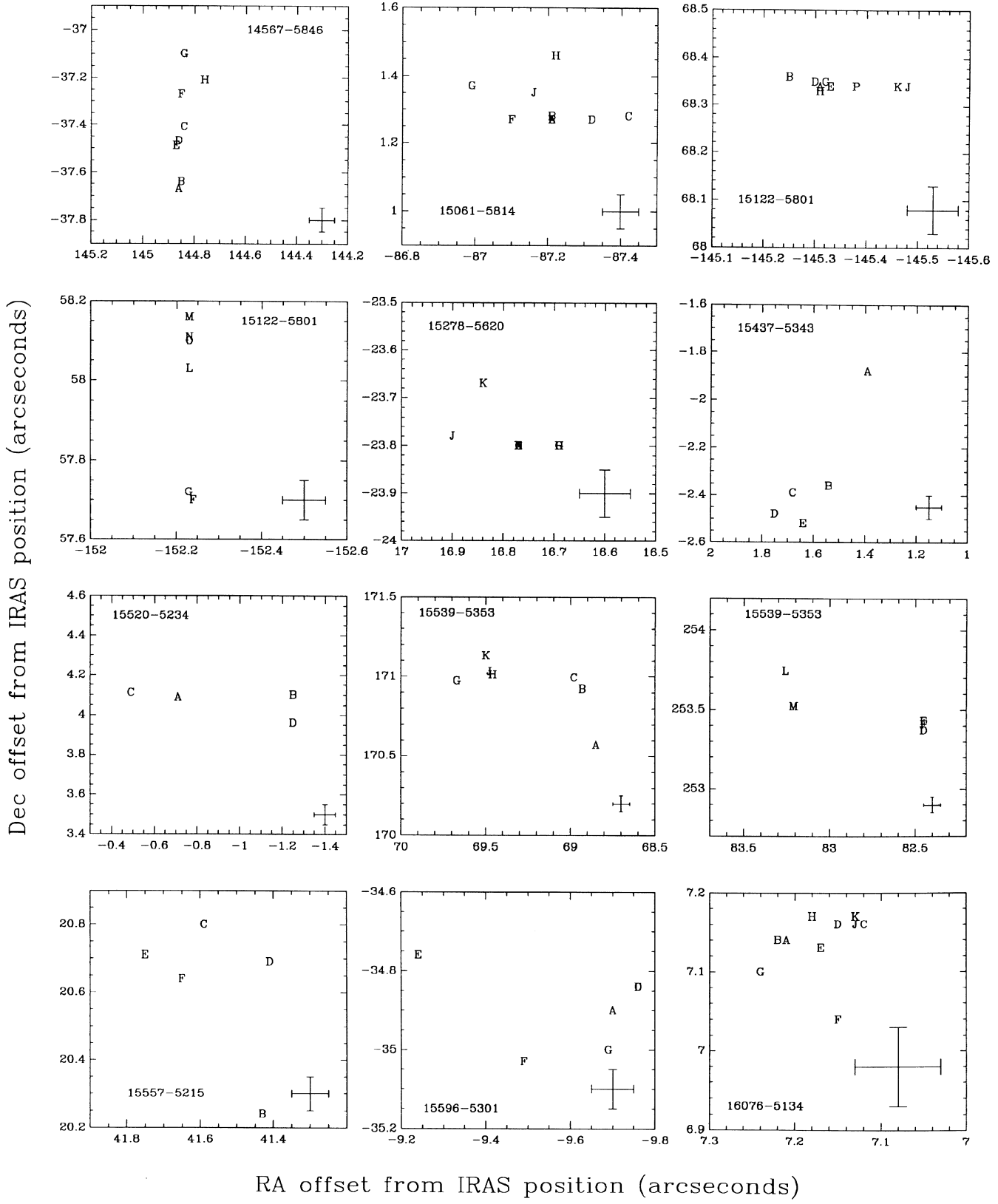


Figure 2 – continued

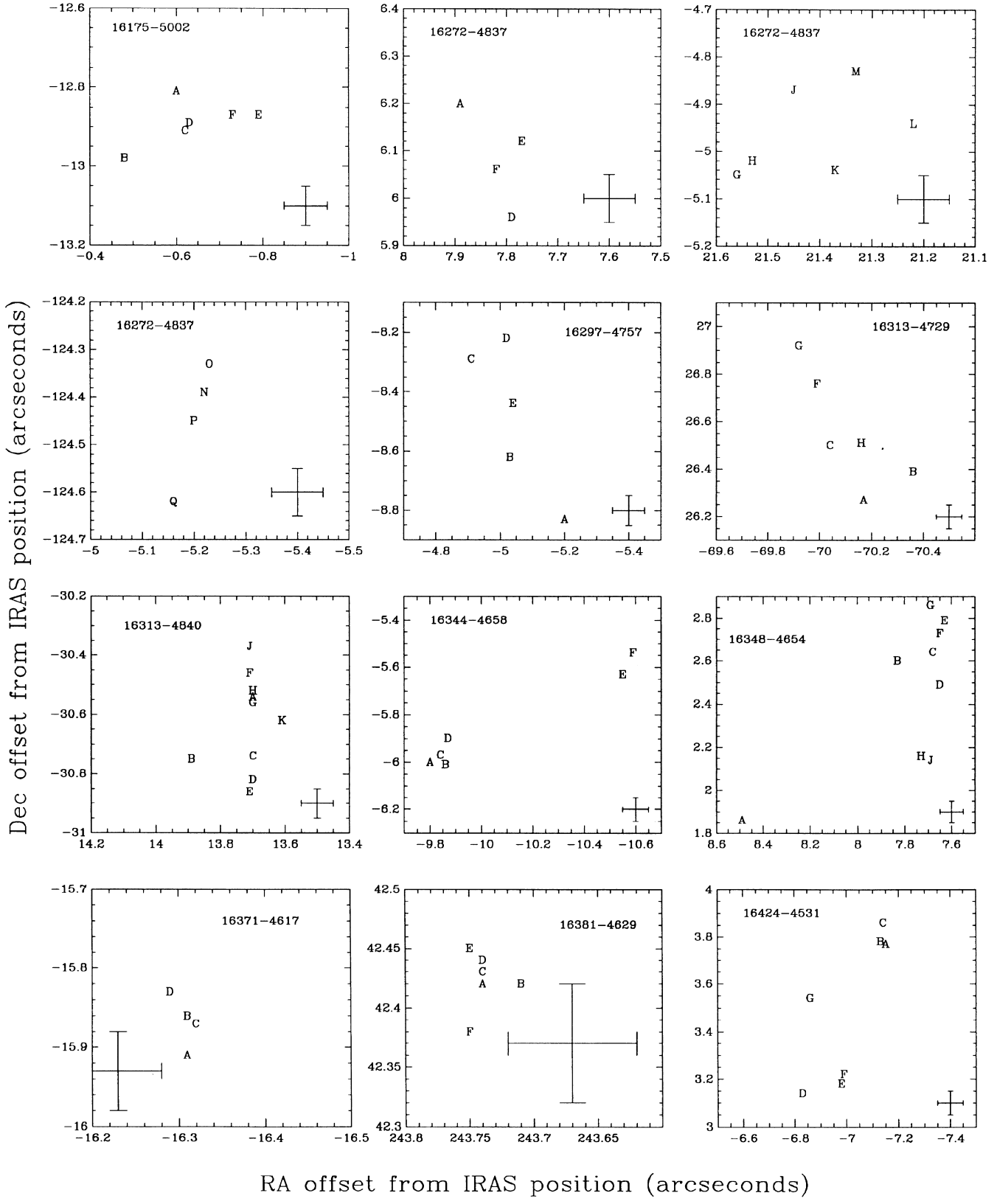


Figure 2 – continued

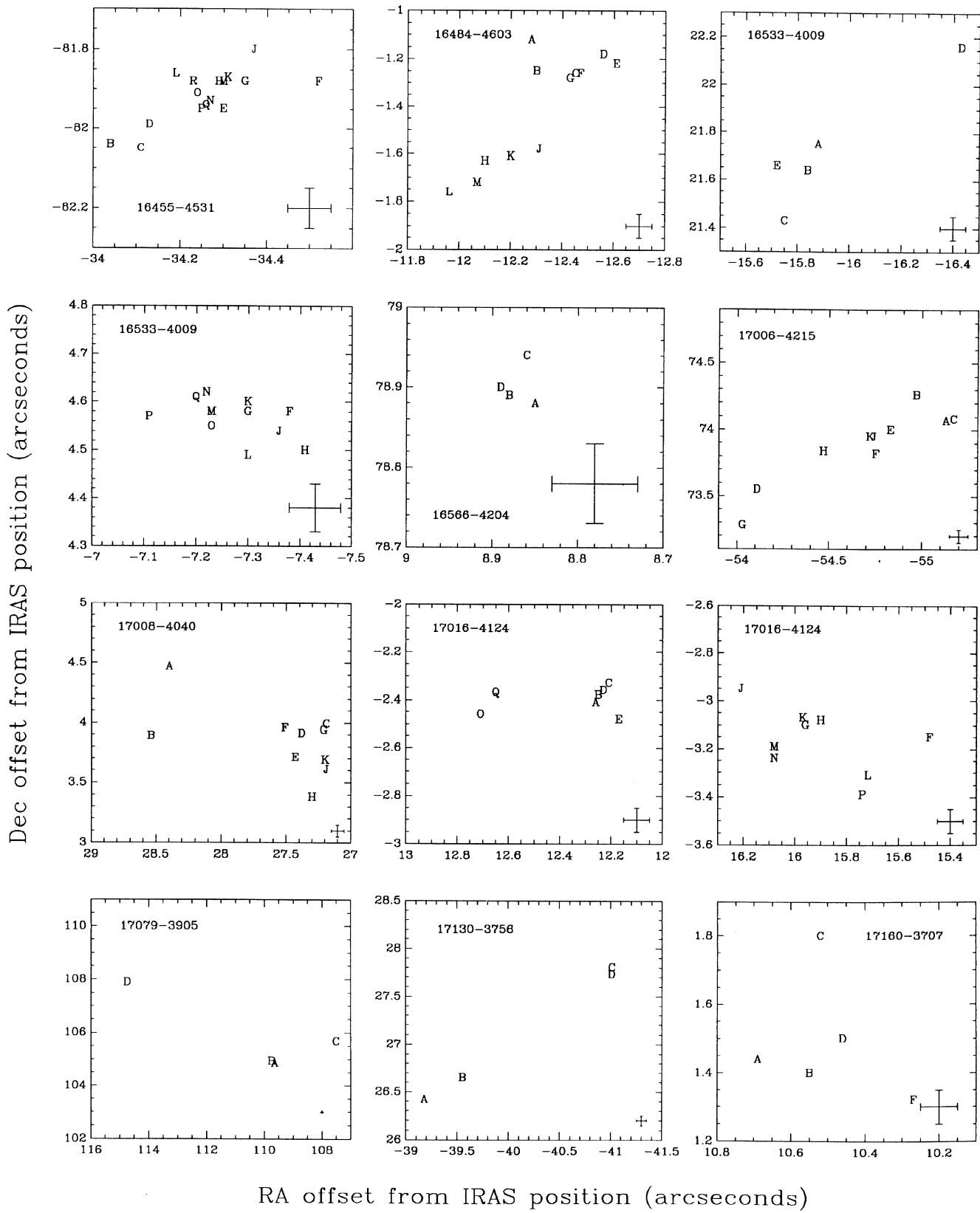


Figure 2 – continued

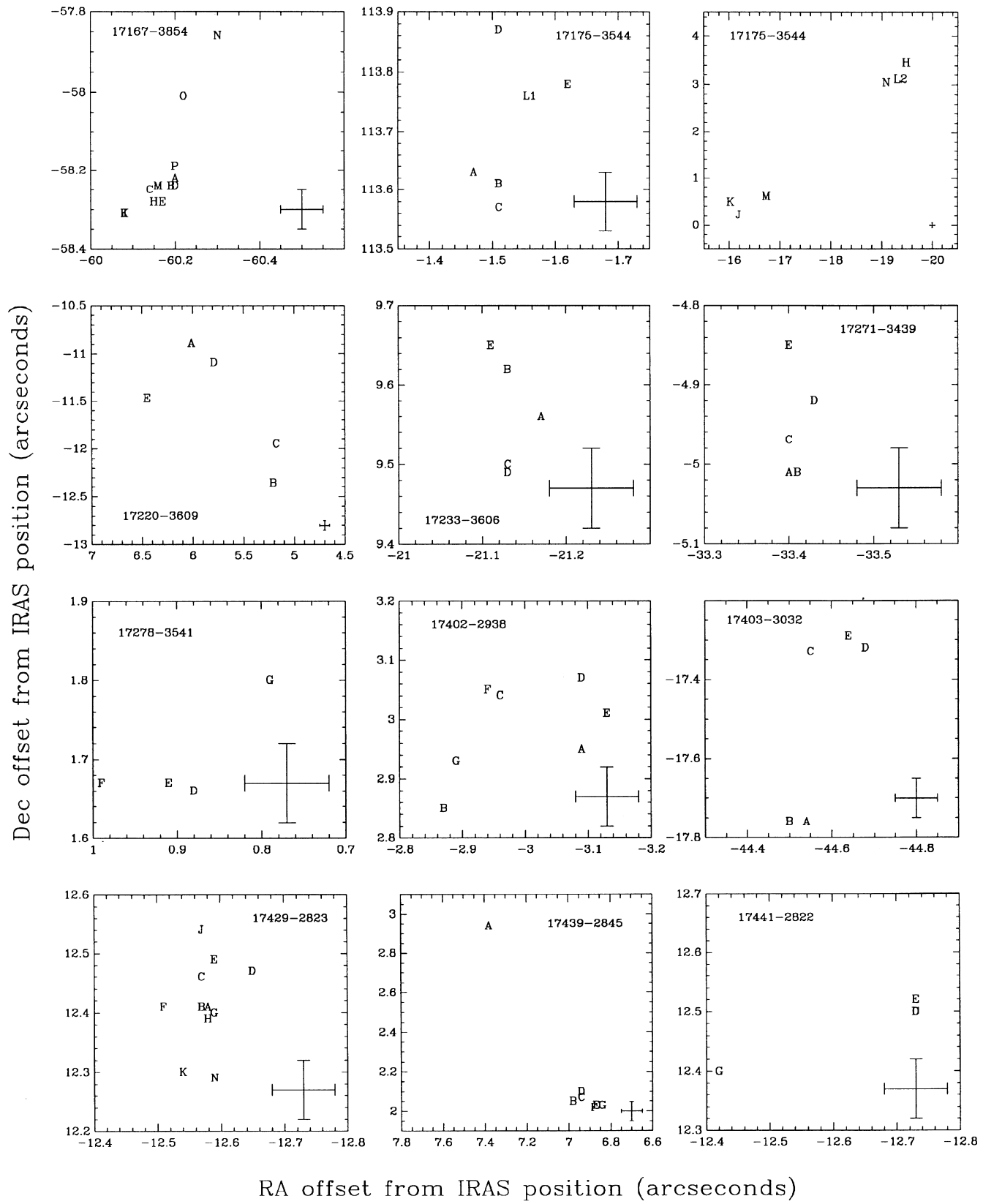


Figure 2 – continued

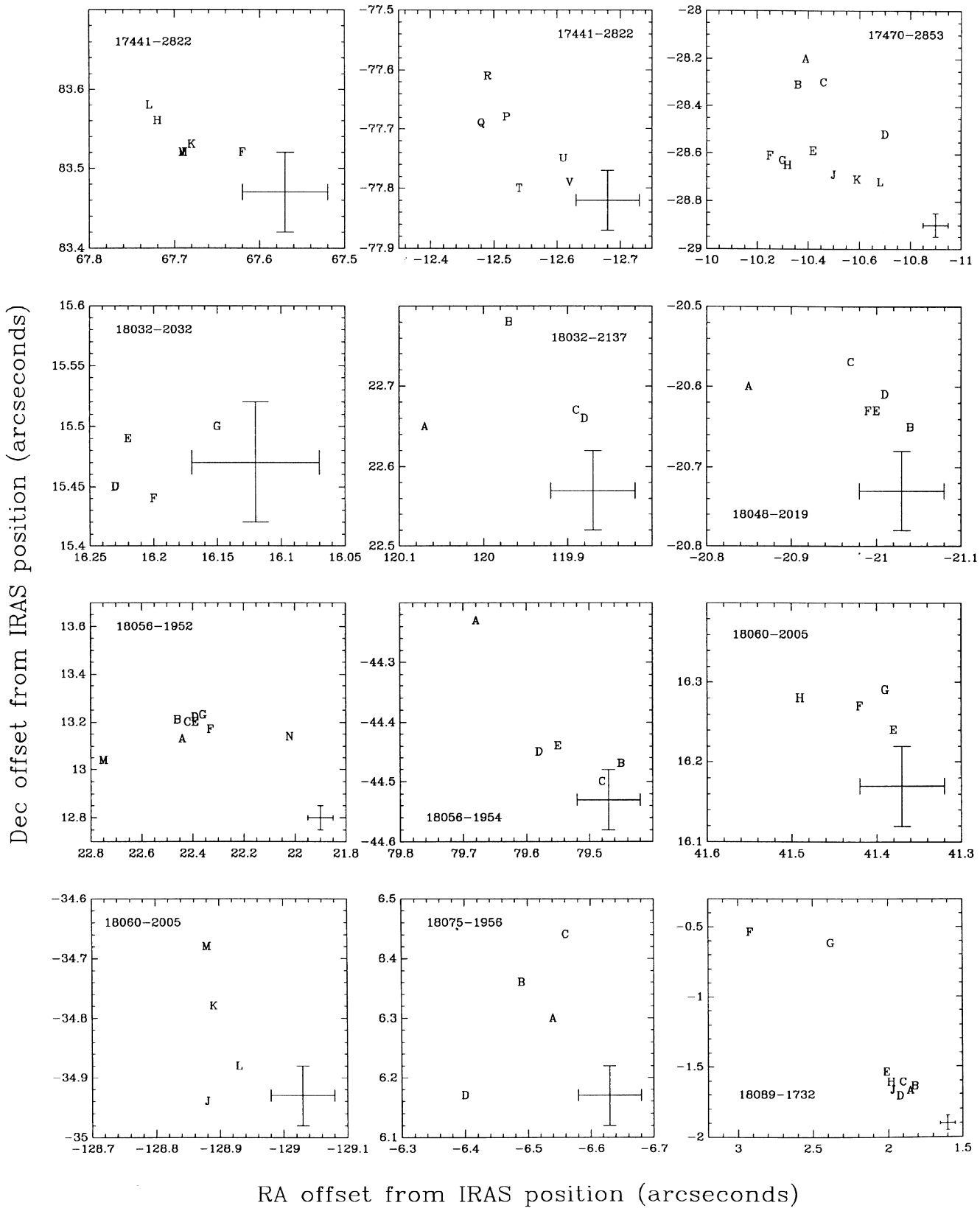


Figure 2 – continued

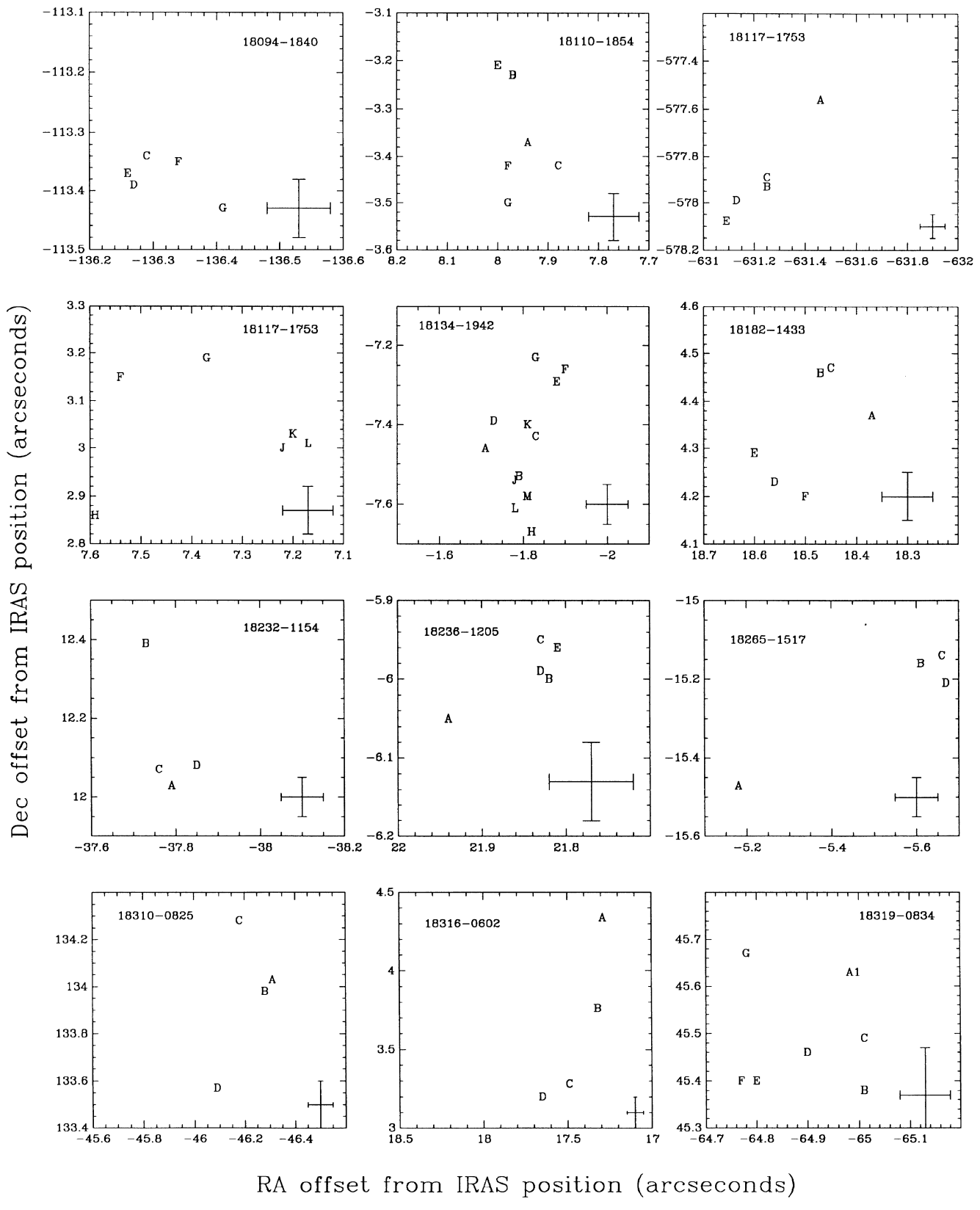


Figure 2 – continued

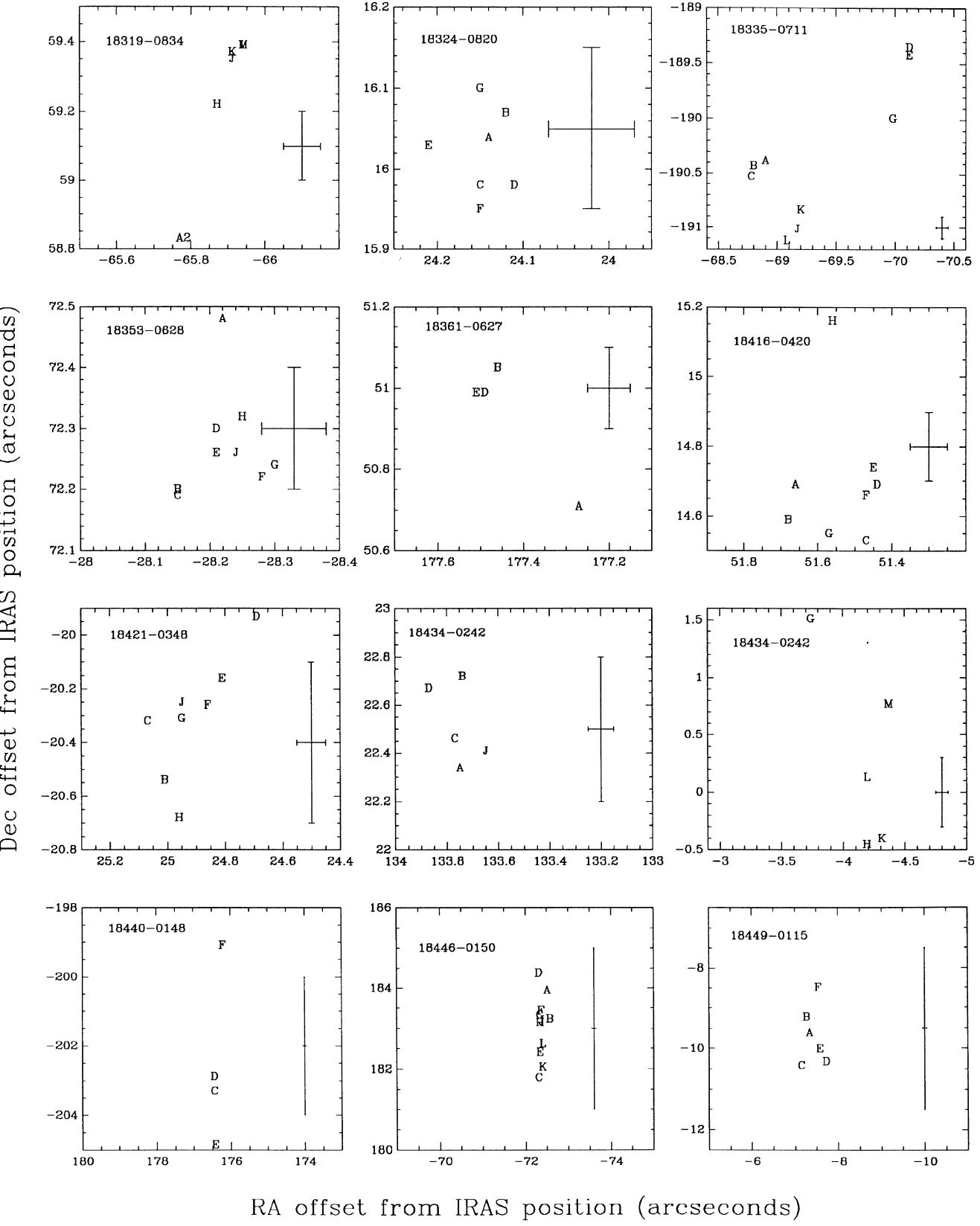
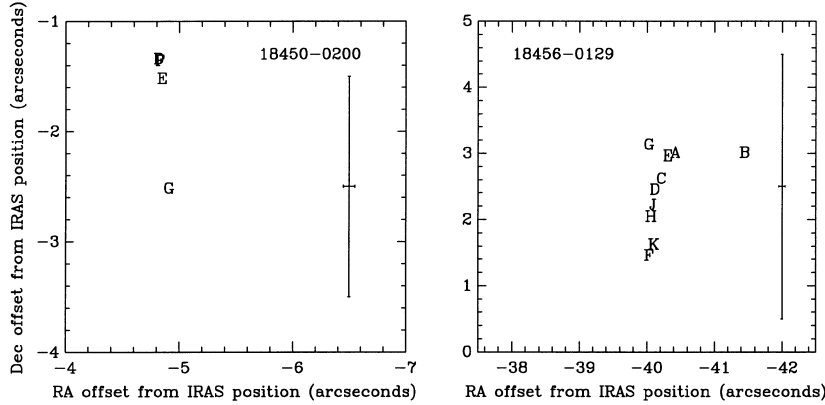


Figure 2 – continued

Figure 2 – *continued*

Also, if maser emission were enhanced by continuum photons, at the maser frequency, along the line of sight, we would find an enhancement in the brightness of maser emission when it overlaid continuum contours. Using a K–S test, we are 51 per cent confident that the bottom histogram in Fig. 4 for maser sites projected on to continuum contours is no different than that for those masers with no associated continuum source (the top histogram). It is also noted that in the limited sample of maser sites that are projected on to observed continuum emission (32 sites), there is no correlation between the brightness of the maser emission and the brightness of the continuum emission. A correlation would be expected if the maser emission were significantly influenced by the continuum photons. Thus, we can find no evidence that the maser emission is enhanced by the presence of an observable background continuum source.

It is possible that the methanol emission that is offset from the observed continuum arises from radio continuum sources which are too small and/or weak to be detected by our observations. The methanol emission, in the majority of cases, may come from UC H II regions that are very young, and not large or bright enough to show up in our data as continuum sources. The observed continuum sources, then, are UC H II regions that are generally older than the regions responsible for pumping the maser transition.

4.3 Morphological type

As a result of the nature of the short cut integrations used, interpretation of any morphologies is restricted to overall shapes as most of the fine detail is hard to distinguish from artefacts. The morphological types identified in Table 2 are cometary, irregular, partially extended, double and unresolved. To compare this with previous surveys, it is necessary to explain the criteria used to classify the objects. We have chosen to use the classification criteria of Wood & Churchwell (1989b, hereafter WCb) for cometary, irregular and unresolved (spherical) morphologies. Other morphologies used here are defined as follows: if the majority of emission can be easily fitted with two two-dimensional Gaussians and is not classified as one of the above, then the morphology is designated as double. Sources that are listed as partially extended are essentially unresolved, but some extended emission can be seen, although this extended emission is not large enough to distinguish between any of the above extended morphologies. Two morphologies used by WCb are not listed here, namely the shell and core–halo morphologies. None of our contour plots show conclusive evidence for such morphologies. There are two reasons for this: first, as noted by WCb, there are only a relatively small number of such regions,

compared to the other morphologies (16 per cent for core–halo and 4 per cent for shell). The second reason is that our data have lower sensitivity, dynamic range and resolution than the data of WCb. The weak extended emission may not be picked up from a core–halo object in our survey, and may be classified as an irregular or unresolved object, as is the case with IRAS 18006-2422. Some shell morphologies identified by WCb are not evident in our data, such as IRAS 17574-2403 and IRAS 18021-1950, where our larger beam was not able to resolve the structure properly, particularly in the central region with less emission (WCb's resolution is 0.4 arcsec). It should be noted that some of our images in Fig. 1 may have some of the characteristics of both cometary and shell morphology. Examples of this are IRAS 10303-5746, IRAS 14095-6102, IRAS 14567-5846, IRAS 14594-5824 and IRAS 16445-4516. Each of these sources has continuum emission that extends in a parabolic shape, but is suggestive of forming a

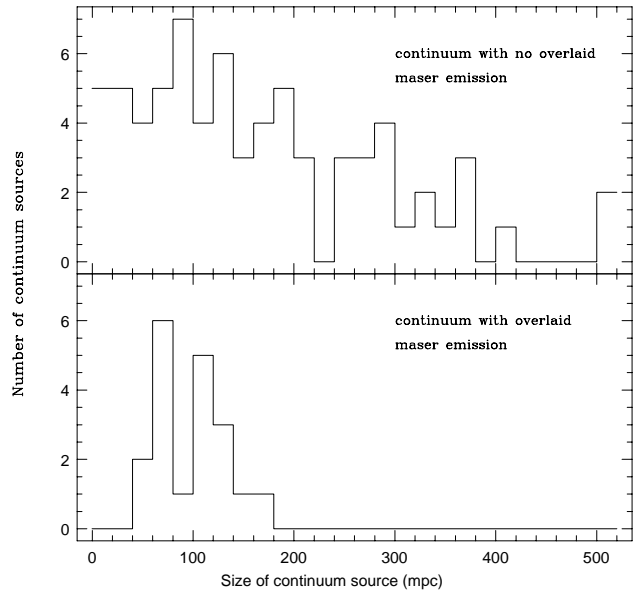


Figure 3. Histograms of the projected sizes of extended radio continuum regions. The upper histogram shows all radio continuum sources without maser emission projected on the continuum contours. The lower histogram shows only those continuum regions where maser emission is projected on the continuum contours (and presumably directly associated with the continuum emission). It is obvious that the continuum regions with maser emission are generally smaller, implying that maser emission is associated with the smallest, and therefore youngest, UC H II regions.

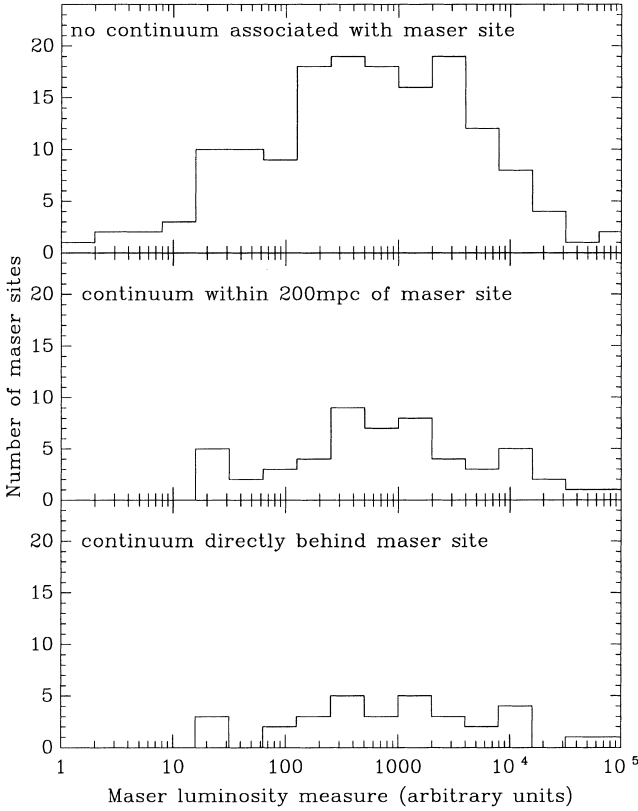


Figure 4. Three histograms are shown for the integrated flux of the maser emission. The top one is for all maser sites that have no associated radio continuum source. The middle one shows those maser sites that have a continuum source within 200 mpc projected distance, and are therefore possibly connected. The bottom one shows those maser sites that are projected on to the continuum contours such that the continuum photons may play a part in enhancing the maser emission along the line of sight. The similarity of the three distributions implies that there is no evidence the maser emission is enhanced by the presence of a continuum source.

complete ellipse towards the tail of the cometary region, although the limited sensitivity does not show this explicitly. It may be possible that shell and cometary morphologies arise from similar circumstances. It has been suggested by Hofner & Churchwell (1996) that the UC H II regions with a cometary morphology may arise from a density gradient, with a high density at the cometary head and low density at the tail. It is possible, then, that shell morphologies occur if the density gradient is not as severe as that for cometary regions. The relative number of morphologies found in this survey is: 30 per cent unresolved, 30 per cent cometary, 28 per cent irregular, 7 per cent partially extended and 4 per cent double peaked.

How are cometary and irregular morphological types related? Previously, a survey by Hofner & Churchwell (1996) of water maser and continuum emission sites has indicated that there is a distinction between the morphological types and the proximity of maser emission. They show that the maser emission associated with non-cometary regions (including irregular morphologies) is often projected against the continuum emission contours, whilst maser emission is more likely to be offset from the continuum emission of cometary regions. For the cometary UC H II regions, this was interpreted as evidence for the maser emission arising from an undeveloped and undetected UC H II region, associated with hot

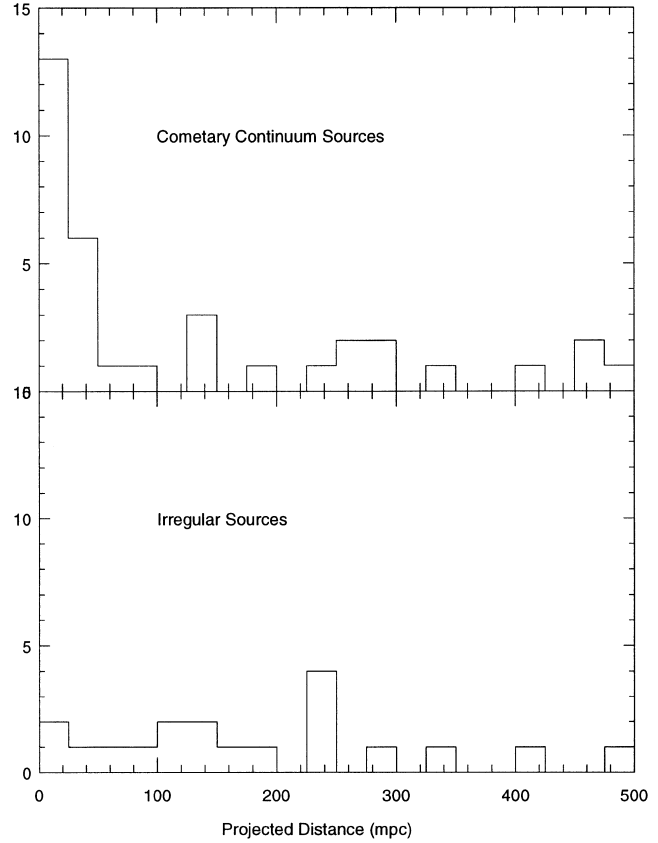


Figure 5. Two histogram plots of the distribution of methanol maser sites from a nearby continuum source are shown for cometary (upper histogram) and irregularly (lower histogram) shaped UC H II regions. The masers are found preferentially closer to the cometary continuum regions, but not to the irregularly shaped continuum sources.

ammonia clumps (Cesaroni et al. 1994). Thus, the dense core associated with the water masers and ammonia emission creates a density gradient that shapes the cometary UC H II region. We can produce a histogram plot similar to fig. 23 of Hofner & Churchwell for the methanol masers, as shown in Fig. 5. This figure shows the projected distance of the sites of methanol emission from the radio continuum source, for the cometary and irregularly shaped continuum morphologies. In comparison to the relative positions of water masers, our data show a contrast for the different morphologies. The continuum sources with a cometary shape do show a significant increase in the occurrence of methanol emission closer to the continuum, whereas no such correlation is found for water maser emission. Also, in contrast to the correlation found with water masers and irregular UC H II regions, there is little correlation between the positions of the methanol maser and UC H II regions of irregular morphology. This difference between water and methanol maser emission highlights the different environments that are conducive to their formation. A K-S test of the distributions of maser sites from the irregular and cometary-shaped continuum sources indicates that there is only a 4 per cent probability that the two are drawn from the same distribution. Thus, we believe that the two morphologies are physically different from each other, and are not the result of some projection effect.

Even though we find that the distribution of methanol and water masers about continuum sources is different, there are a number of sources in which there is good positional coincidence of the two types of masers, for example IRAS 18110-1854 and IRAS

18032-2032. It seems that, in these cases, they are associated with a very young or undeveloped UC H_{II} region that is not currently observable as a continuum source, but may be visible as a hot ammonia clump. This suggests that the masers may in some cases arise in similar circumstances.

It is possible that both maser species have more than one environment in which they may be observed. Both methanol and water maser emission are found associated with ammonia clumps. However, methanol maser emission is also seen preferentially closer to cometary radio continuum sources, where water maser emission is not. Furthermore, water maser emission is also found preferentially closer to irregularly shaped radio continuum sources, where methanol maser emission is not.

4.4 The structure of methanol maser spots within a maser site

It has been previously reported (Norris *et al.* 1993), for a small number of objects, that the relative positions of methanol maser spots tend to lie along a line or arc, with a velocity gradient along the axis. The interpretation given by Norris *et al.* (1993) is that the masers lie within an edge-on protoplanetary disc. This data was for the brightest 15 regions of methanol maser emission known. With our considerably larger data base, we are able to further test this hypothesis. Not all the 238 regions identified with maser emission can be used, as many have few maser spots. Some 97 regions have four or more maser spots, and were used to examine their relative positions. These are shown in Fig. 2. As can be seen there are a variety of shapes, from well defined linear/arc structures to apparently random patterns. As it is hard to make a good quantitative estimate of the proportion of masers lying in a linear/arc structure, we have categorized the maser sites according to the ratio of major to minor axes in the spread of maser spots. If the ratio is less than 3, then the maser site is defined as having no evidence for linear structure; between 3 and 5, some linear structure; and greater than 5 means a well-defined linear structure. Using these definitions we find 61 that have no linear structure, 27 that have some linear structure and 9 that have a well-defined linear structure.

One way to test the hypothesis that the masers originate from a circumstellar disc is by comparing the data we have to the expected Keplerian orbits in a rotating disc. Our method estimates the minimum central mass that will produce the observed radial velocities. Fig. 6 shows P–V (position–velocity) diagrams for those 36 maser sources showing evidence for a linear structure. A P–V diagram shows the relative position of a maser spot along the line which the maser site is extended on the horizontal axis. The vertical axis is the measured radial velocity. The P–V diagram can be used to estimate the central mass in two ways. The positions of the spots are either confined to two quadrants of the P–V diagram (with the origin signifying the position and radial velocity of the central mass), or they lie in a line. These two cases will be dealt with separately.

4.4.1 P–V diagrams with spots in two quadrants

The physical interpretation of maser spots lying within two quadrants of the P–V plane is that they are orbiting around a central

mass, located at the origin, with all orbits on one side being towards the observer and all orbits on the other side moving away, relative to the rest frame of the central mass. Since there is currently no velocity or precise positional information on the central stellar object, the origin cannot be determined. However, all maser spots must lie in one or two quadrants of the P–V diagram. For each maser spot, the mass of the central star can be calculated using the following equation, which describes Keplerian motion:

$$R = \frac{GM}{V^2} \cos^2 \Theta, \quad (1)$$

where V is the radial velocity of the maser spot with respect to the central mass (i.e. the origin), R is the distance of the maser spot from the origin and Θ is the angle between our line of sight and the maser velocity vector. As it is not known what part of the motion of each spot is along the line of sight, the radial velocity, and hence the calculated central mass, will only be a lower limit; we are determining values for $M \cos^2 \Theta$. Furthermore, our choice of the location of the origin has been determined to find a minimum value for the central mass. Each mass listed for those P–V diagrams in Fig. 6 with masers in two quadrants is the largest value of $M \cos^2 \Theta$ found, but is still a lower limit to the central mass. Most of these lower limits do seem to fit in with what would be expected for an O or early B-type star, but in several cases we note that the implied masses are extremely large ($> 100 M_{\odot}$), which we consider unlikely.

Furthermore, the locations of the maser spots (in quadrant diagrams) are not uniformly distributed, as would be expected if observing random orbital positions. A random distribution of spots should lead to an average of half the spots in one quadrant of the P–V diagram and half in the opposite quadrant. In Fig. 6, the distribution of spots is heavily weighted in favour of one quadrant in at least 11 cases out of 36. This is necessary to achieve the lowest possible derived central mass. If the central mass is located such that approximately equal numbers of spots are found in each quadrant, the derived central mass increases to unrealistic values for O and B stars in these cases.

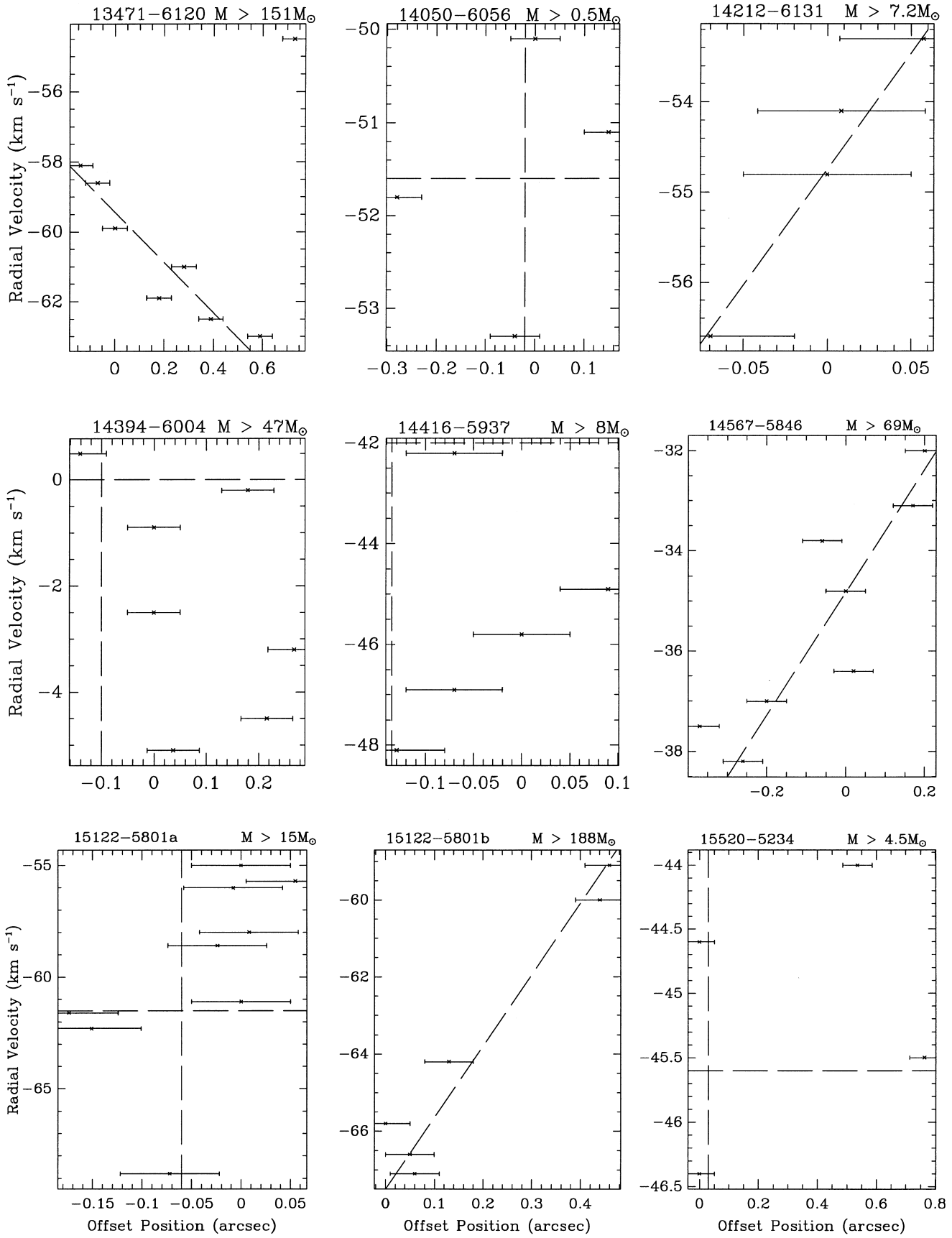
4.4.2 P–V diagrams with spots in a line

A slightly better constrained model is available, for example, when the maser emission is found to be distributed along a line, in the P–V diagrams. The model we adopt here is that the masers are located on the edge of a thin ring, whose annular width is small compared to its radius. The edge of the ring we see is where the maser path length is longest. In this case the maser emission kinematics will follow a straight line in the P–V diagram, with a gradient given by

$$\frac{dV}{dP} = \sqrt{\frac{GM}{R^3}}, \quad (2)$$

where R is the radius of the ring. Since we do not know where the central mass is located, again we can only derive lower limit estimates of the mass of the central star. We have crudely derived it by assuming that the radius of the ring is equal to the linear extent

Figure 6. Position–velocity diagrams of those 36 maser sites that show some evidence of a linear structure are shown. The horizontal axis is the offset in position along the major axis of the maser site, from the strongest maser spot. The vertical axis is the measured radial velocity. Each site has a lower limit central mass estimate (see text for details). Those sites where the central mass has been derived using a linear fit to the maser spots are shown with the linear fit drawn as the dotted line. Those sites where the mass has been determined by separating the maser spots into two quadrants are shown with the quadrant axes drawn on. The origin of these axes indicates the position and radial velocity of the central mass, chosen so that it takes the minimum possible value. Lower case letters (e.g. ‘17016-4124a’ and ‘17016-4124b’) are used to refer to multiple maser sites detected within the same field. ‘a’ refers to the maser site with the lowest maser spot velocity, ‘b’ refers to the maser site with the second-lowest maser spot velocity, and so on.



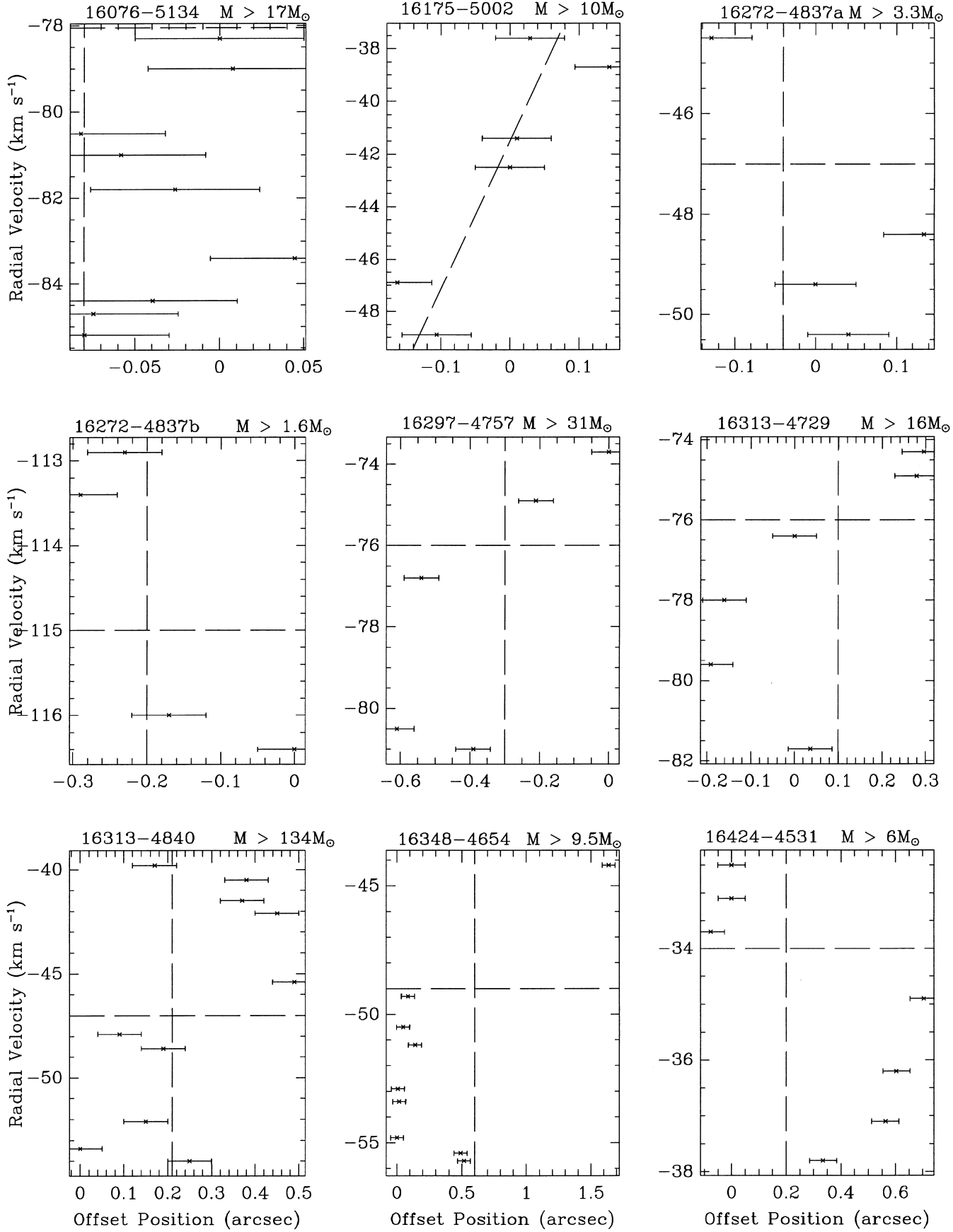


Figure 6 – continued

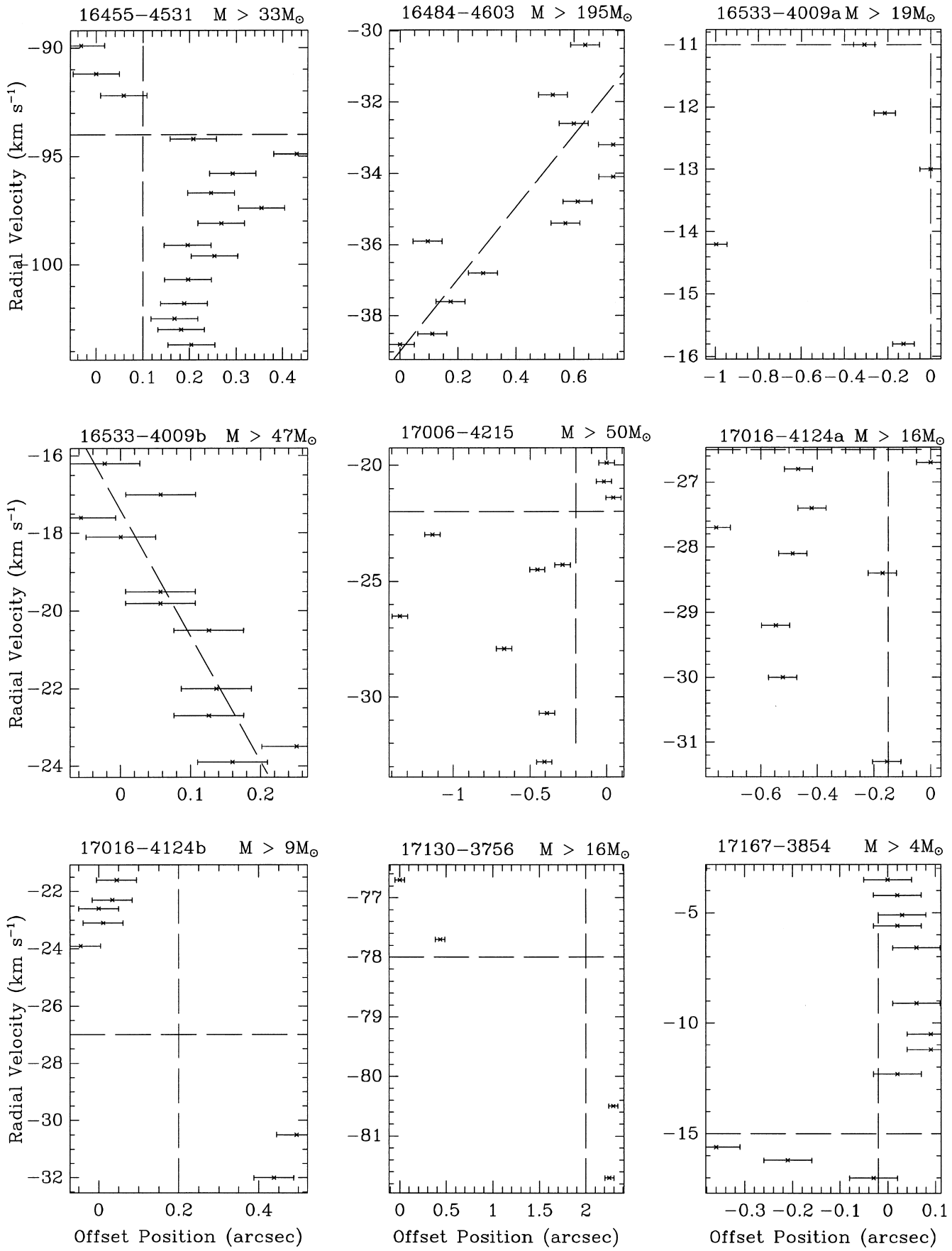


Figure 6 – continued

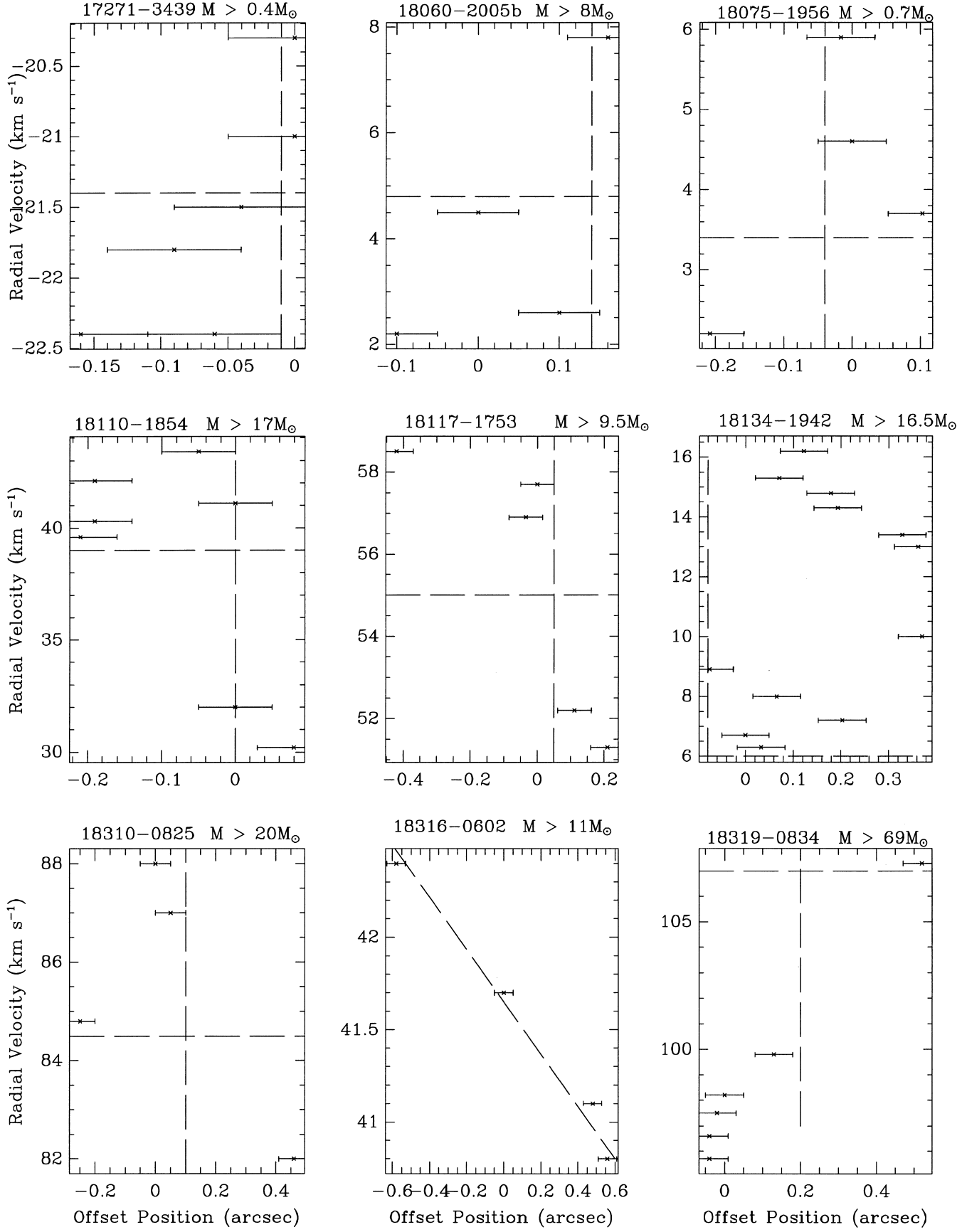


Figure 6 – continued

of the maser spots (i.e. the annular thickness of the ring), which is hardly consistent with the assumption that the ring is thin compared to its radius. These are listed, with their corresponding P–V diagrams, in Fig. 6. Again, it is apparent that the masses derived do follow what would be expected of particularly massive stars.

Since the mass is heavily dependent on the ring radius, the derived masses will be too large to be realistic in all cases if the ring radius is only 2.5 times the annular thickness.

With the uncertainties in both these methods of mass estimation through Keplerian motions, it is hard to categorically conclude that the masers are not in Keplerian orbits about a central massive star. Factors such as the position of the central mass need to be determined before a rigorous test can be applied. Nevertheless, the large values for some of the derived values of the mass make this hypothesis seem unlikely.

Our data do suggest that another interpretation is required to explain the maser emission in many cases. We examine the case of an expanding shock as an example in the next section.

4.4.3 Expanding shock model

There is no doubt that there are a number of maser sites that are linear in extent which cannot be accounted for by chance alignments. A shock viewed from one side can produce such linear structures readily. Norris et al. (1993) argued that a shock was an unlikely explanation of their data, as it cannot produce the velocity gradients seen in many of their maser sites. In our data set (see Fig. 2), it is found that most maser sites do not show a systematic velocity gradient (only 12 out of 97 sites do have a velocity gradient). Thus, we believe that a velocity gradient is not a general feature of maser sites. This is partly the reason why the circumstellar disc hypothesis has difficulty in explaining all our data. It is doubtful that velocity gradients have been smeared out in our short cut integrations as we observe the same features as Norris et al. (1993) in sites that were mapped in both programs (e.g. IRAS 13471-6120 and IRAS 14567-5846).

The shock wave model naturally explains why many maser sites are seen without associated radio continuum emission, as there is no need for an ionizing source to be present. This implies that the maser may also be associated with objects other than UC H II regions.

The shock wave hypothesis for spot locations does not require them to be shock-excited, but rather that they are dense knots of gas that have been compressed and accelerated by the passage of the shock, with a sufficient column of material along our sight line for masing to occur. The velocities of the masing spots reflect the projection on our line of sight of the shock velocity. For instance, for a spherically expanding 20 km s^{-1} shock wave 1500 au from its origin, two spots 100 au apart on the plane of the sky (0.5 arcsec at 2 kpc) would have a velocity difference of 5 km s^{-1} , values quite typical of the data. Any spots in between would show a smooth velocity gradient. In practice, of course, the shock front is unlikely to expand uniformly unless it traverses a homogeneous medium. Thus while velocity shifts may reflect changing projection angle, they could also be produced by varying shock speeds and a convoluted, or even fractal, shock front. A closer analogy might be a wavy sheet. Sight lines through the extrema of the sheet would be most likely to exhibit maser emission due to increases both in column of material and in velocity coherence.

This is a general hypothesis and does not make specific predictions for maser spots. Depending on local conditions, line, clusters

and isolated spots can be produced, and while velocities of adjacent spots are likely to be correlated, they do not show systematic gradients. A test of this hypothesis would be to search for tracers of shock waves associated with the masers, particularly through near-infrared H₂ vibrational–rotational emission, and high velocity HCO⁺ mm line emission. In principle, the spatial and velocity structure of the maser spots could then be used to model the geometry of the expanding shock wave for individual sources, and in particular to determine the degree of inhomogeneity of the molecular cloud.

5 SUMMARY AND CONCLUSIONS

We have obtained high (arcsecond) resolution radio continuum (to a limit of $\sim 1 \text{ mJy}$) and methanol maser (to a limit of $\sim 0.3 \text{ Jy}$) images of a large number of UC H II candidates, using the ATCA. Contour maps are provided for selected continuum sources, showing overall morphologies of the regions, as well as relative position maps of maser spots, with relative positional accuracy up to 0.05 arcsec. Our major findings are as follows.

(i) Most sites of methanol maser emission are not associated with observable continuum emission, and most sites of continuum emission show no signs of methanol maser emission.

(ii) Continuum sources with associated maser emission tend to be smaller than those which lack maser emission.

These first two points suggest that the methanol maser is observable before the UC H II region phase and is probably destroyed as the UC H II region develops. It is possible that a small fraction of these maser sources are associated with embedded non-ionizing stars. We predict that mid- to far-infrared sources should be associated with these sites of maser emission as this radiation is required to explain how the maser is pumped.

(iii) The methanol maser flux is not dependent on the proximity of a continuum source, whether the continuum lies offset from the maser site or is projected behind it.

(iv) A comparison of the positions of water and methanol maser sites, with respect to differing morphologies of UC H II regions, shows a marked difference. Methanol sites are clustered closer to cometary-shaped continuum sources, whilst water masers are not. Water masers, on the other hand, are found clustered towards irregularly shaped UC H II regions whereas methanol masers are not.

(v) Despite differences in the association of methanol and water masers with UC H II regions, there are some cases in which there is good positional coincidence between the two maser types. Such cases are associated with hot ammonia clumps, presumably a stage of star formation before the UC H II region phase. Thus, the environmental requirements for methanol and water maser emission to be observable overlap, but are not the same.

(vi) The hypothesis that methanol masers arise from circumstellar discs is not inconsistent with some of our data. However, in general it seems unlikely to account for the kinematics of most of the masers that are found in a line or arc. The data is too highly unconstrained to rigorously test the hypothesis, and further information, such as the radial velocity and position of the central stellar object, is required to further test this model. Nevertheless, the minimum values derived for the central masses in the most optimistic cases are very high, making the hypothesis seem unlikely. We have provided an alternative model, suggesting that the masers can be formed behind shocks, which

adequately explains the distribution of maser spots within an emission site.

ACKNOWLEDGMENTS

The authors would like to express gratitude to R. P. Norris for helpful information on observing strategy and data reduction and analysis, and to the ATNF for generous allocation of observing time on the ATCA. This work is partially supported by an Australian Research Council grant.

REFERENCES

- Caswell J. L., Vaile R. A., Ellingsen S. P., Whiteoak J. B., Norris R. P., 1995a, MNRAS, 272, 96
- Caswell J. L., Vaile R. A., Forster J. R., 1995b, MNRAS, 277, 210
- Cesaroni R., Churchwell E., Hofner P., Walmsley C. M., Kurtz S., 1994, A&A, 288, 903
- Ellingsen S. P., Norris R. P., McCulloch P. M., 1996, MNRAS, 279, 101
- Forster J. R., Caswell J. L., 1989, A&A, 213, 339
- Gaume R. A., Mutel R. L., 1987, ApJS, 65, 193
- Ho P. T. P., Haschick A. D., Vogel S. N., Wright- M. C. H., 1983, ApJ, 265, 295
- Hofner P., Churchwell E., 1996, A&AS, 120, 283
- Menten K. M., 1991, ApJ, 380, L75
- Norris R. P., Whiteoak J. B., Caswell J. L., Wieringa M. H., Gough R. G., 1993, ApJ, 412, 222
- Ramesh B., Sridharan T. K., 1997, MNRAS, 284, 1001
- Sevenster M. N., Chapman J. M., Habing H. J., Killeen N. E. B., Lindqvist, M., 1997, A&AS, 122, 79
- van der Walt D. J., 1997, A&A, 322, 307
- Walsh A. J., Hyland A. R., Robinson G., Burton M. G., 1997, MNRAS, 291, 261 (Paper 1)
- Wood D. O. S., Churchwell E., 1989a, ApJ, 340, 265 (WCa)
- Wood D. O. S., Churchwell E., 1989b, ApJS, 69, 831 (WCb)

This paper has been typeset from a $\text{T}_{\text{E}}\text{X}/\text{L}^{\text{A}}\text{T}_{\text{E}}\text{X}$ file prepared by the author.